UNIVERSITY OF LONDON THESIS

Degree PhD Year 2006 Name of Author MARTINDALE Hugh Gustav

THE BEHAVIOUR OF FLEXIBLE RISER TENSILE ARMOUR IN THE REGION OF AN END FITTING

HUGH GUSTAV AELRED MARTINDALE

A Thesis Submitted for the Degree of Doctor of Philosophy

University College London

Mechanical Engineering Department
Torrington Place
London
WC1E 7JE

ProQuest LLC
789 East Eisenhower Parkway
P.O. Box 1346
Ann Arbor, MI 48106-1346

ABSTRACT

The Behaviour of Flexible Riser Tensile Armour in the Region of an End Fitting

This is a study of axial and transverse slip in helically wound armour wires on flexible pipe under the influence of end restraint.

Analysis of steel strip layers in order to find the effect of end restraint prompted the development of a new model to describe their behaviour. This avoids the shortfalls of adapting previous models designed either for similar but different structures or for application away from any end fitting restraint.

Previous analytical solutions concerning flexible pipe tensile armour have concentrated on pre-defined paths on the supporting surfaces, these being strained helices or geodesic curves, and have avoided any consideration of end effects. The work presented here is aimed at finding the path adopted by armour wires approaching end fittings, and the resultant stresses and slip.

A model is developed which uses small changes in helical angle along the strip to describe tensile armour configuration as a flexible pipe is bent and stretched. The problem is characterized by a strip on a cylinder at a variable angle to its axis which itself has a variable curvature applied to it. A solution is found by minimizing total strain energy to find stress concentrations and slip characteristics. The simplest case of a straight pipe under tension is solved first, followed by a more typical flexible riser configuration involving bending under tension.

The results show that under frictionless conditions tensile armour wire slips to reduce tension and that near the end fitting this slip leads to increased bending stresses in some or all of the wires. The model is applied to typical riser designs for the transport of oil and gas to find the location and level of the greatest increases in stress. Their sensitivity to pipe design parameters is also assessed.

To my mother and father

Acknowledgements

I would like to thank above all my Supervisor Dr Kevin Drake for all his invaluable help and guidance towards the completion of this work. I also gratefully acknowledge the technical support and encouragement from Professor Joel Witz during the course of my studies. I would like to thank too Professor Minoo Patel and also Mr Niels Rishoj of NKT Flexibles for their initial support.

I have had much support and encouragement from a great many friends and colleagues at UCL. In particular I am grateful to Abed El-Chayeb for our many discussions regarding flexible pipe and umbilicals, and also to Chang-Hsin Chien for his contribution to a stimulating atmosphere for research. The support of Dr Richard Bucknall, Dr Alvin Blackie and Dr Feargal Brennan is also greatly appreciated, along with the help of David Bevan and Mark Iline.

Finally I would like to thank my good friends Carlos Santos, Francisco Lobo, Ângela Vidal and Phil Thomas for their words of support while this work has been going on.

LIST OF CONTENTS

NOMENCLATURE

α	Change in helical angle, change in orientation to loxodromic
α_0	Original helical angle, loxodromic angle
β	Strained helix deviation from loxodromic
β_0	Original lay angle
ε_a, ε_s,	Wire axial strain
ε_b	Wire longitudinal strain due to bending
ε_k	Helix/pipe axial strain
ϕ	Parametric angle, rotations per unit length
ϕ_0	Wire polar angle at restraint (ANSYS)
γ	Wire deviation from loxodromic
κ	Wire normal curvature
κ'	Wire binormal curvature
κ_0	Line curvature
λ	Lagrange multiplier
μ	Decay constant, coefficient of friction
ν	Poisson's ratio
Θ	Wire applied twisting moment per unit length
θ	Wire polar angle
θ_0	Wire polar angle at restraint
θ	2D global coordinate
θ_1	2D global coordinate at restraint
ρ	Radius of applied curvature
σ_a	Wire axial stress
σ_b	Wire longitudinal stress due to bending
τ	Wire twist
τ_0, $\frac{1}{\Sigma}$	Line torsion
ω_i	Deformation variable
ξ	Rate of change of path strain
A	Wire cross-sectional area
b	Unit binormal

C	$L\cos\alpha_0$
E	Young's Modulus
$\frac{df}{ds}$	Secondary component of wire twist
G	Wire normal bending moment
G'	Wire binormal bending moment
G_1	Shear Modulus $E/(2(1+\nu))$
H	Wire twisting moment
I	Second moment of area
J	Polar moment of area
K	Interaction shear stiffness beween wire and surface
K	Wire applied normal moment per unit length
K'	Wire applied binormal moment per unit length
K_p	Pipe applied curvature, $1/\rho$
k	$R\tan\alpha_0$, Ratio $\frac{\delta\theta}{\delta s}$
k_1	Cross-section torsion constant
L	Original wire length
L_p	Unloaded pipe length
N	Wire normal shear force
N'	Wire binormal shear force
$\mathbf{n}$	Unit normal
R	Wire helical radius
R_{cr}	Critical radius of curvature (minimum bend radius)
s	Original arc length variable
S_l	Lateral slip
T	Wire tension
$\mathbf{t}$	Unit tangent
X	Wire applied normal force per unit length
Y	Wire applied binormal force per unit length
Y	Strained helix deviation from loxodromic
Z	Wire applied axial force per unit length
Z	Pipe applied curvature at $s = 0$

LIST OF TABLES

LIST OF FIGURES

1 INTRODUCTION

1.1 AIMS

Each component of flexible pipe has its own limitations which have led to problems in operation, often in severe service conditions of deep water, high temperature, high pressure and sour service. Constant flexure of flexible risers requires that the components be resistant to wear and fatigue. Sour service reduces flexible pipe service life; steel armours in the pipe are sensitive to the presence of sea water and H_2S leading to defects caused by localized corrosion. Polymers used for fluid barriers degrade with age either becoming brittle over time or shrinking through loss of plasticiser depending on which material is used. Polymer extrusion under pressure through gaps in their supporting layers is also a problem which leads to pipe failure.

By the mid 1990s several extrusion failures above 80°C had occurred at end fittings, examples of which were brought to UCL. It is clear that the sealing mechanism for a barrier manufactured from a material displaying creep and stress relaxation dependent on operating temperature is a complex problem. Also large bending effects take place in dynamic applications near the end fitting due to the joining of rigid and flexible system elements, and it is evident that stress concentrations and higher fatigue will result. Although flexible pipe distant from any restraint has been extensively analysed, there has been little work concentrating on the design and operational issues regarding end fittings. Together with the greater likelihood of failure at a pipe termination, this calls for a detailed study of the mechanics of end fittings.

This work concentrates on the analysis of flexible pipe tensile armour slip and stresses in the region of an end fitting, with the aim being to provide a dedicated analytical solution to the problem, allowing greater insight than that provided by numerical means or by adaptation of free field analytical results.

1.2 OFFSHORE HYDROCARBON PRODUCTION

When producing oil offshore, the system equipment can be broken down into the following five general areas :- sea-bed, risers, production support, storage and export.

The number of wells drilled will depend on the optimum rate of depletion, chosen to maximize the quantity of hydrocarbon recovered. The result may be a number of satellite wells, or a number of directionally drilled wells, drilled from a template. Wells may be drilled for production or for injection of flow enhancing fluid such as steam or methanol. Each wellhead is terminated by a 'christmas tree', which consists of valves and controls for the monitoring and control of fluid flow. A manifold provides the sea-bed site at which connection is made between the risers and all the production and injection wells.

The main purpose of production support, other than control of extraction, is to process the hydrocarbon extracted so that it is fit for export. Structures used for production support include jackets, which are steel structures built into the sea bed, and gravity structures, which are platforms based on very large hollow steel or concrete structures, some flooded when in position, others providing oil storage space. These permanent structures are not always the optimum solution, especially if the total reserve is small, and jack-up facilities may be preferred. These have the same advantage as the smaller drilling jack-ups in that they are easily moved from field to field. For large water depths, such structures are no longer practical, and so floating facilities such as semi-submersibles and converted tankers are employed. Hybrid forms also exist including tension-leg platforms and guyed towers.

In many cases, no pipe-line infrastructure exists. Export under these circumstances must be by tanker, a process limited by sensitivity to the weather. Hence processed hydrocarbon may need to be stored, albeit briefly, ready for export. Where there is no capacity on the production support platform, storage usually is provided separately by moored tanker or barge, the vessel being free to weathervane about the mooring point. In some cases the vessel is rigidly joined to the mooring buoy swivel, a configuration which improves storage vessel response making shuttle tanker loading operations more

easy. Alternatively, oil storage may be possible in the mooring buoy itself or within the structure of an articulated column. Connections to tanker manifold and pipeline end manifold are by flexible hose.

These separate items all require connection by flowlines, some static and some dynamic. Advantages of connection by flexible pipe include compliance with floating structures and ease of installation when compared to the much smaller tolerances involved with rigid piping.

The connection between sub-sea installation and surface production platform for the extraction of oil or gas, electrical connection and hydraulic control is made by marine risers, of which there are three different types; platform risers, rigid risers and flexible risers. The term 'riser' describes a tubular between sea-bed and surface, installed for the transport of fluids in either direction. Risers are required for several purposes including production of hydrocarbons from well to platform, export of processed hydrocarbons from platform to pipeline, and gas or water injection for the starting or enhancement of production. Service risers provide water for testing and cleaning, and control lines permit hydraulic control of sub-sea installations.

Platform risers are vertical steel pipes connecting seabed flowlines to the surface, clamped to the steelwork of a jacket platform and possibly carrying bundles of other risers and umbilicals. Secondly, a tubular steel pipe suspended freely between surface and sea-bed constitutes a rigid riser, such as for example, the original drilling pipe. It will be tensioned to confer stability on account of its high slenderness ratio, and because of its rigidity the surface vessel needs to be prevented from making large excursions from its position directly above the sea-bed installation.

The flexible riser is the most recently introduced kind of riser, consisting of a length of flexible pipe suspended freely between sea-bed and surface facilities, often arranged in bundles with other risers and umbilicals. Thus much larger horizontal deflections of the surface platform can be accommodated than with rigid risers, the pipe being designed to allow significant flexure. Such pipe is, as already mentioned, of composite construction including helical steel strip or wire reinforcement layers and cylindrical

polymer barrier layers for fluid impermeability, the result being compliant while axially and radially strong. Additional polymer layers between helical layers reduce wear as layers continually slip relative to eachother. This is no longer a static application of flexible pipe, and it is now exposed to greater loads with a greater degree of variation. Due to its flexibility there are several different configurations in use which provide optimum design solutions for each situation.

1.3 FLEXIBLE PIPE

1.3.1 Some Early History

Flexible pipe was first used for seabed transportation of fluids in 1944, when the Allied forces in northern France were supplied by up to twenty 3" I.D. pipes laid across the English Channel, at an operating pressure of about 1,200 psi. Called PLUTO, for Pipe Line Under The Ocean, the first laying test for this had been carried out across the Bristol Channel in 1942. The type of pipe used had already been developed for land use through hills in Iran, by A.C. Hartley, the Chief Engineer of Anglo-Iranian Oil. 'Hais' pipe (short for Hartley-Anglo-Iranian-Siemens) consisted of a lead pipe covered by insulation, reinforced by steel wire and coated in tar and yarn. It was manufactured remotely and could be laid in long lengths simply by unreeling from a large drum. In the case of PLUTO, each floating reel provided 70 miles of pipe and weighed 1600 tons.

Modern flexible pipe, consisting of separate steel and thermoplastic layers and manufactured in long continuous lengths, was first introduced to the offshore industry in 1972. It had previously been developed by the French Institute of Petroleum (I.F.P.) for use by the drilling industry, but was then marketed to the offshore oil and gas industry by Coflexip for use in static flowline applications, beginning with Elf Aquitaine in the Emeraude and Grondin fields in the Congo. The choice of flexible pipe for static application was due to easier laying and retrieval procedures than those required for rigid pipe. For the next ten years the market grew as gradual increases in pipe length and diameter were made together with increases in operating depth and pressure. By the end of 1982, Coflexip had installed a 12" I.D. line off Spain, set a new depth record

of 230m with flowlines for Shell in Tunisia, with the ability to reach 300m depth, and had developed flexible pipe for dynamic application. By 1991, 2300km of flexible pipe had been installed world-wide with service in excess of 15 years in some cases and at depths of up to 1000m.

1.3.2 Flexible Pipe Composition.

There are two categories of flexible pipe - bonded and unbonded. Bonded pipe consists of helically wound steel strip layers embedded in elastomeric compound layers, all bonded together by a vulcanisation process involving application of heat and pressure. The steel strip layers give axial, bending, torsional and burst strength to the pipe while the elastomeric layers provide a barrier against permeability. The helical steel strip geometry combined with the low elastic moduli of the elastomer layers gives a fair degree of flexibility to the overall pipe.

However, today unbonded pipes are far more widely used than bonded. Unbonded flexible pipe consists of polymer sheaths acting as barriers together with steel strip layers in helical configuration to provide strength or protection, but without the layers being bonded together. This allows them to slip relative to each other. The result is a pipe which is both radially and axially strong while remaining flexible. As it is this kind of flexible pipe that this study concerns, any reference from now on to flexible pipe implies unbonded flexible pipe unless specifically mentioned otherwise. An example cut-away diagram of the unbonded structure is shown in Figure 1.1

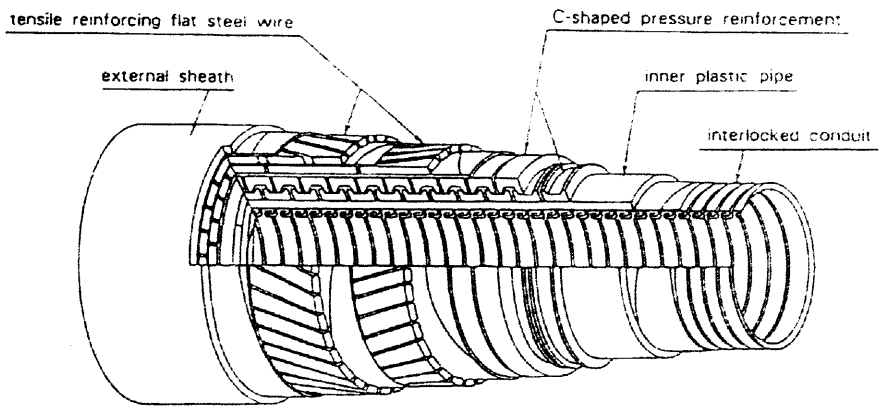

Figure 1.1 Basic structure of flexible pipe (Fuku, Ishii).

The following lists the component layers of flexible pipe and explains the purpose of each, beginning on the inside and working outwards. A description of the materials employed is given in Section 1.3.3.

Carcass

A steel strip layer which interlocks, hence having a small helical angle. If required, it protects the barrier layer from abrasion and collapse under external pressure loads, and also helps to prevent blistering of the barrier should permeated gases try to escape after a rapid decompression of the pipe. It sees external hydrostatic pressure, although on account of inevitable pressure paths between each turn it is not impermeable and does not see any pressure differential from internal fluid pressure. Pipes with a carcass are termed Rough Bore, as opposed to those with an exposed inner barrier which are called Smooth Bore. An example cross-section is shown in Figure 1.2.

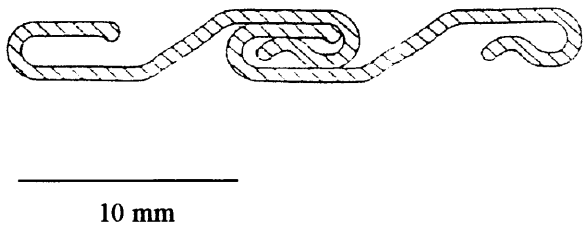

Figure 1.2 Carcass cross-section showing two turns (Wellstream).

Barrier / Inner Sheath

The polymer layer which carries the pipe contents – the actual pipe which is protected and supported by all the other layers. Barrier layers provide the pipe with impermeability but the inner barrier requires careful protection against high pipe internal pressure. The impermeability of the inner barrier is not generally perfect as high temperature (c. 100°C) high pressure (c. 50MPa) gases can gradually pass through. Care has to be taken at the end fitting to ensure a lasting seal and to prevent extrusion of the polymer into gaps.

Interlocking Spiral – Pressure Armour

A continuous interlocking steel strip wound around the barrier layer to give it radial (pressure) support. This requires a continuous surface with minimal gaps so that there is no risk of polymer extrusion due to high pressure while maintaining pipe flexibility. The strip profile has to withstand stresses due to pressure and from neighbouring turns and is also subjected to wear at the interlocking face. This layer may consist of two separate strips interlocking with each other, as shown in Figure 1.3.

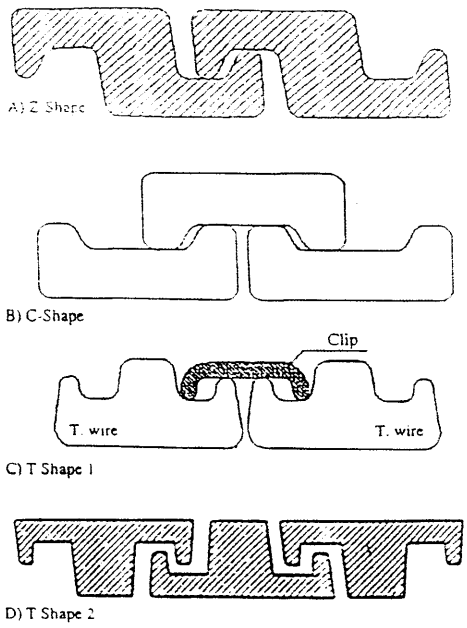

Figure 1.3 Pressure armour strip sections (Marinflex, 1995).

Tensile Armour Wires

Two or four layers of contra-wound helical steel strips with a much larger helix angle (in the region of 45 to 55 degrees) than the interlocking spiral. These give axial tensile strength to the pipe. The even number of contra-wound layers reduces the torsional effects of the axial loading of the helices. In flexible pipe, tensile armour is of a flat, rectangular cross section (Figure 1.4). The pipe owes its flexibility to the occurrence of slip between armour wires and their surrounding layers, and a distinguishing feature for dynamic application is that thin polymer sheaths or anti-friction ribbon will be included between steel strip layers to encourage slip, contolling interlayer friction and protecting

against wear. Where free from any restraint, wire axial slip reduces axial strain thus reducing pipe stiffness. Wire transverse slip will also reduce bending stiffness by reducing wire transverse curvature, the extent of such slip being dependent on wire cross section and wire tension. Rotational slip is not possible due to the rectangular cross section. Such slip is only allowed by a circular cross section as employed in umbilicals. It is clear that at the end fitting no slip of any kind is allowed, leading to stress concentrations where this affects the strip behaviour.

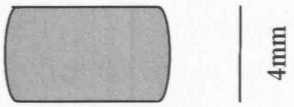

Figure 1.4 Tensile armour example cross-section.

Tapes and Yarns

Yarns and woven fabric tapes are also widely used for interlayer cushioning, helping against wear between layers and against extrusion of polymer layers into steel armour layers. They also assist in the manufacturing process, maintaining structural integrity during assembly.

External Sheath

This polymer layer is the finished surface of the pipe giving protection during installation and also from the external environment, preventing the ingress of sea water. Together with the inner barrier, the external sheath forms an annulus inside which reside the steel strip layers. Permeated gases from the interior, which may well include CO_2, H_2S and HCl, can build up in this annulus, creating a corrosive atmosphere and also causing a risk of collapse of the inner barrier. Ventilation is usually provided at the end fitting, although ingress of water must also be guarded against.

Some typical pipe weights, pressure ratings and dimensions are given in Table 1.1 overleaf.

Nominal Bore (inches)	2	4	6	8	10	12	16
Maximum Pressure (bar)	690	690	517	345	310	172	52
Weight Empty in Air (kg/m)	31.0	77.2	109.4	148.5	208	158	-
External Diameter (mm)	108	178	229	292	353	388	505

Table 1.1 Typical flexible pipe characteristics (Patel, Witz and Tan, 1993).

1.3.3 Flexible Pipe Materials

Polymers

Polymers in flexible pipes must be capable of sustaining high long term static and dynamic strains, while exhibiting good long term chemical resistance, internal and external fluid tightness, low permeability and low swelling. They must also be compatible with the high temperature products being transported, and show good wear resistance. Where there is no protection, resistance to abrasion and blistering is also important. As the mechanical properties of polymers are generally time and temperature dependent, creep and stress relaxation must be fully characterized and understood, particularly in the region of any sealing forces.

Most thermoplastics will satisfy the strain requirements, and the technique of extrusion for the manufacture of barrier layers will provide a porous-free sheath. All thermoplastics are susceptible to vapour permeability and thus also to a risk of blistering on sudden decompression. Resistance to blistering decreases as temperature increases. Degradation while in use, or ageing, is similarly temperature dependent. It may take the form of deplasticisation, oxidation of the plastic or be due to hydrolysis.

Polymers used for barrier layers consist of High Density Polyethylene (HDPE), Polyamides PA11 and PA12 (Nylons) and Polyvinylidene Fluoride (PVDF or Coflon). PA11 has been chosen as most suitable by Coflexip for work up to 100°C yielding a possible 10 year design life. Rilsan, a specially designed grade of Nylon 11, is more

flexible and has good resistance to blistering. HDPE displays excellent durability in the presence of water or acid, but has a relatively low melting point. Thus HDPE is suitable for lower temperature use (< 50°C) and is less vulnerable to ageing from hydrolysis. PVDF is safe to use at temperatures up to 130°C, or even higher for short term use, and is thus used where the temperature limit for Rilsan is exceeded. Regarding extrusion, PA11 has been shown to be more suitable for use than PVDF. A particular design solution was to use PVDF on account of its superior chemical and heat resistance properties coated with a layer of PA11 to minimize polymer extrusion.

Steels

Steels used for radial and axial strength layers are low alloy carbon steels. These steels exhibit mechanical properties superior to plain carbon steels due to additions of elements such as nickel, chromium, and molybdenum.

Examples of stainless steels for carcassing are AISI 304/304L, 316/316L and 409/430. Austenitic stainless steel 304 and its low carbon version 304L offer a good combination of strength and corrosion resistance, and are easy to form. 316 is an austenitic stainless steel which has an increased molybdenum content to improve its resistance to corrosion when compared to other 300 series alloys. 409 is an alloy designed principally for car exhausts, combining good elevated temperature corrosion resistance with medium strength, good formability and low overall cost. 430 is a basic ferritic non-heat treatable stainless steel. Its strengths include ductility, formability and good corrosion and oxidation resistance.

1.4 FLEXIBLE RISER DEVELOPMENT

The first flexible risers were installed in the Campos Basin off Brazil in 1978, being simple catenary risers and operating from up to 100m water depth. These include the Enchova field production riser bundle with the Penrod-72 semi-submersible, and several other jack-up based production systems. In 1979 flexible risers were used for oil production off Spain. These were supplied by Coflexip, and throughout the 1980s

Coflexip has supplied risers to Brazil, the United Kingdom, the Middle East, Norway, Holland, the Gulf of Mexico, Australia and the Mediterranean. As smaller, deepwater fields are being exploited, the interest in flexible risers has increased, especially as floating production systems using flexible risers are an attractive form of surface installation for such oil and gas recovery. The greater compliance and relatively low installation and operating costs of flexible risers combine with the obvious advantage of the possibility of relocation afforded by semisubmersibles.

By 1986 the Balmoral field in the North Sea was employing four Steep S flexible riser bundles operating from a depth of 145m up to the support semisubmersible, riser diameters varying between 4"and 10". Also a 165m length of 5" inner diameter production riser was in use in the Steep Wave configuration for production from 105m depth to the Norsk Hydro Petrojarl 1 monohull in the Norwegian Oseberg field. Naturally, operational depth records were repeatedly broken at the time. In 1989 Coflexip installed 8" and 10" risers in 540m on the Jolliet Gulf of Mexico Conoco TLWP, and 2 years later set a 750m depth record on Marlim off Brazil.

Another manufacturer, Wellstream, entered the market in 1989 and has since been very active. In 1991 they delivered 2.5" and 4" risers for Petrobras Marlim rated for 1000m water depth at 3000psi. In 1992 Wellstream installed an 18km 5.3" gas line in Greece, while their 5" risers installed in the same year for Alcorn International in the West Linapacan field in the Philippines at 350m depth completed the deepest subsea/floating production system outside Brazil at the time.

Pirelli decided not to continue their small flowline program begun in the early eighties while Furukawa, another cable manufacturer which started with flexibles at the same time, supplying Conoco Dubai in 1984, continued and passed Shell's tests for static and dynamic applications. They delivered flexible pipe to Petrobras off Brazil in 1992 for 500m water depth application.

With the continued increase in depth of oil field development, flexible pipe technology is having to overcome the problems created. The considered limit for flexible riser depth of 1000m has already been reached off Brazil, and the current depth record is

1900m, achieved by Coflexip Stena Offshore at the Roncador field, also in the Campos Basin, with a 7.5" 10,000psi water injection riser. On account of the weight of a 2000m riser, new risers from lighter materials such as aluminium alloys and composite materials are being considered.

1.4.1 Configurations of Flexible Risers

With such a range of water depths and other environmental conditions, it has become necessary to develop several different types of installation configuration in order to reduce riser stresses and stress variations from riser excursions. The general configurations that have been employed to date are described in the following.

Simple Catenary

The riser is suspended freely from the surface vessel, with a length lying on the sea bed before reaching the sea bed facility (see Figure 1.5), a configuration which matches that already encountered in pipelaying by the 'J-lay' method. The slack region on the sea bed accommodates some change in profile due to vessel movement or environmental change without subjecting the sea-bed connection to unnecessary loading. Two regions of maximum bending are at the top end connection and in the touch-down region, where the catenary profile is modified by the riser stiffness. Some form of bending control will be required at the top. This is a configuration that has been widely used, but in larger water depths higher bottom end curvature and higher top end tension make it unsuitable.

Steep S

Suitable for greater depths, this geometry consists of two sections of flexible pipe with a buoyancy module in between (Figure 1.5). This configuration can be a help if the sea bed is congested with equipment. The bottom pipe rises vertically to the buoy while the connection to the surface vessel is allowed to sag. The buoy may take one of three forms. Firstly it may be tethered to the sea-bed and have a pipe support arch. Secondly, it may be supported by the lower section and have a conduit through it

joining the top and bottom pipes together. This usually needs bend restrictors at the joints. Finally the buoy may be tethered by a combination of support lines and transport pipes, the support lines reducing tension in the lower section. The buoy should be located at sufficient depth to avoid wave induced excitation of the lower vertical section. Bending control will also be required at the sea bed connection.

Lazy S

Similar to the Steep S, but with a simple catenary for the lower section; this configuration is used where large horizontal offsets between sea-bed and surface installations are required. It eliminates the top tension difficulties for catenaries in deep water and the buoy is better balanced horizontally by the lower catenary than in the Steep S case, thus reducing buoy size.

Steep Wave and Lazy Wave

These are natural progressions of the Steep S and Lazy S configurations, providing buoyancy distributed along a length of the pipe to create a positively buoyant pipe arch, thus eliminating the time and expense caused by sub-sea installation. The drawback with these is in their dynamic performance; the riser has greater freedom to move, leading to more fatigue and wear, and greater influence of upper section movement on the lower part of the pipe. In the case of the Steep Wave, buoyancy positioned too high on the riser can lead to wave induced motions while buoyancy placed too low creates a large sag bend leading to higher excitation. For the Lazy Wave configuration, vessel induced motions can directly affect the portion of the pipe lying on the sea-bed, causing lift-off.

Pliant Wave

This is simply a hybrid development retaining the advantages of a lazy wave installation but with a number of tethers to maintain the dynamic performance advantages of a steep wave profile.

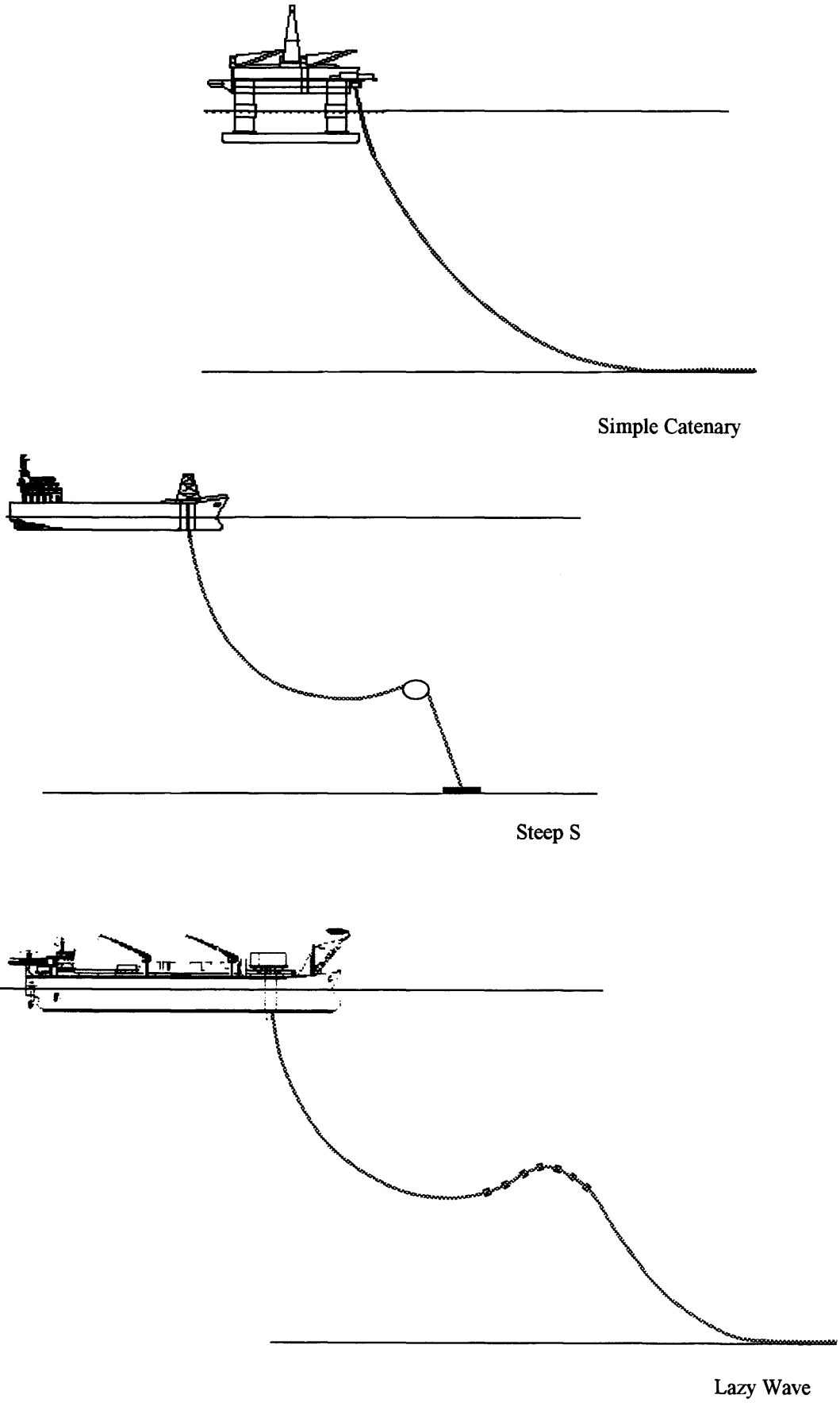

Figure 1.5 Some flexible riser configurations (Technip, SUT).

1.5 END FITTINGS

1.5.1 Basic End Fitting Composition

The end fitting provides all the interfaces between the end connector and each layer of the flexible pipe. The end fitting as a whole therefore has a simple rigid steel pipe at one end and a multi-layered flexible pipe at the other consisting of the components already listed. Figure 1.6 is a section through an example 6" bore end fitting showing its component parts. Completion of the assembly shown is as follows.

The inner body is welded to a flange assembly at its top end. Its base presents an area for the attachment of sealing and retaining rings, while its conical shape allows for retention of the armour wires by epoxy. There is a threaded area to receive the outer jacket forming one end of the fitting enclosure.

The inner barrier layer is gripped in order to form a seal between the pipe end and the inner body and to prevent it from being pulled out of the end fitting. In this example, a steel sleeve is fitted inside the end of the layer against which the polymer is pinched by a steel seal ring on the outside. This ring is sloped on its outside so as to be forced against the pipe as it is held in place by a retaining collar bolted to the inner body. The seal is thus effected by pressure between the seal ring and the barrier, and also by an O-ring seal positioned between the inner body and retaining collar.

The interlocking spiral pressure armour layer is on account of its completeness finished off flat, allowing a butt joint against the back of the inner seal collar. Care is taken to avoid possible extrusion of the barrier layer into a gap at this point, any resultant gap being filled with epoxy. In this example the pressure armour then provides the central support for a second polymer gripping arrangement to hold an anti-wear layer between it and the first tensile armour layer.

The layers of armour wire are axially restrained as they provide the axial strength of the pipe. In this case the last 400mm of armour wires are opened out and bent over the

conical inner body in the base of which are the inner gripping and sealing arrangements. They are banded and set in place by a surrounding epoxy.

The jacket is threaded to the inner body at one end and surrounds the fitting. The other end receives the outer collar completing the external seal arrangement which is similar to that for the inner barrier. Holes are provided for injection of epoxy and expulsion of displaced air which are then plugged, thus completing assembly.

In addition, vents may be incorporated to allow ventilation of any annulus between the pipe's barrier layers.

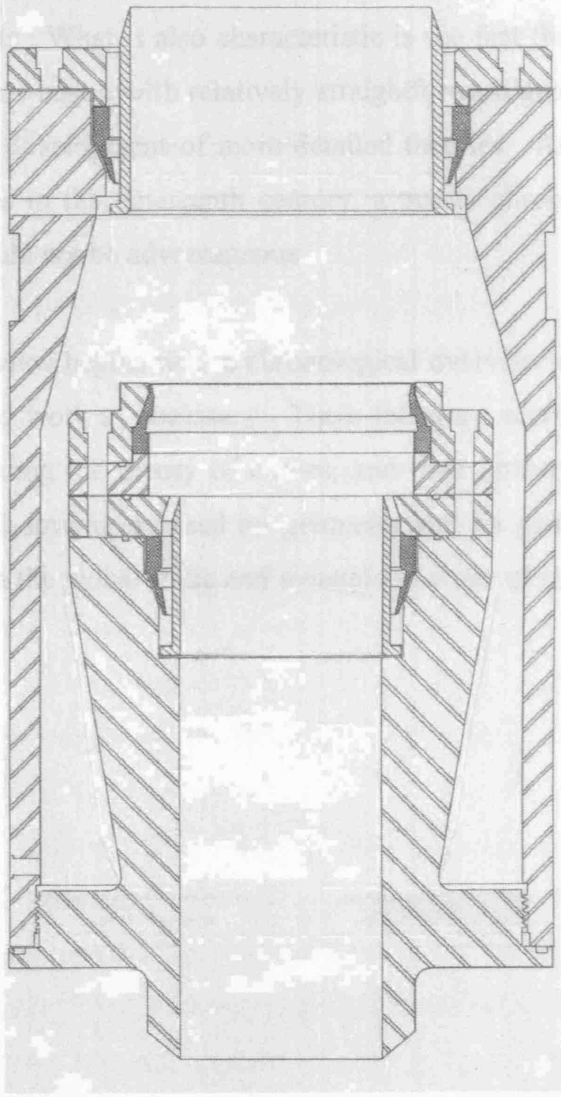

Figure 1.6 Example end fitting section showing components (Wellstream).

2 LITERATURE REVIEW

2.1 INTRODUCTION

The aim of this review is to prepare for an analysis of flexible pipe tensile armour in the region of an end fitting. It covers material on both structural analysis and global dynamic analysis.

Although very little analysis has been carried out on end fittings, significant results exist in the literature from the free field analysis of flexible pipe and similar structures such as wire rope and armoured cables. Flexible pipe analysis naturally draws from previous works on these similar structures, all being characterized by the inclusion of helical components. What is also characteristic is the fact that the structural analysis of each of these has begun with relatively straightforward geometrical considerations, before the use or development of more detailed theories. As the basis for the more complex work lies in the nineteenth century, a purely chronological presentation of relevant work would not be advantageous.

As a result the review begins with a chronological overview of flexible pipe analysis, introducing related work as necessary. There follows a section covering background information regarding the theory of curves, and then further detail on the structural analysis of helical structures based on geometry and on general thin rod theory. A review of work on the global static and dynamic analysis of cables and flexible pipe is also included.

2.2 PREVIOUS WORK

Unbonded flexible pipe is not the first structure to make use of helically wound wires, and on their introduction in the 1970s there already existed ongoing analysis of related structures such as wire rope and armoured electrical cables. Hruska (1951, 52, 53) carries out an elementary analysis of wire rope under axial loading to find the resulting axial forces in individual wires, radial inter-wire forces and rope tangential forces. The analysis is based on geometry which remains helical after stretch and rotation of the rope. Rotation of wire rope due to an imbalance in tangential forces is shown to be able to cause significant increases in wire stresses.

An analysis of cable bending is carried out by Lutchansky (1969). It is based on the interaction between a helical armour wire and the supporting cylindrical core as it is bent into a toroid. The wire is considered to slide along the initial path (axial slip) only, and not laterally from it, as it is deformed due to the applied bending. The wire strain depends on an interaction shear force between it and the path, the resulting axial strain being the only strain considered. A fixed boundary condition is used which means that an increase in stress due to end restraint can be examined, and a significant result is that maximum stresses are found at a neutral axis position rather than an extreme fibre position.

Raoof and Hobbs (1984) use a similar model to Lutchansky's for an analysis of armour wire stresses and slip for comparison with multi-layer cable bending tests under tension. Free field analysis is carried out by treating armour wire layers as orthotropic sheets, with shear compliances derived using a Hertzian contact analysis, thereby covering the entire range from zero friction to infinite friction. The results show a 13% change in cable bending stiffness over this range. Nearer terminations or clamps, the cable is treated as a solid core with an outer layer of wires, with shear interaction calculated using an oblique contact Hertzian analysis, reflecting a cross-laid or contra-wound construction. As the shear interaction force is found to be much larger than that chosen by Lutchansky, greatest stress is predicted at an extreme fibre position rather than at the neutral axis. However, maximum slip would occur in a neutral axis position near the clamp, which is exactly where the first cable fractures

are observed in the tests. Hence cable failure is taken to be due to internal fretting near the termination.

Lanteigne (1985) derives a stiffness matrix for cable, consisting of several helical wire layers wrapped around a straight wire core, to relate forces and displacements. Terms are derived by independent consideration of axial strain in constituent helical wires under cable tension, torsion and constant curvature bending. Variation of the total strain energy of the cable and external potential energy gives axial, torsional and flexural rigidities and coefficients for coupled tension-torsion, tension-bending and torsion-bending. The flexural rigidity is affected by slip, dependent on friction between layers, and in the limit reduces to the sum of the flexural rigidities of the individual wires. Interwire friction between wires in the same layer is disregarded, as radial forces render interlayer frictional forces much more significant. Good correlation is observed with Costello, summarized later (Costello 1990), for frictionless bending, a 2% difference being attributed to his inclusion of Poisson's ratio.

Jolicoeur and Cardou (1991) collect and compare several load-deformation relations to axial load test results for a single strand cable. All relations assume a helical geometry after deformation, and no end effects are considered. The most accurate relations allow for axial, bending and torsional stiffness of the outer wires and axial and torsional stiffnesses of the core, and include variation in core radius due to compression from the outer wires. Inclusion of Poisson's ratio has little effect on the results.

With the growing application of flexible pipe offshore for flowlines and risers, the OTC Paper by D'Oliveira et al (1985) addresses the need for a better understanding of flexible pipe behaviour, by using analytical methods to assess mechanical performance. In it they examine flexible pipe strength and stiffness characteristics and flexible riser static configurations. Expressions for pipe axial, torsional and bending stiffnesses and burst and collapse strength are given by simple addition of contributions from cylindrical layers and helical wires, with radial compatibility but otherwise acting independently. For static configuration, the riser is modelled by a catenary and a beam tie with zero moment at the join. The beam tie accounts for a

boundary layer near the termination where its orientation and the pipe bending stiffness render a catenary solution void.

Rather than assessing pipe global behaviour in a dynamic environment, Feret and Bournazel (1987) examine the behaviour of the internal structure. The paper shows calculation of free-field stresses and contact pressures for layers of flexible pipe under axi-symmetric loads. A simplified solution is found by taking contributions from helical strip layers only, assuming helical form after deformation, the same change in radius for each layer and considering strip axial stress only. The stresses obtained agree well with test results.

Also in the same paper and in contrast to previous analyses, the authors suggest that, under bending and far from any end restraint, flexible pipe tensile armour will slip towards the new geodesic curve on the supporting surface. A slip vector from helix to toroid geodesic is calculated with axial slip and transverse slip components. Changes in strip twist and curvature accompanying this slip will lead to a bending stiffness greater than that of an equivalent free spring. Friction will reduce slip, inducing strip tension, compression and transverse curvature. Also highlighted are test results showing that flexible pipe bending is hysteretic, with various bending moment-curvature relationships dependent on tensile armour slip and also on the closing of gaps between individual wires.

Baradaran Seyed (1989) presents improved equations for the static profiles of flexible risers. These are catenary equations with modified tension and weight terms to account for the effects of pressure and fluid flow. Simplified versions can be solved to give first approximations to riser configurations, although of course no end effects are included. Riser dynamic response is approximated by a modal decomposition technique.

Also in regard to pipe global analysis, Sødahl (1991) addresses flexible riser bend-stiffener design, whereby curvature is controlled in the approach to the riser termination. An iterative method is given which allows graphs of design pipe tension and design curvature as functions of tension angle and a dimensionless stiffness parameter.

Witz and Tan (1992, i) derive a model to predict the free-field response of flexible pipe to axial-torsional loading. The pipe is considered as an assembly of cylindrical layers and helical strip layers, all subjected to the same change in length, twist per unit length and radius, and with compatible inter-layer pressures. For the first time in flexible pipe analysis, the helical strip layer force and moment equations involve Love's non-linear equations, thereby including strip bending and twisting effects. This requires solution by numerical means. The results however show very linear axial and torsional stiffness relations which agree well with test results.

A second model is derived (1992, ii) to examine flexible pipe free-field behaviour under flexure. Strain energy contributions per unit length from each layer are differentiated with respect to the applied curvature giving the pipe bending moment-curvature relation. Steel strip layer energy is dependent on axial slip relative to the supporting surface, being dominated by axial strain in the absence of slip but with only contributions from changes in strip twist and curvature after full slip. Therefore the relation is non-linear, consistent with the test results shown by Feret and Bournazel.

The use of Love's equations represents a shift in the analysis from purely geometrical to analysis involving equilibrium equations. This mirrors a similar development in wire rope and cable analysis. Love's treatise on elasticity (Love, 1944, originally published 1893) includes a general theory on the bending and twisting of thin rods, based on linear elasticity and small local deformation. Six non-linear equations are derived for force and moment equilibrium involving twist and curvature of the rod. These equations were given previously by Kirchoff in 1859. Euler-Bernoulli 'approximate theory' constitutive relations are shown to yield good approximations to rod stress couples 'at a distance from any place of loading or support'. Love concludes that the most important strains in a bent and twisted rod are extension due to curvature, shear due to torsion and relative displacement of cross-section elements parallel to the plane of the section. The equations are used to study forms of the elastica (plane curve, zero twist), and for an analysis of rods held in helical form by terminal forces and couples, following results from St. Venant (1843). Solutions in these cases are obtainable as the equations can be considerably simplified.

Hay (1942) develops a general theory for thin rods with uniform cross sections and loaded only at the ends, where strains are described in terms of metric tensor components. All quantities are expanded in power series in the ratio of rod width to rod length, a small dimensionless parameter, allowing approximations to be introduced in a more systematic way than by Love. A particular case of the first approximation solution, for small strain and finite bending, yields the appropriate form of Love's non-linear equations.

Ericksen and Truesdell (1958) present a complete theory of stress and strain in a rod. A general theory including strain of displacement and strain of orientation is given first, the mathematics of which is particularly suitable for the description of stress and strain in a thin rod. An example is given which coincides with Hay's work mentioned above.

Ramsey (1988) derives a new theory of thin rods for application to helical wires in cables, using kinematic variables which are absent from Love's theory. Expressions are derived linking rod strains to centre-line twist and curvature, although solutions to case studies are obtained using a linearized form of Love's equations. Axial loading from one helical form to another is examined, as are bending with infinite friction and zero friction. The infinite friction solution suggests that circular wires will rotate with respect to the supporting surface and will be subject to fretting damage.

Costello (1990) develops a theory of wire rope using Love's equilibrium equations and uses it to analyse a single strand consisting of wires wrapped helically around a core. Results are obtained by assuming wire final twist and curvature directly from the geometry of curves. For axi-symmetric loading, wire forces and moments are obtained for prescribed rope strain, while for bending outer wires are considered to behave like springs under pure bending and an expression for bending stiffness is found which is the same as D'Oliveira's. For a strand under tension bent over a sheave these two results are superimposed. Costello also shows that external frictional forces and moments, applied to individual wires through contact with the core, have little effect on his solutions.

Ramsey continues his cable analysis to study the effects of inter wire friction when a cable is subjected to uniform extension and twisting (Ramsey 1990). Wire contact between wires in the same layer is considered as well as contact between different layers. The only resulting friction forces form couples opposing changes in the lay angles of the wires.

Ramsey (1991) also extends his analysis to look at the effect of end fittings or clamps on helical wires in cables. The case of axi-symmetric loading in the absence of friction is examined, and a boundary layer effect is observed in wire stresses, although the increases are small. In contrast, the resulting relative motion between adjacent layers is more significant. This extends all along the cable, although in reality friction would cause this also to be a boundary layer effect.

The development of finite element analysis methods has allowed numerical analyses of flexible pipe internal structure. Saevik (1993) develops a curved beam element for finite element modelling of a flexible pipe tensile armour strip. The strip has a rectangular cross-section and is constrained to lie flat on the supporting surface as it slides from the strained original curve towards equilibrium. Bending results with no end fitting restraint and no friction compare well with the Feret and Bournazel geodesic slip calculations. Results for bending including end effects are also given but are only compared with constant curvature geodesic slip analytical expressions. The effects of friction on reducing transverse slip are shown to be significant, but again only a simple analytical model is provided for comparison. Stresses from the model are also compared with results from pipe tension and bending tests. Both test and model results show typical friction effects on axial slip, leaving residual regional variations in axial stresses.

McIver (1995) derives a highly detailed stiffness matrix for flexible pipe section strain energy and uses an iterative technique to minimize the resulting energy functional. Helical strip layer contributions are for wires of constant but arbitrary cross section and include energy per unit length from axial, torsional, bending and transverse sectional strains and thermal potential. The model is for axially uniform pipe conditions and so no end effects are accounted for. Results allow wire stresses, deformations and relative displacements to be calculated and pipe constitutive

relations to be examined. They suggest piecewise linear relations, with a hysteretic bending moment – curvature relation and a dependence of the axial stiffness on applied torque, highlighting a directionality characteristic of flexible pipe. The author points out that although the results seem simple, the high degree of detail involved is necessary for accurate fatigue and wear calculations.

Continuing with a geometric approach, Out and von Morgen (1997) consider the limit of tendon slip on a toroid to be given by the geodesic curve, and derive an approximate expression for it from which strip axial and transverse slip can be calculated. Values of slip are calculated for strips of only one turn in length, and maximum slip for a strip restrained at the neutral axis is found to be double that for one restrained on the inside of the curvature. Changes in strip curvature are also compared for geodesic and original curves, the geodesic having the larger overall change in curvature. This suggests that the strip position will therefore be somewhere between these two limiting curves.

McIver (1998) focuses on flexible pipe helical armour wire slip, considering wires of rectangular or circular cross-section wound on a cylinder bent with constant curvature. A stiffness matrix is developed for wire axial and transverse displacement and rotation, with wire stresses due to axial strain, bending, twist and also pre-tension. The wire is considered to be stressed as if under infinite friction and then allowed to slip. A continuous representation is used for the regional friction force which varies between static and dynamic values. Results suggest that rectangular wires retain more stress after slip than circular wires, and that low levels of friction are enough to supress lateral slip.

Saevik (1998) presents a second finite element method for predicting stresses in tensile armour. This method uses sandwich beam theory to find tendon layer potential energy for the model. Each tendon interacts with the core via a virtual shear layer, and displacement is confined to the original path in the same way as in Lutchansky's model. Results for plane section bending (infinite friction) and constant curvature without friction compare very well with analytical results for these cases, and comparison with a 15 inch riser bending test also shows very good correlation.

This completes the overview of previous work from which the material in the following sections on pipe structural analysis, wire equilibrium and pipe global analysis is drawn. Before expanding on these subjects, Section 2.3 outlines some important details with regard to the use of curves in the description of wire behaviour.

2.3 CURVES AND THIN RODS

In analysing thin rods which are supported on or between curved surfaces, it is not unnatural to talk of curves when describing aspects of the rods. It is important at this stage to set out some definitions regarding curves, and also to make clear the distinction between the curve which may be used to describe the central line of a rod and the material cross-section of the rod itself.

2.3.1 Curves

Arc Length, Curvature and Torsion

In three dimensional Euclidean space a curve is defined completely, apart from its actual position, by three invariants, namely arc length s, curvature κ_0 and torsion τ_0 (Ramsey, 1988). Put another way, it is a line of some length which may have curvature and torsion. The Seret-Frenet equations as set out below show how these invariants govern the curve (Lipschutz, 1969, p. 80).

$$\begin{aligned} \mathbf{t}' &= \kappa_0 \mathbf{n} \\ \mathbf{n}' &= -\kappa_0 \mathbf{t} + \tau_0 \mathbf{b} \\ \mathbf{b}' &= -\tau_0 \mathbf{n} \end{aligned} \tag{2.1}$$

or, in matrix form,

$$\begin{pmatrix} \dfrac{d\mathbf{t}}{ds} \\ \dfrac{d\mathbf{n}}{ds} \\ \dfrac{d\mathbf{b}}{ds} \end{pmatrix} = \begin{pmatrix} 0 & \kappa_0 & 0 \\ -\kappa_0 & 0 & \tau_0 \\ 0 & -\tau_0 & 0 \end{pmatrix} \begin{pmatrix} \mathbf{t} \\ \mathbf{n} \\ \mathbf{b} \end{pmatrix} \tag{2.2}$$

These relate the rates of change of the vectors tangent **t**, normal **n** and binormal **b** of the curve **x**(s) to its curvature $\kappa_0(s)$ and torsion $\tau_0(s)$. The normal, or principal normal, gives the direction in which the curve is turning. The tangent is defined as the limiting position of a line passing through two neighbouring points on a curve as they approach a single point. The binormal completes a right handed orthonormal triplet

with the other two vectors. Torsion is referred to as tortuosity by some authors and is also called the second curvature.

$$\mathbf{t}(s) = \mathbf{x}'(s) = \frac{d\mathbf{x}}{ds} \qquad \mathbf{n}(s) = \frac{1}{\kappa_0}\mathbf{t}'(s) = \frac{1}{\kappa_0}\mathbf{x}''(s) \qquad \mathbf{b}(s) = \mathbf{t}(s) \times \mathbf{n}(s) \tag{2.3}$$

Torsion and curvature are measures of change in orientation, curvature indicating the rate at which the curve is turning, torsion being a measure of the change in direction of curvature. They are in radians per unit length, therefore with units m^{-1}, as indicated by the equations. It must be remembered that the curvature and torsion are functions of a natural co-ordinate such as arc length. This is not a Lagrangian co-ordinate, and therefore does not take any account of strain.

The Seret-Frenet equations show that the curvature and torsion represent rotations about the binormal and tangent vectors respectively. They are components of the total curvature, or third curvature, which is the full change in orientation per unit length of the curve.

Helices

A circumferential line on a cylinder perpendicular to its axis is a circle, a plane curve with no torsion, with curvature equal to the reciprocal of the radius, while an axial line parallel to its axis is straight, without curvature or torsion. A line at a constant angle to each of these is a helix, and a unit length along this helix corresponds to a shorter length around the circumference and hence a smaller change in orientation. This total curvature is about an axis parallel to the cylinder axis and can be represented by a vector drawn so that the change in orientation corresponds to a clockwise rotation about it when viewed from start to finish (see Figure 2.1). The components of this vector in the helix binormal and tangential directions give respectively the curvature and torsion of the helix.

$$\left.\begin{matrix}\kappa_0 \\ \tau_0\end{matrix}\right\} = \frac{1}{R}\cos\alpha_0 \left\{\begin{matrix}\cos\alpha_0 \\ \sin\alpha_0\end{matrix}\right. \tag{2.4}$$

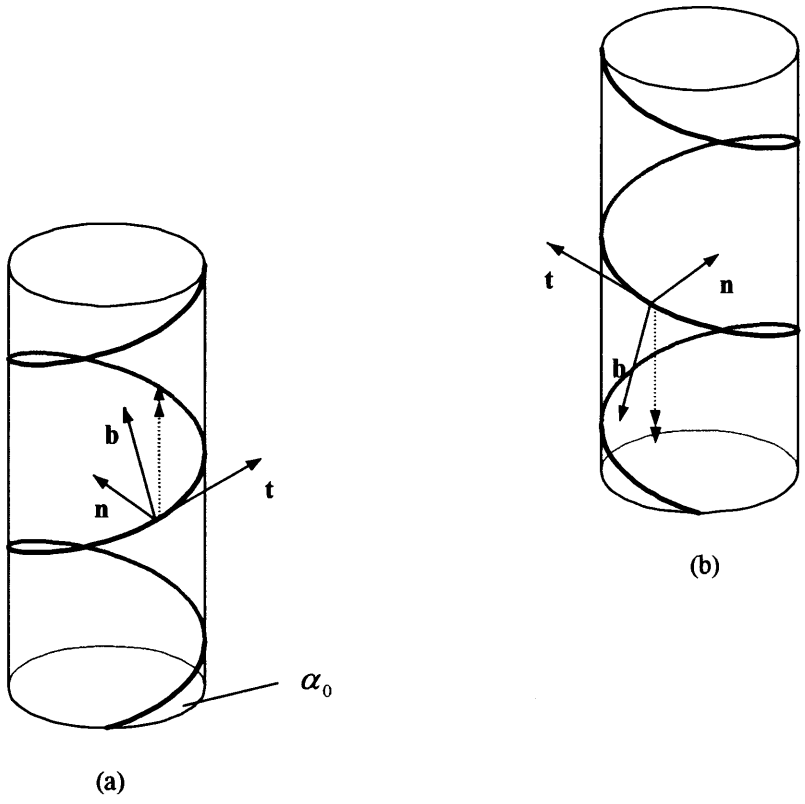

Figure 2.1 Right-hand (a) and left-hand (b) helices, showing tangent, normal and binormal vectors, and direction of positive curvature for each. Also shown is helical angle α_0. A left-hand helix is a right-hand helix with helical angle between $\pi/2$ and π.

Strained Helices

If the above mentioned cylinder is bent into a toroid, a helical line on the cylinder surface will experience axial strain and changes in torsion and curvature, and will therefore change into a completely different curve. Assuming plane section bending of the cylinder, some conclusions regarding this strained helix can be written down as follows. The angle which the curve makes with the bent cylinder axis is no longer constant owing to changing axial strain of the surface. The initial curvature and torsion of the helix are altered by this variation in angle, and are also augmented by the applied curvature of the toroid.

Loxodromes

A loxodrome is an entirely different curve to a strained helix but previous flexible pipe literature has confused the two. While the definition is generally made with regard to a sphere, the extension to a toroid is easily made. On a sphere, a loxodrome is defined as a line which cuts lines of constant longitude, or meridians, at a constant angle. This is also called a rhumb line. Figure 2.2 shows a differential element and defines the parameters from which the following relation is easily derived.

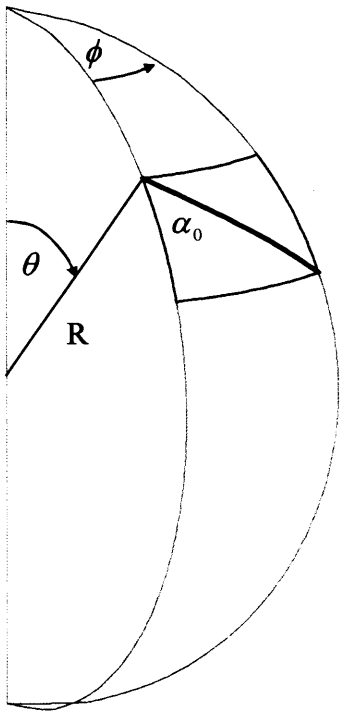

Figure 2.2 Element of Loxodrome and spherical co-ordinates.

$$R\sin\theta\, d\phi = \sin\alpha_0\, ds$$

$$R\, d\theta = \cos\alpha_0\, ds$$

$$\phi = \tan\alpha_0 \int \frac{d\theta}{\sin\theta}$$

$$= \tan\alpha_0 \left(\ln(1-\cos\theta) - \ln(\sin\theta)\right) + C \qquad (2.5)$$

It is interesting to note that this shows that such a line cannot ever reach either pole, a result clearly correct as all meridians meet there and consequently no line can arrive at a constant angle to all. However, although infinitely spiralling, the arc length does converge. Figure 2.3 shows a truncated example.

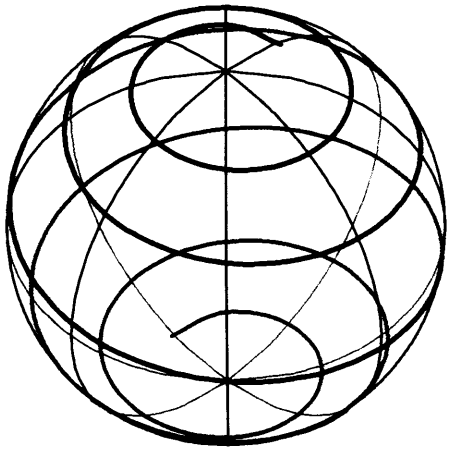

Figure 2.3 Example loxodrome, $\alpha_0 = 14\pi/30$.

The same analysis can be applied to a toroid, replacing meridians with lines parallel to the axis as in Figure 2.4. The resulting equation is

$$(\rho_0 + R\sin\theta)\,d\phi = \sin\alpha_0\, ds$$

$$R\,d\theta = \cos\alpha_0\, ds$$

$$\phi = \tan\alpha_0 \int \frac{d\theta}{\frac{\rho_0}{R} + \sin\theta} = \frac{-2\tan\alpha_0}{\sqrt{\left(\frac{\rho_0}{R}\right)^2 - 1}} \tan^{-1}\left[\sqrt{\frac{\frac{\rho_0}{R} - 1}{\frac{\rho_0}{R} + 1}} \tan\left(\frac{\pi}{4} - \frac{\theta}{2}\right)\right] + C \qquad (2.6)$$

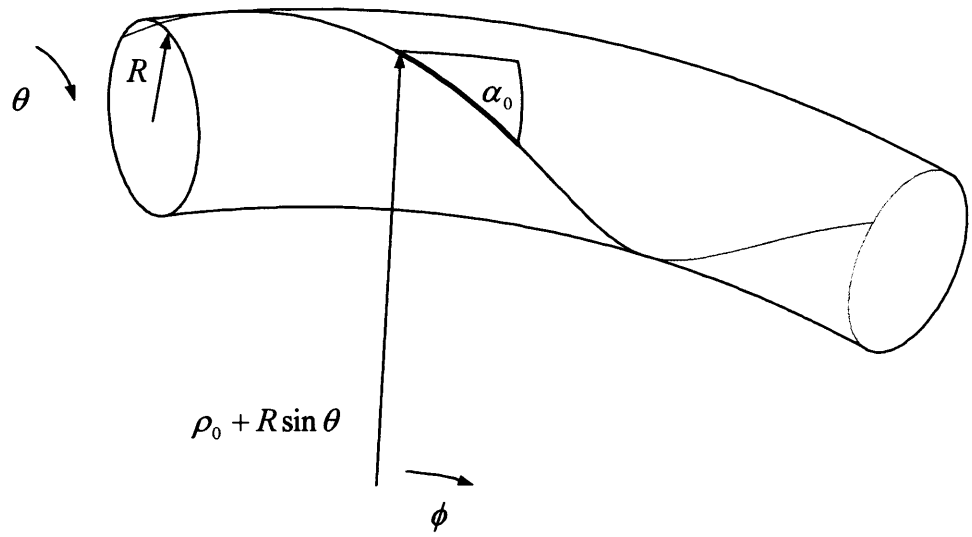

Figure 2.4 Element of toroidal loxodromic curve and co-ordinates.

Figure 2.5 shows for comparison a full circle toroid with a strained helix and a loxodrome drawn on it. The departure of each curve from the other is clear to see.

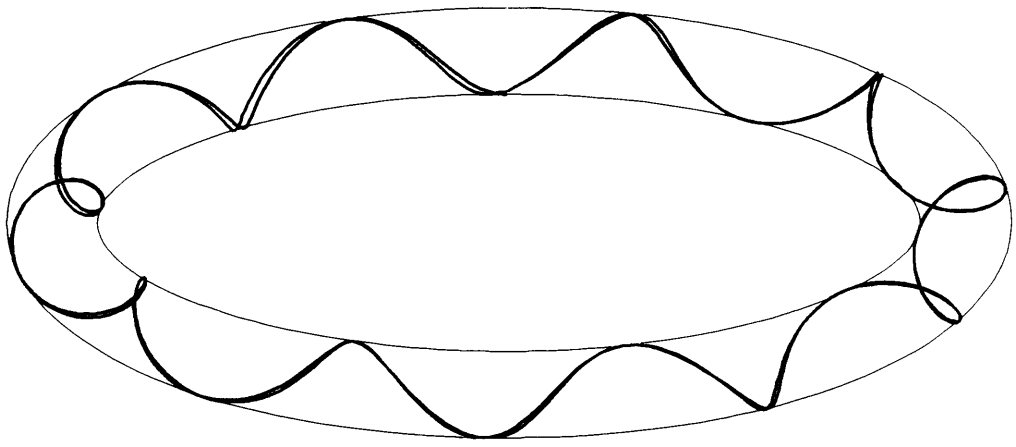

Figure 2.5 Loxodromic and strained helix curves.

Geodesics

Rhumb lines were sometimes mistaken for lines of shortest distance, or geodesics. On a sphere geodesics are of course great circles, and on a cylinder, helices. They are characterized as having the least curvature possible, and therefore as they traverse the surface they have no lateral curvature, only the curvature of the surface in the direction of the tangent to the line. Geodesic curve equations can be derived from Euler-Lagrange minimisation of the arc length integral, although sometimes, such as in the case of toroids, solution for the arc length can be analytically unobtainable.

2.3.2 Thin Rods

A full description of the analysis of stress and strain in thin rods is left for later in the review, the aim of this section being to introduce some basic concepts. Thin rods are characterized as having cross sections with dimensions considerably smaller than the rod length. Tensile armour wires are particularly good examples, with cross sections millimetres wide and lengths of hundreds of metres. In the initial unloaded state, the central line or line of centroids of a rod is a curve, with curvature and torsion as already described. However, the orientation of the cross section is a separate issue, not at all related to the curve invariants. Therefore to assess rod strain, the curvature of the centre line curve must be split into components κ and κ' to coincide with the chosen principal axes of the rod cross section. Also, if the measure of the twist of the rod includes the torsion of the centre line it must also include a secondary twist to account for rod cross section twist with regard to the centre line. Hence

$$\tau = \frac{df}{ds} + \frac{1}{\Sigma} \quad , \tag{2.7}$$

where τ is the total twist of the rod, $\frac{df}{ds}$ is the twist of cross section, and $\frac{1}{\Sigma}$ is the tortuosity, or torsion, of the rod centre line.

2.4 GEOMETRIC APPROACHES

2.4.1 Introduction

This section of the review covers the structural analysis of flexible pipe and other structures containing helically wound wires which is based on assumptions regarding the geometry of the component wires. The important mechanism of slip is introduced whereby, under bending, pipe or cable cross-sections do not remain plane as wires move to reduce stress gradients.

2.4.2 Definitions

Lay angle may be used instead of helical angle when describing a helically wound wire, and this is simply the angle which the wire makes with the helix axis (see Figure 2.6), or $\pi/2-\alpha_0$. The developed cylindrical surfaces in Figure 2.7 show compatible stretch, radial expansion and twist from one helical form to another.

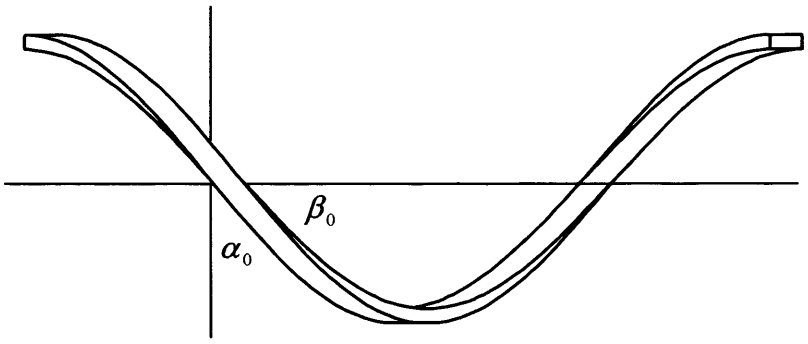

Figure 2.6 Helical angle α_0 and lay angle β_0.

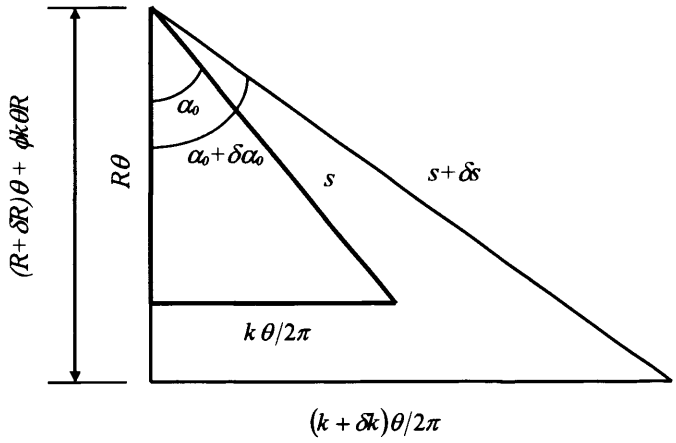

Figure 2.7 Geometry of helical strip before and after deformation (with twist ϕ rotations per metre along helix axis), showing relationships between helical radius R, pitch k, helical angle α_0, arc length s and parametric (polar) angle θ.

2.4.3 Structural Analysis – Axi-Symmetric Loading

Wire Strain

A small strain ε_k in the pitch k of a helix, with no change in the radius, leads to a small strain ε_s in the length s, related as follows (see Figure 2.7).

$$(s+\delta s)^2 = \left((k+\delta k)^2 + R^2\right)\theta^2$$

$$2s\delta s = 2k\delta k\theta^2 \qquad \left(s^2 = \left(k^2 + R^2\right)\theta^2\right)$$

$$\delta s = \delta k\theta \sin\alpha_0 \qquad \left(s\sin\alpha_0 = k\theta\right)$$

$$\varepsilon_s = \frac{\delta s}{s} = \frac{\delta k}{k}\sin^2\alpha_0 = \varepsilon_k \sin^2\alpha_0 = \varepsilon_k \cos^2\beta_0 \qquad (2.8)$$

This simple derivation was used by Hruska to show that helical layers in wire rope under tension are under less strain than the core (Hruska, 1951) where there is sufficient friction to maintain the same axial elongation.

In the same way, a small strain ε_r in the radius leads to

$$\varepsilon_s = \varepsilon_r \cos^2 \alpha_0 = \varepsilon_r \sin^2 \beta_0 \tag{2.9}$$

Also referring to Figure 2.7, a twist ϕ rotations per unit length is equivalent, in terms of the developed geometry only, to a radial strain of $2\pi\phi k$, leading to

$$\begin{aligned} \varepsilon_s &= 2\pi\phi k \cos^2 \alpha_0 \\ \varepsilon_s &= 2\pi\phi R \sin \alpha_0 \cos \alpha_0 \qquad (k = R \tan \alpha_0) \\ \varepsilon_s &= \phi\pi R \sin 2\alpha_0 = \phi\pi R \sin 2\beta_0 \qquad (\sin(\pi - 2\beta_0) = \sin 2\beta_0) \end{aligned} \tag{2.10}$$

Summing these possible contributions to strain and defining an equivalent Poisson's ratio $\nu = -\varepsilon_r / \varepsilon_k$ gives the following expression suggested by D'Oliveira (D'Oliveira et al, 1985) for the axial strain in helical constituent wires in flexible pipe.

$$\varepsilon_s = \varepsilon_k (\sin^2 \alpha_0 - \nu \cos^2 \alpha_0) + \phi(\pi R \sin 2\alpha_0) \tag{2.11}$$

While the tension in helical armour wires provides axial equilibrium it also leads to radial forces and tangential forces. The former, due to curved wires under tension, can cause high contact stresses in wire rope but this is not such a problem for flexible pipe armour where the wires have flat surfaces and the layers are usually separated by intermediate polymer layers. Tangential forces, on the other hand, may lead to rotation and an associated redistribution of load. Applied rotation, if severe enough, can create compressive forces in armour wires sufficient to cause buckling and layer separation, often referred to as birdcaging.

Pipe Behaviour

Axial and Torsional Stiffness

Using 2.11, first approximations for pipe axial and torsional stiffnesses can also be written down by combining independent contributions from cylindrical layers and wire layers, based on compatibility of displacements but on no further interaction between layers (D'Oliveira et al, 1985).

Axial stiffness can be estimated from axial equilibrium of the pipe cross section. If flexible pipe is considered to consist of a cylindrical core and *m* helical wire layers, the following combination gives pipe axial stiffness, where ε_k is the pipe axial strain, ε_i is the wire axial strain in the *i*th layer from (2.11), n_i is the number of wires in the *i*th layer and A_i is the cross sectional area of wires in the *i*th layer. $E_c A_c$ is the core axial stiffness.

$$EA = E_c A_c + \sum_{i=1}^{m} n_i E_i A_i \sin\alpha_i \varepsilon_i / \varepsilon_k \tag{2.12}$$

The expression is reliant on the assumption that the helical layers remain helical when the pipe is strained, and that the new helices fit exactly with the stretched and twisted cylindrical elements of the pipe. It is a free-field expression and no end effects are considered to be present.

Similarly, from torsional equilibrium, pipe torsional stiffness can be given by

$$JG = J_c G_c + \sum_{i=1}^{m} \left[\varepsilon_i n_i E_i A_i R_i \cos\alpha_i / \phi + n_i J_i G_i \sin^2 \alpha_i \right] \tag{2.13}$$

The first term under the summation is from torque due to the axial force on each wire while the second term is due to wire rotation about its own axis. Here, because of the helical angle α_i the wire twist per unit length is less than that of the pipe, and only a

component of the wire torque is in the plane of the pipe cross section. The term can be used with an equivalent stiffness in the case of rectangular wires.

Linear Stiffness Matrix

The axial-torsional responses in (2.12) and (2.13) can be expressed in matrix form, both being dependent on strain ε and twist $2\pi\phi$, as follows.

$$\begin{pmatrix} F \\ M \end{pmatrix} = \begin{pmatrix} k_{F\varepsilon} & k_{F\phi} \\ k_{M\varepsilon} & k_{M\phi} \end{pmatrix} \begin{pmatrix} \varepsilon \\ 2\pi\phi \end{pmatrix} \tag{2.14}$$

The stiffness matrix terms relating force F and moment M to the strain and twist are, for the simplest case in which ν is considered to be zero,

$$\begin{aligned} k_{F\varepsilon} &= E_c A_c + \sum_{i=1}^{m} n_i E_i A_i \sin^3 \alpha_i \\ k_{M\phi} &= G_c J_c + \sum_{i=1}^{m} n_i G_i J_i \sin^2 \alpha_i + \sum_{i=1}^{m} n_i E_i A_i R_i^2 \sin \alpha_i \cos^2 \alpha_i \\ k_{F\phi} &= k_{M\varepsilon} = \sum_{i=1}^{m} n_i E_i A_i R_i \sin^2 \alpha_i \cos \alpha_i \end{aligned} \tag{2.15}$$

In accordance with Maxwell's reciprocal theorem for a linear elastic system the stiffness matrix is symmetric (Jolicoeur and Cardou, 1991). The change from one helix to another indicated in Figure 2.7 requires twisting and bending strains as well as the axial strain already considered, partially accounted for by the second term under the summation in (2.13). Hruska makes the point (Hruska, 1953) that even the simplest wire rope strand will not unwind when loaded because wire twisting and bending stresses due to change in the lay angle will prevent it from becoming 'a bundle of parallel wires'. However, some attempts reported by Jolicoeur and Cardou to improve the accuracy of the stiffness matrix, by including wire bending and twisting moments, augment $k_{M\varepsilon}$ and $k_{M\phi}$ without changing $k_{F\phi}$ and this violates the symmetry. While Jolicoeur and Cardou leave this unexplained, it is because the changes considered come from a comparison of helical lines and not from wire

equilibrium. Use of wire equilibrium equations, introduced in the next section, restores symmetry.

Figure 2.7 shows that pipe axial strain increases the helical angle while the rotation ϕ reduces it. A small change in helical angle leads to the following changes in curvature and twist.

$$\kappa' = \frac{\cos^2 \alpha_0}{R} \qquad \delta\kappa' = \frac{-2}{R} \sin \alpha_0 \cos\alpha_0 \delta\alpha_0 \tag{2.16}$$

$$\tau = \frac{1}{R} \cos\alpha_0 \sin \alpha_0 \qquad \delta\tau = \frac{1}{R}\left(1 - 2\sin^2 \alpha_0\right)\delta\alpha_0 \tag{2.17}$$

The original geometry gives simply

$$s\cos\alpha_0 = R\theta \qquad s\sin\alpha_0 = k\theta \tag{2.18}$$

Changes in the geometry due to pipe axial strain only, assuming small strains and using (2.18), give

$$\begin{aligned} &s(1+\varepsilon_s)\cos(\alpha_0 + \delta\alpha_0) = R\theta \\ &s(1+\varepsilon_s)(\cos\alpha_0 - \delta\alpha_0 \sin\alpha_0) = R\theta \\ &\varepsilon_s \cos\alpha_0 = \delta\alpha_0 \sin\alpha_0 \end{aligned} \tag{2.19}$$

Substituting into 2.16 and 2.17 and using 2.8,

$$\begin{aligned} \delta\kappa' &= \frac{-2}{R} \sin^2 \alpha_0 \cos^2 \alpha_0 \varepsilon_k \\ \delta\tau &= \frac{1}{R}\left(1 - 2\sin^2 \alpha_0\right)\sin\alpha_0 \cos\alpha_0 \varepsilon_k \end{aligned} \tag{2.20}$$

In the same way, changes in the geometry due to pipe twist alone give

$$s(1+\varepsilon_s)\sin(\alpha_0+\delta\alpha_0)=k\theta$$
$$s(1+\varepsilon_s)(\sin\alpha_0+\delta\alpha_0\cos\alpha_0)=k\theta$$
$$\varepsilon_s\sin\alpha_0=-\delta\alpha_0\cos\alpha_0 \qquad (2.21)$$

leading to

$$\delta\kappa'=4\pi\phi\sin^3\alpha_0\cos\alpha_0$$
$$\delta\tau=2\pi\phi(1-2\cos^2\alpha_0)\sin^2\alpha_0 \qquad (2.22)$$

These changes in curvature and twist in all wires combine to provide a moment about the pipe axis (Figure 2.8) and the moment terms in (2.15) can be rewritten as follows.

$$M_\varepsilon=\sum_{i=1}^{m}n_i\left[E_iA_iR_i\sin^2\alpha_i\cos\alpha_i-2\frac{E_iI_i}{R_i}\sin^2\alpha_i\cos^3\alpha_i+\frac{G_iJ_i}{R_i}\sin^2\alpha_i\cos\alpha_i(1-2\sin^2\alpha_i)\right] \qquad (2.23)$$

$$M_\phi=G_cJ_c+\sum_{i=1}^{m}n_i\left[E_iA_iR_i^2\sin\alpha_i\cos^2\alpha_i+2E_iI_i\sin^3\alpha_i\cos^2\alpha_i+G_iJ_i\sin^3\alpha_i(1-2\cos^2\alpha_i)\right] \qquad (2.24)$$

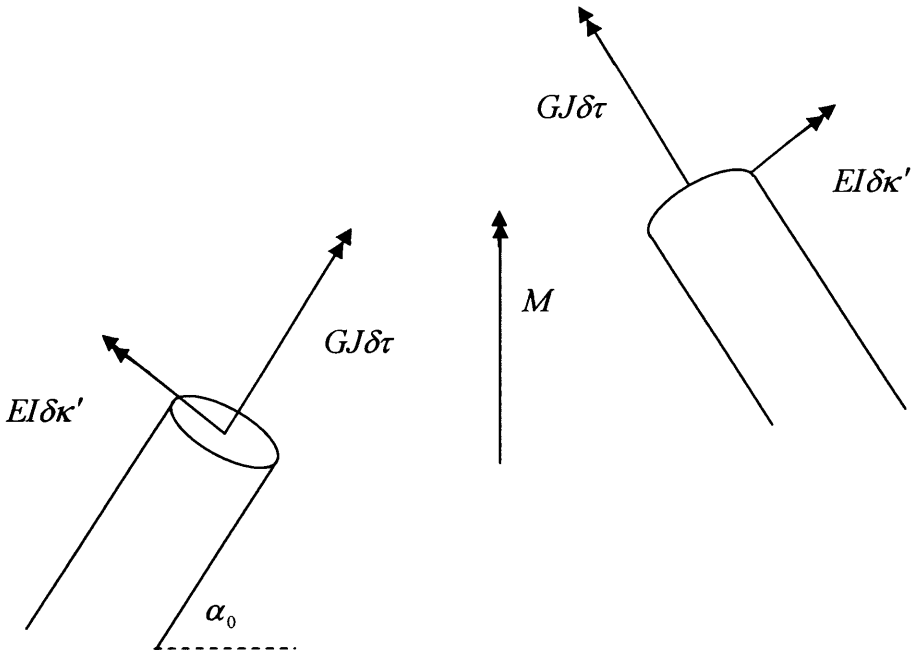

Figure 2.8 Moment M due to wire bending and twisting in opposite wires.

Expression (2.11) includes the effect of core contraction due to pipe axial strain although it does not take into account core compression by radial forces from the tensile armour due to ϕ and ε_p. Core radial contraction is derived by Knapp (Knapp, 1979) using Lame's thick cylinder analysis together with an expression for average external pressure from circumferential equilibrium, including small changes in the helix radius and lay angle. Stiffness matrix expressions (2.15), (2.23) and (2.24) are obtained with small correction factors dependent on material properties of the central core, and shown to give stiffnesses for electrical cable which agree well with experimental results.

Pressurized Pipe Equilibrium

For a flexible pipe under pressure, approximate wire stresses can be found from a simplified set of equations based on the assumptions that deformations are small, all pressure and tension resistance is provided by the wires and none by the polymer cylinders and that all layers remain in contact (Feret and Bournazel, 1987).

Equilibrium in the axial direction for a pipe subjected to internal and external pressure, an axial force F and twisting moment M is

$$\sum_{i=1}^{m} n_i \sigma_i A_i \sin \alpha_i = F + \pi P_{\text{int}} r_{\text{int}}^2 - \pi P_{ext} r_{ext}^2 \tag{2.25}$$

Likewise in the circumferential direction, equilibrium over one lay length gives (Figure 2.9)

$$\sum_{i=1}^{m} \frac{n_i \sigma_i A_i \cos \alpha_i}{2\pi r_i \tan \alpha_i} = P_{\text{int}} r_{\text{int}} - P_{ext} r_{ext} \tag{2.26}$$

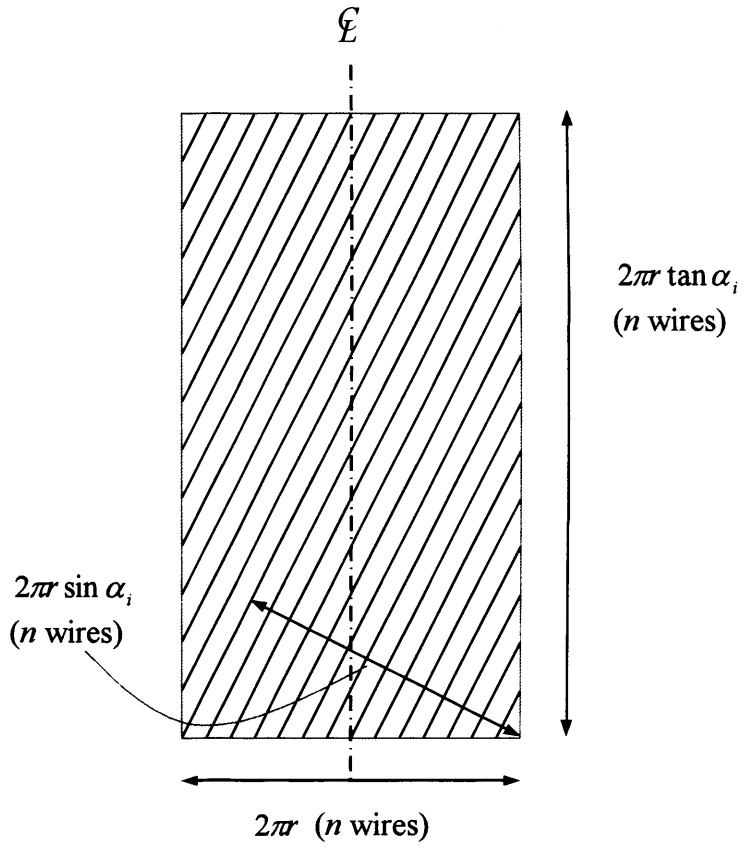

Figure 2.9 Developed cylinder radius r, one pitch with n helical wires at helical angle α_i.

Also pipe twisting moment equilibrium gives

$$\sum_{i=1}^{m} n_i \sigma_i A_i \cos\alpha_i = M \tag{2.27}$$

From (2.11), for each layer,

$$\frac{\sigma_i}{E_i} = \varepsilon_k \sin^2 \alpha_i + \varepsilon_r \cos^2 \alpha_i + \phi(\pi R \sin 2\alpha_i) \tag{2.28}$$

With no rotation ϕ, (2.25) – (2.28) can be used with further simplification to give an indication of pipe performance. As flexible pipe structure for high pressure work has dedicated pressure and tensile armour steel strip layers, a pipe can be idealized as consisting of a pressure layer wound at a helical angle of zero inside a tensile layer at a helical angle of α_0, both with the same radius r (Feret and Bournazel, 1987).

Axial equilibrium is therefore only provided by the tensile armour and (2.25) gives, for a pipe exposed to a pressure difference ΔP and an axial force F,

$$\sigma_t \sin\alpha_0 (nA) = F + \pi r^2 \Delta P \tag{2.29}$$

The total wire cross sectional area represented by nA can be replaced by an equivalent layer thickness e_t multiplied by its width $2\pi r \sin\alpha_0$ (perpendicular to the wires, see Figure 2.9). This is equal to the area A divided by the wire width plus the gap between the wires. Hence the *tensile armour* axial stress becomes

$$\sigma_t = \left(\Delta P + \frac{F}{\pi r^2}\right) \frac{r}{2e_t \sin^2 \alpha_0} \tag{2.30}$$

Radial equilibrium involves an intermediate pressure P_1 between layers and leads to the following simultaneous equations.

$$e_p \sigma_p = (P_{\text{int}} - P_1) r \qquad e_t \sigma_t \cos^2 \alpha_0 = (P_1 - P_{ext}) r \tag{2.31}$$

Hence *pressure armour* axial stress is

$$e_p \sigma_p = \Delta P\, r - e_t \sigma_t \cos^2 \alpha_0$$

$$\sigma_p = \frac{\Delta P\, r}{e_p}\left(1 - \frac{1}{2\tan^2 \alpha_0}\right) - \frac{F}{\pi r e_p}\frac{1}{2\tan^2 \alpha_0} \tag{2.32}$$

The change in pressure through each layer is easily calculated by substitution for the armour stresses in (2.31). Finally, with radial strain given by the pressure armour strain, pipe strain can be written down in terms of armour strains using (2.28).

$$\varepsilon_r = \frac{\sigma_p}{E_p} \qquad \varepsilon_k = \frac{\sigma_t}{E_t \sin^2 \alpha_0} - \frac{\sigma_p}{E_p \tan^2 \alpha_0} \tag{2.33}$$

More detailed analysis including changes in layer radius, thickness and helical angle and contributions from polymer sheath layers has been carried out by, for example, the Institut Français du Pétrole, via computer modelling, but the simplified expression (2.30) shows the significance of pressure on the tensile armour tension.

2.4.4 Structural Analysis – Flexural Loading

Wire Strain

A stiffness matrix for helically armoured cables including bending is developed by Lanteigne (1985), which includes the terms in (2.15), though ignoring wire torsional stiffness, together with the bending stiffness

$$EI = \sum_{i=1}^{m} n_i A_i E_i \left(\frac{r_i^2/2 + R_i^2}{2} \right) \sin^3 \alpha_i + E_c I_c \tag{2.34}$$

where r_i is the wire radius in the ith layer, in the absence of any broken wires. In this case terms coupling bending with axial strain and twist are zero. This is also in the absence of any radial strain. Expression (2.34) is based entirely on the understanding that there is no axial slip of the wires and that therefore they experience the same strain as a strained helix, all cross-sections remaining plane.

In cables the contact forces between successive wire layers increase towards the centre, owing to wire curvature and tension, while tension and compression due to plane cross-section bending increase away from the centre, owing to distance from the cable neutral axis. If the contact forces are not sufficient then the tension gradient developed leads to slip, whereby regions in compression expand while regions in tension contract. On the assumption that all slip happens in the wire axial direction, Lanteigne gives an intermediate bending stiffness

$$EI = \sum_{i=1}^{j} n_i E_i A_i \left(\frac{r_i^2/2 + R_i^2}{2} \right) \sin^3 \alpha_i + \sum_{i=j+1}^{m} n_i E_i I_i + E_c I_c \tag{2.35}$$

to account for full slip in the outer $(m-j)$ layers. This reduces to the sum of the individual stiffnesses

$$EI = \sum_{i=1}^{m} n_i E_i I_i + E_c I_c \tag{2.36}$$

in the case of full slip in all wire layers, which is 'the lower flexural rigidity commonly used'.

Friction forces are considered to exist at contact points between circular wires in contra-wound layers, and in an example analysis of an aluminium conductor of radius 15.2 mm consisting of 49 wires, stiffness had reduced by 96% of the range from maximum to minimum by an applied curvature of 1 m^{-1}, or a ratio of $r/\rho = 0.015$.

Axial Slip

As mentioned above, axial slip along a strained helical path would be a mechanism by which sinusoidal axial stresses in wires following the path could be relieved. The surface strain along an originally helical path on a bent cylinder would therefore be different to the strain experienced by a wire following the path. If the surface and wire were considered to interact to restrain the slip, then the resulting axial stresses in the wire could be modelled. This is the approach taken by Lutchansky (1969) in examining armour wire stresses in bent cables, considering axial stresses only and ignoring local wire bending and twisting.

For an original helical angle α_0 the strained helical path strain ε_s is, on a cylinder bent into a toroid, (see Figure 2.10, and using (2.8))

$$\varepsilon_s = \frac{R}{\rho}\cos(\theta + \theta_0)\sin^2\alpha_0 \tag{2.37}$$

and therefore the new arc length s_t as a function of θ is

$$s_t = \sqrt{R^2 + k^2}(\theta - \theta_0) + \frac{R}{\rho}\sin^2\alpha_0(\sin\theta - \sin\theta_0) \tag{2.38}$$

where the first term is the original path length (see Figure 2.7). A wire, following the strained helical path and clamped at $\theta = 0$, is considered to interact with the central core so that it receives an axial force proportional to the difference between the surface

and wire axial displacements. This results in the following second order ordinary differential equation in the wire axial displacement u.

$$\frac{d^2u}{ds_c^{\,2}} - \frac{K}{AE}u = -\frac{KU}{AE}\left(\sin\frac{s_c}{a} - \sin\frac{s_{c_0}}{a}\right) \tag{2.39}$$

where where $a = \sqrt{R^2 + k^2}$, s_c is the original arc length co-ordinate on the cylinder, s_{c_0} is the length of wire between the clamp and where the wire crosses the top of the cable, furthest from the centre of curvature, K is the interaction shear stiffness, A is the wire cross sectional area and

$$U = \frac{R}{\rho}\frac{k^2}{a}$$

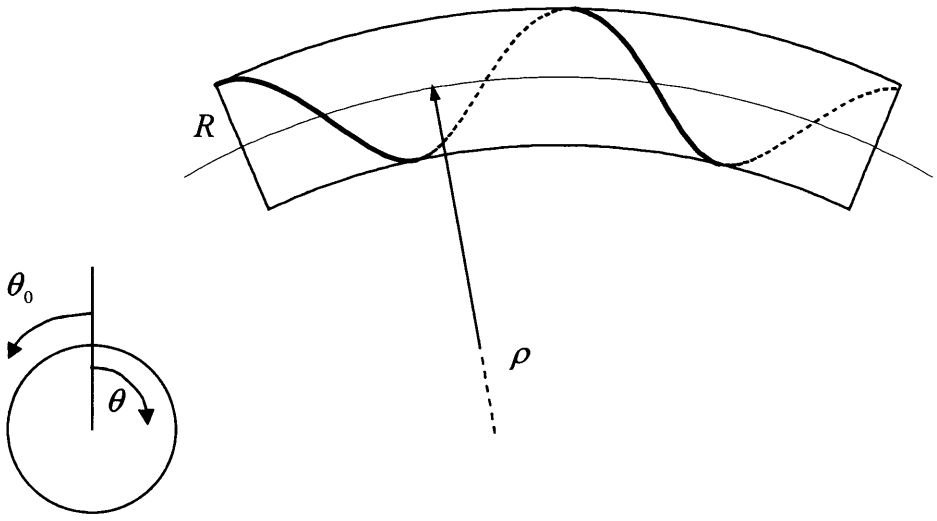

Figure 2.10 Helical groove and definitions

This results in the following expressions for wire axial displacement and stress, taking wire displacement at the clamp to be zero.

$$u = \frac{U\sin\theta_0}{\left(1+\frac{a^2K}{AE}\right)}e^{\sqrt{\frac{K}{AE}}a(\theta_0-\theta)} + U\left[\frac{Ka^2}{AE+a^2K}\sin\theta - \sin\theta_0\right] \tag{2.40}$$

$$\sigma = \frac{UaK}{A\left(1+\frac{a^2K}{AE}\right)}\left[-\frac{1}{a}\sqrt{\frac{AE}{K}}e^{\sqrt{\frac{K}{AE}}a(\theta_0-\theta)}\sin\theta_0+\cos\theta\right] \tag{2.41}$$

This expression for stress shows that at the clamp $(\theta = \theta_0)$ the restriction of wire motion imposed by a clamp results in stress concentration at that point varying with circumferential position θ_0. Differentiation of the above with respect to position θ_0 gives the location of the wire with the greatest stress as

$$\hat{\theta}_0 = \tan^{-1}\left(\frac{1}{a}\sqrt{\frac{AE}{K}}\right) \tag{2.42}$$

This expression is clearly, for a given wire geometry, dependent only on the interaction shear stiffness K, and with Lutchansky's choice for K based on cable bending tests this suggests a maximum stress location somewhere near the neutral axis position.

Shear stiffness orthogonal to the wire path has been disregarded as transverse deflections and forces are felt by Lutchansky to be small and therefore to have little effect on the wire stresses. There is some sense in this approach, particularly as such a groove may well exist due to extrusion of the supporting core into inter-wire gaps, especially if the cable is subjected to significant external pressure. However near any such end or clamp restraint, there is no guarantee that the wire will remain on the strained helical path, and local bending stresses which may become significant have therefore been disregarded. Lutchansky's is the first investigation of the effect on normal wire-core interaction that a clamp or restraint has.

Lutchansky's model is adopted by Raoof and Hobbs (1984) to investigate the bending of spiral strand and armoured cables close to terminations, free from any other external restraints. Although comparison is made with bending tests involving considerable axial tension, a constant curvature model is used with finite interactive shear modulus between wire and solid core in the same way as Lutchansky, the solid core undergoing

plane section bending. The difference is that the shear modulus is allowed to vary, being dependent on cable axial tension and slip. This renders Lutchansky's model non-linear, requiring a numerical solution. Also the no-slip values used for the shear modulus are much higher than those selected by Lutchansky giving a close to extreme fibre location for the wire with the greatest axial stress and not a neutral axis location as given before. This result is clear from the $\hat{\theta}_0$ equation (2.42).

As the first bending test fractures reported by Raoof and Hobbs (1984) are near the neutral axis it is concluded that no-slip axial wire strains at a fixed termination are not the factor controlling cable fatigue life, and that as slip near the termination is greatest near the neutral axis it is this phenomenon which is responsible, by a fretting process, for the initiation of wire breakages.

Lateral Slip

In contrast to the foregoing, a wire under tension that is not restrained to follow the strained helix may have a tendency to follow a geodesic path. Free-field analysis of tensile armour in flexible pipe has been carried out on this basis by Feret and Bournazel (1987) and Out and von Morgen (1997). In both cases comparison is made between the strained original helix and a geodesic derived using the Euler-Lagrange equation to minimize distance, on the assumption that applied curvature is constant. The wire-core axial and transverse slips are given as

$$\begin{aligned} \Delta_a &= -\frac{R^2}{\rho}\frac{\sin^2\alpha_0}{\cos\alpha_0}\sin\theta \\ \Delta_t &= \frac{R^2\tan\alpha_0}{\rho}\left(\frac{\sin^2\alpha_0}{\cos\alpha_0}+2\cos\alpha_0\right)\sin\theta \end{aligned} \tag{2.43}$$

Note the dependence on $1/\rho$ and θ. For high α_0, as in the pressure layer, slip is negligible, these formulas being relevant to tensile armour slip.

Wires which now follow the geodesic on a toroid rather than a helix on a cylinder have added curvature and twist. The twist induces small shear stresses but the bi-normal

curvature variation has a significant effect on tension layer stiffness. The change quoted by Feret and Bournazel (1987) is

$$\Delta(\kappa') = \frac{\sin^2 \alpha_0}{\rho} \frac{\cos\theta}{1 + \frac{R}{\rho}\cos\theta} \tag{2.44}$$

but this is actually the case for the loxodromic curve at angle α_0 and not the geodesic. The comparative bi-normal curvatures for the helix, strained helix and geodesic from Out and von Morgen (1997) are

$$\begin{aligned} \kappa_1 &= \frac{\cos^2 \alpha_0}{R} \\ \kappa_1 &= \frac{\cos^2 \alpha_0}{R}\left(1 + \frac{R}{\rho}\sin\theta \frac{\cos 2\alpha_0}{\tan^{-2}\alpha_0}\right) \\ \kappa_1 &= \frac{\cos^2 \alpha_0}{R}\left(1 + 3\frac{R}{\rho}\sin\theta \tan^2 \alpha_0\right) \end{aligned} \tag{2.45}$$

while transverse curvature for the deformed helix is

$$\kappa_2 = \frac{1}{\rho}\cos\theta \sin\alpha_0 \sqrt{3\cos^2 \alpha_0 + 1}\left\{1 + \frac{R}{\rho}\sin\theta \frac{7\tan^{-2}\alpha_0 + 1}{\left(\tan^{-2}\alpha_0 + 1\right)\left(4\tan^{-2}\alpha_0 + 1\right)}\right\} \tag{2.46}$$

The normal and transverse curvatures in (2.45) and (2.46) will correspond to the wire normal and binormal axes if the rectangular strip is constrained to lie flat on the surface. The geodesic change in normal curvature from the original helix is more than three times as large as that of the deformed helix, while the deformed helix transverse curvature change is larger than its normal curvature change. This suggests that neither curve will be a path of least strain energy. Movement to the geodesic will remove strain energy due to transverse bending and will, on account of its actual shortening, relieve some of any tension that the tendon may be under, though strain energy will be increased due to normal bending. The curve of least elastic strain energy will be between the geodesic and strained helix boundary curves.

Friction may also need to be taken into account if the final position due to pipe curvature is to be accurately predicted. Friction will limit slip, in the axial case leading to extra tension or compression σ_T, which will induce stresses which are a maximum on the inside and outside of the curved pipe ('extreme fibre' position), and in the transverse case leading to transverse curvature ΔC_B independent of the bending radius, which will induce stresses which are a maximum on the sides of the pipe (neutral axis position). The friction factor f has to be known reliably.

$$\sigma_T = \frac{\pi P_c f R}{2 e_t \cos\alpha_0} \qquad \Delta C_B = \frac{\pi^2}{8} \frac{P_c f \left(1+\cos^2\alpha_0\right)}{E e_t \sin\alpha_0 \cos\alpha_0} \sin\theta \tag{2.47}$$

Feret and Bournazel also point out that due to slip the helical angle of the tendons is no longer constant, increasing on the inside of the curvature and decreasing on the outside. It is suggested that the increase on the inside, together with the shortening of this distance due to curvature, will lead to contact between tendons at a radius of $\rho = R/\left(j \sin^2\alpha_0\right)$, where j is the relative clearance between tendons. This would be responsible for an increase in pipe stiffness and an increase in the stresses in the tendons. Such a level of curvature, particularly if reached periodically, would lead to an increase in fatigue.

The geodesic considerations introduced in this section are only applicable to free field analysis, and have simply compared lines on a toroidal surface, and not wires with a rectangular cross section. Furthermore, regarding the effect of end restraint, such a comparison is totally inappropriate and would be made while ignoring the fact that the end of the wire is fixed in the original orientation and not aligned along the geodesic, and that the applied curvature is likely to vary along the pipe's length.

2.5 WIRE EQUILIBRIUM

2.5.1 Introduction

Equations of equilibrium for a thin rod have existed in elasticity theory since at least 1859, and these have also been used to model armour wires in flexible pipe and similar structures containing helically wound wires. This approach has led to the development of complete sets of equilibrium, compatibility and constitutive equations for the analysis of structural response, some of which include end effects. The complexity of the solutions either limits the analysis to simple cases or requires numerical procedures for evaluation.

2.5.2 Love's Thin Rod Equations

The principal torsion flexure axes *(x,y,z)* of a thin rod cross section, as distinct from the tangent, normal and binormal vectors associated with the central line, are constructed by consideration of three linear elements in the directions of the central line and cross section principal axes issuing from the centroid in the unloaded state. After deformation these three elements will in general no longer be at right angles but they can be used to construct a new orthogonal triad. The tangent to the strained central line gives the z axis, which is clearly the same tangent axis as defined in the Serret-Frenet relations. The new x axis is such that the new *(x,z)* plane contains the element originally in the direction of the cross section x axis when unloaded, this plane being a principal plane of the rod. The y axis is then mutually perpendicular to these. Thus curvatures before and after deformation refer to the same planes of the rod.

Curvatures and twist can then be found by considering, as a visualization tool, this triad of axes moving with unit velocity along the central line. The triad's resultant angular velocity, on resolution along each axis, gives curvatures and torsion. Note the existence of two curvatures which, when combined, will give a vector directed along the binormal as defined in the Serret-Frenet relations with magnitude equal to the curvature of the strained central line. Ericksen and Truesdell (1958) point out that choice of the x or y axis for this construction can lead to two different results for twist after deformation. However, as by definition a rod has one dimension much larger

than the others, even large deflections will lead only to small local deformation and so small strain theory can be used to advantage.

The curvature direction along the binormal is due to consideration of angular velocity, represented by a vector directed along the axis of revolution, as shown in Figure 2.1. This is a source of confusion in the literature, as the mathematical curvature given by differential geometry is the magnitude of a vector in the direction of curvature, i.e. the normal direction. This same curvature would be referred to by Love (1893) and Costello (1990) as being in the binormal direction of the curve (a nonsense in differential geometry terms), that being the direction of the axis of curvature.

As already shown by (2.7), this resolution of the curvature along two torsion-flexure axes reveals the possibility of twist additional to that of the central line which may be experienced by the rod if its cross section changes orientation with respect to the normal of central line curvature. For example, a curved rod of rectangular cross section confined to lie flat on the surface of a cylinder will have its normal axis concurrent with the surface normal. Only when this rod follows the geodesic are these normals also colinear with the rod's curvature normal. If the rod is following a line other than the geodesic it will experience transverse curvature indicating that the cross section is twisted with respect to the central line which itself will be twisted.

In Love's work, and in Costello's literature (1990) on the same subject, curvature in the *(x,z)* plane, i.e. about an axis parallel to the y axis, is represented by κ', the 'curvature in the y direction' (see Figure 2.11). Similarly κ is the curvature in the x direction and τ is the twist per unit length as already defined. Consideration of internal and external force and moment equilibrium of a differential element of rod, length *ds*, gives the following six Equilibrium Equations for a thin rod.

$$\begin{aligned}
&\frac{dN}{ds} - N'\tau + T\kappa' + X = 0 && \frac{dG}{ds} - G'\tau + H\kappa' - N' + K = 0 \\
&\frac{dN'}{ds} - T\kappa + N\tau + Y = 0 && \frac{dG'}{ds} - H\kappa + G\tau + N + K' = 0 \\
&\frac{dT}{ds} - N\kappa' + N'\kappa + Z = 0 && \frac{dH}{ds} - G\kappa' + G'\kappa + \Theta = 0
\end{aligned} \qquad (2.48)$$

Axial strain due to T is ignored. If the six applied forces and moments are known, these equations contain nine unknowns, therefore three more equations are needed. Investigation of strain in a bent and twisted rod leads to the conclusion that simple beam type equations connecting stress couples and curvatures are sufficient, i.e.

$$G = EI_x\kappa, \qquad G' = EI_y\kappa', \qquad H = GJ\tau \tag{2.49}$$

and for the case where the rod already has curvature and twist in the unloaded state,

$$G = EI_x(\kappa_1 - \kappa), \qquad G' = EI_y(\kappa_1' - \kappa'), \qquad H = GJ(\tau_1 - \tau) \tag{2.50}$$

and the rest of Love's examination of thin rods proceeds with these equations. This is not before explaining that the equations given give good approximations to the stress couples and tension away from any place of loading or support but that close to these regions the equations are of doubtful validity.

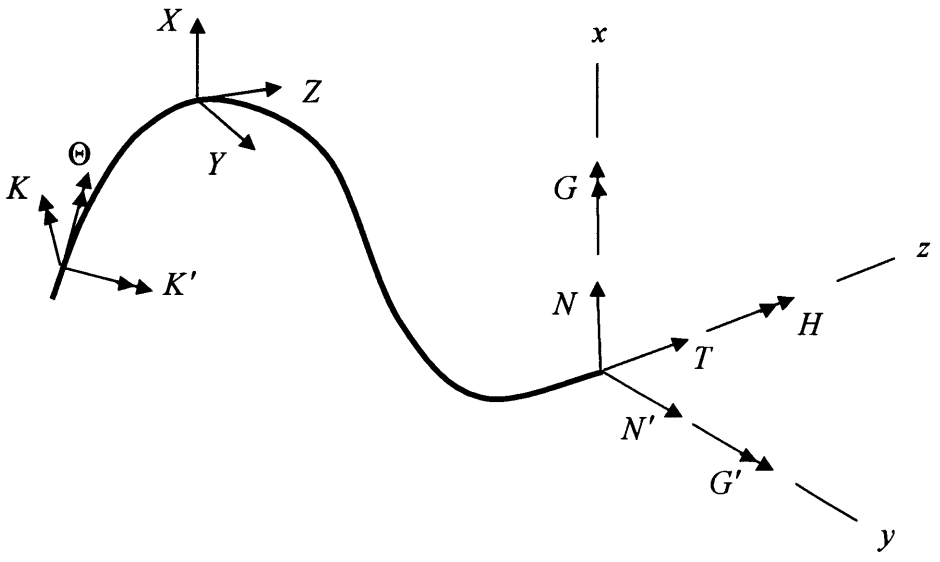

Figure 2.11 Thin rod applied forces X, Y, Z and moments K, K', Θ per unit length, and resultant tension T, shear forces N and N', and moments.

The equilibrium equations are greatly simplified if forces and couples are only applied to the rod at its ends. They are used by Love to develop a theory of spiral springs, in which a rod is maintained in a helical form by the application of a force R in line with the helix axis and couple C about the axis, although only applicable to rods for which $I_x = I_y$. R and C can be arranged to provide at the rod end a terminal force alone or a terminal couple alone, both cases leading to an additional twist of the rod. However they can also be arranged to hold the rod in a helical form without any additional twist and in this case they are

$$R = GJ\frac{\cos\alpha_1}{r_1}\left(\frac{\sin\alpha_1\cos\alpha_1}{r_1} - \frac{\sin\alpha_0\cos\alpha_0}{r}\right) - EI\frac{\sin\alpha_1}{r_1}\left(\frac{\cos^2\alpha_1}{r_1} - \frac{\cos^2\alpha_0}{r}\right)$$
$$K = GJ\sin\alpha_1\left(\frac{\sin\alpha_1\cos\alpha_1}{r_1} - \frac{\sin\alpha_0\cos\alpha_0}{r}\right) + EI\cos\alpha_1\left(\frac{\cos^2\alpha_1}{r_1} - \frac{\cos^2\alpha_0}{r}\right) \quad (2.51)$$

where α_0 and α_1 are initial and final helical angles respectively. If the change in helical angle is small, then substitution of the relations (2.19) and (2.21) into the first of (2.51) and using (2.8) and the appropriate form of (2.10) yields the missing F_ϕ component in the revision of the stiffness matrix terms in (2.15).

2.5.3 Application of Love's Equations Away from End Restraint

Witz and Tan (1992, (i)) present an analytical model for predicting axial-torsional load-displacement relationships for a generic flexible structure, where the mechanical behaviour of the helical components is based on Love's non-linear formulae. Results for elongation and angle of twist are found to be very linear in spite of the non-linearity of the model, and agreement with experimental results is good. The model also predicts the formation of gaps between layers due to separation under, for example, twisting.

Consideration of a simple shell element, radius R and thickness t_c, leads to the following equations showing linear relationships between deformations and forces and moments, and that the twisting moment M_t and axial force F are uncoupled.

$$F = \frac{2\pi R t_c E(1-\nu)}{(1+\nu)(1-2\nu)}\left[\varepsilon_x + \frac{\nu}{1-\nu}\left(-\frac{\Delta R}{R} + \frac{\Delta t}{t_c}\right)\right]$$

$$M_t = G2\pi R^3 t_c \phi \tag{2.52}$$

Also the pressure difference can be written

$$q_{out} - q_{in} = \frac{t_c E(1-\nu)}{R(1+\nu)(1-2\nu)}\left[\frac{\Delta R}{R} - \frac{\nu}{1-\nu}\left(\varepsilon_x + \frac{\Delta t}{t_c}\right)\right] \tag{2.53}$$

The corresponding expressions for the axial force and twisting moment for a helical strip layer containing m wires with new helical angle α_1 are

$$\begin{aligned} F &= m(T\sin\alpha_1 + N'\cos\alpha_1) \\ M_t &= m[H\sin\alpha_1 + G'\cos\alpha_1 + T(R-\Delta R)\cos\alpha_1 - N'(R-\Delta R)\sin\alpha_1] \end{aligned} \tag{2.54}$$

which are coupled and nonlinear in ΔR, ε_x & ϕ. Also the following nonlinear expression arises for the pressure difference:-

$$q_{out} - q_{in} = \frac{1}{b}[(-G\tau_1 + H\kappa_1')\tau_1 - T\kappa_1'] \tag{2.55}$$

where b is the effective width of the wire strip, accounting for inter-wire gaps.

For a multiple layer pipe, combination of the above expressions for inter layer pressure differences leads to an expression for the difference between pipe internal and external pressures which is a function of the inner layer constriction ΔR_1 only. Solution of the function is by Newton Raphson as it is nonlinear and of complex form. Care has to be taken to replace any negative pressures obtained with gaps.

Witz and Tan (1992, (ii)) also present an analytical model for predicting the flexural structural response for a generic flexible structure which shows that flexure is dependent on relative slip between layers once a critical curvature has been reached. A hysteretic bending moment - curvature relationship exists due to re-establishment of frictional restriction when deformation is reversed. The linear theoretical relationship agrees reasonably well with experimental results.

If the axial strain of a helical strip wound on a cylinder is examined as the cylinder is bent (plane section bending) with the strip assumed to be firmly attached to the side of the cylinder, the final expression for strain is

$$\varepsilon(\theta) = \left[1 - 2R\cos^2\beta_0 \sin\theta\,\kappa_0 + R^2\cos^2\beta_0 \sin^2\theta\,\kappa_0^{\,2}\right]^{1/2} - 1 \qquad (2.56)$$

where R and θ are the usual helical line parameters and κ_0 is the bending curvature. For small curvature this expression can be linearized to

$$\varepsilon(\theta) = -R\cos^2\beta_0 \sin\theta\,\kappa_0 . \qquad (2.57)$$

which is the same as (2.37). The strain energy per unit length of an armour layer is then found by including local bending and twisting in addition to the axial strain of one strip. Differentiation of the resulting average energy with respect to curvature gives the bending moment contribution before slip of a layer consisting of n strips to be

$$M = \tfrac{1}{2}nEAR^2\cos^4\beta_0\,\kappa_0 + \tfrac{1}{2}n\left(EI_n + EI_b\cos^2\beta_0 + GJ\sin^2\beta_0\right)\kappa_0 \qquad (2.58)$$

subscripts n and b referring to the normal and binormal directions of the helix.

As curvature increases it reaches a critical curvature at which slip will begin to occur. The previous result for bending stiffness relies on wire restriction, either structural or frictional. Frictional restriction can be overcome leading to slip occurring in the strip's axial direction (the strip in the case of a flexible riser being of rectangular cross

section, no twisting slip can occur). Slip will first happen in areas where the rate of change of strain is greatest, allowing strain redistribution according to the principle of minimum elastic strain energy. As bending continues these areas will meet leading to, by virtue of very low dynamic friction, zero axial strain in the strip. Strip strain energy after slip is therefore only due to local bending and twisting, removing the first term from the bending moment contribution expression given above.

This is an important departure in the analysis of flexible pipe behaviour, as for the first time energy has been considered in an analytical model. Wire axial, bending and torsional strain energies have been included, while deformation due to shear has been considered negligible.

A thorough, if idealized, analysis of some configurations of wire rope by application of Love's equations is provided by Costello (1990). For the simplest case of an axially loaded strand, which consists of outer wires (not in contact with each other) wound helically around a straight wire core, where it is assumed that the outer wires are not subjected to external bending moments and that their tension is constant, Love's equilibrium equations for each outer wire reduce to

$$\begin{aligned} &-N'\tau_1 + T\kappa_1' + X = 0 \qquad\qquad -G'\tau_1 + H\kappa_1' - N' = 0 \\ &Y = Z = N = \Theta = 0 \end{aligned} \tag{2.59}$$

All wires in the strand have circular cross-sections. Outer wire initial curvatures and twist per unit length are

$$\kappa = 0\ , \qquad \kappa' = \frac{\cos^2 \alpha_0}{R}, \qquad \tau = \frac{\sin \alpha_0 \cos \alpha_0}{R} \tag{2.60}$$

with α_0 and R being the initial helical angle and radius respectively. The deformed configuration is assumed also to be helical, with corresponding curvatures and twist as in (2.60) but with new helical angle and a new radius dependent on Poisson's ratio, and with no additional twist. Initial and subsequent curvatures and twist are related by

(2.50). From these assumptions the strand forces and moments can be found, and the resulting load-displacement relation is linear.

In the separate case of a helical spring under pure bending, the forces and couples X,Y,Z,K,K',Θ,N,N' and T are all equal to zero. This reduces the new equilibrium equations to

$$\begin{aligned}
&\frac{dG}{ds} - G'\tau_1 + H\kappa_1' = 0 \\
&\frac{dG'}{ds} - H\kappa_1 + G\tau_1 = 0 \\
&\frac{dH}{ds} - G\kappa_1' + G\kappa_1 = 0
\end{aligned} \tag{2.61}$$

Substitution for subsequent curvatures and twist from (2.50) into the equilibrium equations yields the following set of coupled non-linear differential equations for the moments and twist at any cross section:-

$$\begin{aligned}
&\frac{dG}{ds} + \left(\frac{1}{EI_y} - \frac{1}{C}\right)G'H - \frac{\sin\alpha_0\cos\alpha_0}{R}G' + \frac{\cos^2\alpha_0}{R}H = 0 \\
&\frac{dG'}{ds} + \left(\frac{1}{C} - \frac{1}{EI_x}\right)GH + \frac{\sin\alpha_0\cos\alpha_0}{R}G = 0 \\
&\frac{dH}{ds} + \left(\frac{1}{EI_x} - \frac{1}{EI_y}\right)GG' - \frac{\cos^2\alpha_0}{R}G = 0
\end{aligned} \tag{2.62}$$

If the spring wire is of circular cross section of radius r and considering the case where $\nu = 0$, the above equations become linear. If the linear solution is used in Picard's method for cases where $\nu \neq 0$ the following expression for spring curvature results where m_s is the applied bending moment.

$$\frac{1}{\rho} = \frac{\left(2 + \nu\cos^2\alpha_0\right)}{2\sin\alpha_0}\frac{4m_s}{\pi r^4 E} \tag{2.63}$$

Assuming that friction has very little effect on bending stiffness, the final expression for the bending stiffness of a strand consisting of m outer wires with a centre wire of radius r_c is given as

$$EI = \frac{\pi E}{4}\left[\frac{2m\sin\alpha}{2+\nu\cos^2\alpha}r^4 + r_c^4\right] \tag{2.64}$$

Where the lay angle is large, Poisson's ratio has little effect, therefore the linear solution can be used to find wire stresses.

2.5.4 Further Thin Rod Equations

A theory of thin rods for use in cable analysis is developed by Ramsey (1988). Cross-sections of the rod are considered to remain plane and normal to the centre line, and not to experience transverse shear deformation. The rod is described by a centre line with a right-handed set of three orthonormal base vectors $\mathbf{a}_i$ associated with all points along it. As the rod deforms, one of these remains aligned along the centre line tangent and the other two rotate as in St Venant's theory of torsion. The rate of change of each vector with respect to the initial arc length co-ordinate S must be of the form

$$\frac{d\mathbf{a}_i}{dS} = \kappa_{ij}\mathbf{a}_j \tag{2.65}$$

using standard summation notation. Furthermore, as $\mathbf{a}_i$ are orthonormal, κ_{ij} is skew-symmetric and can be written

$$\kappa_{ij} = \begin{bmatrix} 0 & (\bar{\tau}+\omega_3) & -(\bar{\kappa}+\omega_2) \\ -(\bar{\tau}+\omega_3) & 0 & \omega_1 \\ (\bar{\kappa}+\omega_2) & -\omega_1 & 0 \end{bmatrix} \tag{2.66}$$

where $\bar{\tau}$ and $\bar{\kappa}$ are the initial centre line torsion and curvature invariants, on the assumption that in the initial unloaded state $\mathbf{a}_i$ are aligned along the centre line normal, binormal and tangent respectively, and ω_i are unknown deformation

variables. From the Seret-Frenet relations and using the fact that $\mathbf{a}_3$ is always aligned along the tangent, the deformed centre line curve curvature and torsion can be written

$$\kappa = \bar{\kappa}(1-\varepsilon)+\omega_2 \qquad \tau = \bar{\tau}(1-\varepsilon)+\omega_3+\frac{1}{\bar{\kappa}}\frac{d\omega_1}{dS} \tag{2.67}$$

where ε is the centre line strain. To accompany (2.67) a linearized set of equilibrium equations the same as Love's equations is needed and, in the case of circular wires, the constitutive relations (2.68),

$$T = EA\varepsilon \qquad G = EI\omega_1 \qquad G' = EI\omega_2 \qquad H = GJ\omega_3 \tag{2.68}$$

in contrast to (2.50) used by Love (1893) and Costello (1990). These equations constitute a theory of thin rods which can be applied to the analysis of wires in cables, and Ramsey gives some examples as follows. For frictionless axi-symmetric loading, wire strained centre line curvature and twist are assumed to be specified. Uniform bending with friction is treated using the deformed cylindrical surface covariant metric tensor to give, again, strained centre line invariants.

For uniform bending without friction, two extra variables are included to account for wire movement across the supporting core surface. The result given shows these movements to be sinusoidal and that the wire is deformed by bending and twisting moments applied at its ends only, so long as there is no contact with adjacent wires.

The effect of an end fitting on the axi-symmetric response of constituent wires is also considered by Ramsey (1991). In a time-dependent version of the theory, the two extra displacement variables are included again, and along the wire length in the absence of friction only the normal contact force per unit length is non-zero. Two simultaneous fourth order ordinary differential equations in the displacement variables result, and boundary conditions are applied by considering loading as an applied angular velocity of the end fitting. The results for the strains ε and ω_i are naturally in two parts, with one giving the constant values away from the end fitting

and the other decaying exponentially with distance from the restraint. The decay constants are dependent only on the cable radius and the initial helical angle, radius and Poisson's ratio of the wire.

2.5.5 Numerical Procedures

Saevik (1993) aims to formulate a local mathematical model to find stresses and slip of tensile armouring tendons including proper consideration of tendon-pipe interaction due to friction (in the asence of an anti-friction layer between tensile layers), geometric stiffening as tendons come under tension, non–constant curvature varying with position and proper representation of end restraint boundary conditions.

Love's non-linear coupled equilibrium equations as explained before can be used to describe the equilibrium of each tendon. In straightforward cases of axisymmetric loading analytical solutions are possible through simplification. Analytical solutions in cases involving pipe flexure are also obtainable but only if constant curvature is assumed. For an arbitrary curvature distribution a finite element model is required, via the Principle of Virtual Displacements.

One individual tendon is considered, on the assumption that it acts independently of neighbouring tendons in its layer, when the pipe has a given curvature distribution. The pipe is then divided into segments each of constant curvature. The intention is to use Washizu's formulation using Green's strain tensor, given large displacements and small strains, and to develop a tailor made curved beam element for finite element modelling.

The stresses at an end fitting for a tendon starting at the neutral axis position are calculated and examined for the effects of load sequence, friction, restraint axial stiffness and pipe radial stiffness. For a pipe under tension and with a prescribed end angle at the restraint, Saevik uses an exponential curvature distribution (from 2D rod analysis, as discussed later in Chapter 4). This, together with choice of tendon position, creates axial stresses due to friction and axial displacement. Load sequence (tension and bending) has no effect on maximum stress range, although the stress-curvature relationship varies significantly. An increase in radial stiffness increases

tendon axial stresses, the effect attenuating, as stiffness level increases, to an almost linear variation over the first two pitches, thereafter settling towards a constant value. The same kind of increase is noted for variation in end restraint axial stiffness.

The effect of friction on tendon maximum bending stresses near the end fitting is shown to be significant. Without friction, secondary bending at the end restraint due to tendon tension causes high stress levels. An increase in friction restrains the tendon, keeping it closer to the strained original path, thus reducing secondary bending effects. The limiting value of stress corresponds to the analytical expression for the normal curvature increment on the strained helix as the pipe is bent.

A theoretical basis for modelling the detailed component and overall structural behaviour of flexible pipe away from any end fitting restraint is presented by McIver (1995). A numerical method is developed including loading consisting of pipe tension, torque, shear forces, bending moments, internal and external pressure, temperature differential and the effects of friction. Layer separation and the possibility of wire contact within the tensile armour layers are important phenomena which are also addressed. Unlike previous analysis of the helical strip components of flexible pipe, McIver allows for the non-symmetrical cross-sections encountered. The main aim in developing the model has been to provide information for wear and fatigue estimation by finding material stresses and slip. Constitutive relations between pipe loads and deformations are also determined. Some results are summarized as follows.

Pressurized pipe response to axial tension alone gives the obvious result that nearly all the load is taken by the tension layers. Barrier layer axial compression due to internal pressure is also resisted by the armour wires, and the inner carcass separates from the barrier due to barrier radial compression.

The application of axial compression causes separation between pressure armour and neighbouring tensile armour layers allowing radial displacement of the tensile armour which leads to significant loss of axial stiffness. Positive torque in conjunction with tension encourages separation between pressure barrier and pressure armour, while when in conjunction with compression causes separation between inner carcass and

pressure barrier. This has no effect on axial stiffness as the tensile armour layers are unaffected. Similarly a negative torque, while causing a different pattern of separation, has no effect on stiffness. The strain-tension and strain-compression relations are linear though with a marked difference in stiffness, while the torque-torsion relationship is virtually linear throughout.

The response to bending is, as already made clear, dependent on the phenomenon of slip. The bending moment-curvature relationship for a pipe under both axial tension and internal pressure is investigated. For zero internal friction nearly all bending stiffness is due to the thermoplastic layers, the armour wires having slipped to allow uniform tension. There is no interaction between bending and axial loads unless wire gaps close due to bending and produce point contact. In the presence of friction, there is a change of stiffness corresponding to the onset of slip. If the dynamic friction is considerably less than the static friction, an abrupt increase in curvature will occur at the onset of slip. The relationship is clearly hysteretic, as on reversal of bending static friction will have to be overcome again. Simple Coulomb friction may not be an adequate modelling of the interlayer friction forces as deformation of thermoplastic layers could lead to greater resistance of neighbouring armour wire movement.

McIver (1998) also examines the simpler problem of the sliding of helically wound strips on a cylinder, without any influence from end fitting restraint. From previous analysis of wire kinematics the displacements, strain, curvatures, torsion and internal and external forces and moments for a helical wire fixed to a cylinder as it is bent into a toroid with constant curvature are expressed. This configuration corresponds to the theoretical infinite friction case and is unrealistic. As a result the wire will slip, with the internal stresses being the driving mechanism acting against friction until equilibrium is reached. This slip can be expressed in components corresponding to strip axial and lateral displacement and rotation about the strip axis. Where there is a rectangular strip as in flexible risers, the rotation component can be assumed to be zero allowing further simplification.

The incremental rotations and changes in strain, curvatures and torsion due to displacement along the wire axes are considered separately from those due to the cylinder curvature, which provide the forcing terms which induce the sliding

displacements. Consideration of a virtual slip displacement allows the construction of the system stiffness matrix by way of substitution of the expressions for strain, curvature and torsion into the virtual work equation, written for one pitch length of the wire. Wire boundary stresses and forces will be the same at each end, with the harmonic virtual displacements being equal and opposite, eliminating them from the equation.

Friction at inner and outer surfaces of the wire is dependent on inter-layer contact pressures, the former enhanced by wire tension and curvature. Where slip takes place the (lower) dynamic friction acts. This results in a discontinuous force distribution, represented by a one-term Fourier expansion (sine curve) in the model.

Results are presented for the extreme cases of infinite and zero friction and also for an intermediate case with assumed friction coefficient, contact pressure and zero initial tension. In each case the wire has a 30 degree lay angle on a cylinder of radius 150mm with 10m radius of curvature, and there is no applied tension. In the infinite friction case, the most significant result is the fact that the transverse restraining force is 'several orders of magnitude smaller' than the axial restraining force, indicating that under finite friction, transverse slip will be much less likely to occur than axial slip.

In the zero friction case, as the rectangular wire is not allowed to rotate, tension, shear and constraining load components remain. Also the relative displacement given in the transverse direction is almost twice that in the axial direction, showing that transverse slip is a significant natural tendency where slip is encouraged by the reduction of friction coefficients. However, the intermediate case with low friction (and no applied tension) shows zero lateral movement indicating that the friction resistance is already sufficient to prevent it, the strip remaining on the strained original path. Strip axial slip is almost the same as in the zero friction case. In comparison, a circular wire displays rotational slip and slightly more axial slip, and all internal and external forces and moments are less apart from the internal moment about the transverse axis which is almost double.

As contact pressure increases from zero, axial slip remains the same while lateral slip 'attenuates smoothly to zero' over quite a small range. Stress in a rectangular wire is

dominated at small curvature by induced tension whereas at higher curvatures the significant component is due to wire bending about its radial principal axis. At high curvatures, maximum stress occurs at the intrados and extrados (inside and outside of the pipe as it is bent), while at lower curvature the location is nearer the neutral axis position.

Saevik (1998) presents a second method for calculation of tensile armour stresses in flexible pipe. Each tendon is considered to interact with the supporting pipe structure by way of a shear interaction force, an approach similar to that of Lutchansky. The Principle of Virtual Displacements is applied by minimisation of the potential energy equation for the sandwich beam representation of the pipe, in which there is a virtual shear layer between core and tendons. From this the local tendon stiffness matrix is calculated. Standard beam formulation is used for the core involving the Green strain tensor.

Layer contact is formulated using a combination of hyperelastic springs and elastoplastic springs for hysteretic forces. External contact is modelled for the situation where a guide tube with bellmouth is in use while the pipe is being terminated. Contact force is modelled by a spring in the tube surface normal direction at point of contact, with force as a function of the difference in pipe and tube diameters and relative displacement between pipe and tube reference nodes.

Three test results are presented. For the first a beam is held against displacement and rotation at one end and rotation at the other, which is displaced a prescribed amount. A very large shear stiffness is used to model the no slip case. Comparison with plane cross section bending results shows excellent correlation. In the second case, a region of pipe is exposed to constant curvature, with zero friction. The results for tendon slip amplitude agree very well with the analytical answer for such an idealized case. The numerical results are not, however, harmonic as in the analytical case, but this is simply due to the test length being two and a half pitch lengths long. Where the tendon is arranged symmetrically along the length of the pipe a harmonic result is duly obtained.

The third test is to find stress ranges in a lifetime test of a 15" riser. The method is compared with actual test results, where loading was by internal pressure, applied tension and bending by rotating bellmouth. In the model, shear interaction is modelled by elastoplastic springs applying the full value of friction after 0.5mm displacement, with friction factor 0.2. Zero relative displacement at the end fitting is prescribed by large shear stiffness in the shear springs along the end fitting elements. Good correlation is achieved between calculated results and strain gauge measurements.

2.5.6 Remarks Regarding Flexible Pipe Structural Analysis

This concludes the review sections on structural behaviour. The flexural behaviour of flexible pipe has been shown to depend on slip of the tensile armour wires, with analysis based on the assumption that the wires will follow a particular curve. The analysis of the effects of an end fitting is limited, with the most significant study being carried out on pipes not suited to dynamic application, and this consisting of a numerical solution for comparison with tests.

Flexible pipe end restraint causes a change from a fully flexible structure to a rigid inflexible structure. This means that there must be a significant change in the modelling of armour wire as its free-field behaviour is dominated by slip which is no longer permitted at the point of restraint. This suggests that an analytical model to study the effects of end restraint on flexible pipe tensile armour should aim to establish with greater reason the path adopted by the wires, from which a new assessment of wire stresses at an end fitting can be made.

Before proceeding with the development of such a model, the final review section presents results from global analyses of flexible pipe behaviour, in which the natural profiles adopted by flexible risers are examined. This is particularly important in establishing the type of profiles and curvatures to be expected in the region of an end fitting.

2.6 GLOBAL PIPE ANALYSIS

Early analysis of flexible pipe characteristics is presented by D'Oliveira et al (1985). For global analysis, a flexible riser is modelled by a cable attached to a beam element in tension with a zero moment condition at the join. The differential equation for a beam-tie is used (small deflections, shear effects negligible) for the beam element part. In this way the catenary profile is modified to take into account the effects of pipe stiffness, which will only be significant near any restraint which adjusts the natural cable gradient.

Assuming small deflections and negligible shear deformation effects, the bending moment distribution pertaining to a long beam tie with fixed support at the origin is

$$M(x) = \left(M + {}^{w}/_{k^2}\right)e^{-kx} - {}^{w}/_{k^2} \tag{2.69}$$

where M is the end bending moment, w is an evenly distributed load and $k^2 = N/EI$, where N is the axial load and EI the pipe bending stiffness (constant). Clearly for a small EI, the bending effects rapidly attenuate and this bending is often referred to as a boundary layer effect. As a result, for the purpose of determining the total bending moment at the riser termination, the riser can be modelled as a cable connected to a beam element under tension. For a value for kx of 5, the bending moment distribution in the beam tie is within 1% of the corresponding cable solution. If it is assumed, then, that the bending moment at the join is zero, an expression for the bending moment at the support is

$$M = w\left[\frac{x(L+x)}{2} - \frac{Lv}{8\gamma}\right] \tag{2.70}$$

where x is measured from the join, L is the horizontal distance between the cable supports, $v(x)$ is the beam deflection and $\gamma = h/L$, h being the cable sag at $x_1 = L/2$. Using the maximum cable tension for N, the beam k can be found, giving the length x of the beam element. From the boundary conditions $y(0) = y'(0) = 0$, $y'(x) = 4\gamma$,

$$v = 4\gamma\frac{(kx-1)}{k} - \frac{wkx\left(1 - {}^{kx}/_{2}\right)}{k^2 N} \tag{2.71}$$

which can be substituted to give the support bending moment.

The analysis highlights the fact that riser profiles are essentially catenary profiles, but that because the pipe has stiffness, the profile is likely to be altered in the region of any restraint. This alteration will be local, the rest of the unrestrained riser following the natural profile, and hence is only a boundary layer phenomenon.

For a further perspective on riser global behaviour, work has been done at UCL to investigate the dynamics of the various configurations of flexible risers and presented by Baradaran Seyed (1989) and Patel, Witz and Tan (1993). Baradaran Seyed gives an exact result for the integration of fluid pressure over the surface area of a pipe, assuming constant curvature, (an assumption which makes it ideal for finite element analysis,) and also an approximation to slug flow forces for an assumed steady flow.

Inclusion of hydrostatic pressures in the beam column analysis leads to an altered governing differential equation for a vertical marine riser, valid for small deflections only :-

$$\frac{d^2}{dy^2}\left(EI\frac{d^2x}{dy^2}\right)-\left[T(y)+A_0p_0-A_ip_i\right]\frac{d^2x}{dy^2}-\left(\gamma_sA_s-\gamma_0A_0+\gamma_iA_i\right)\frac{dx}{dy}=f \qquad (2.72)$$

A_0 and A_i are the cross sectional areas of the riser bore and the riser cross-section respectively, p_i and p_0 are internal and external pressures and γ_s, γ_0 and γ_i are specific weights of the riser wall, external fluid and internal fluid respectively. Comparison of (2.72) with the simple beam column equation leads to the concepts of effective weight and effective tension, as given by the coefficients of the first and second derivatives of y respectively. As this equation is only valid for small deflections, a more rigorous analysis is required for the more arbitrary geometry of a flexible riser. Considering equilibrium of axial forces, vertical and horizontal forces due to hydrostatic pressures, normal drag force, pipe weight and forces due to slug flow, a more general equation is

$$\left(T + p_0 A_0 - p_i A_i - \rho_i A_i U_i^2\right)\frac{d^2 y}{dx^2}\left[1+\left(\frac{dy}{dx}\right)^2\right]^{-1} - \left(\gamma_s A_s - \gamma_0 A_0 + \gamma_i A_i - N_y\right) - \frac{dV}{dx} - N_x \frac{dy}{dx} = 0 \tag{2.73}$$

where $\rho_i A_i U_i$ is the fluid rate of change of momentum, N is an external drag force and V is the shear force. Note the complete effective weight and effective tension terms in (2.73). This equation is difficult to solve and thus flexible riser static and dynamic analysis is carried out using finite element or finite difference methods. The formulation of finite element models is given by Patel, Witz and Tan (1993).

The polar form of the equation is

$$\left(T + P_0 A_0 - P_i A_i - \rho_i A_i U_i^2\right)\frac{d\theta}{ds} - \frac{dV}{ds} + \left(\gamma_0 A_0 - \gamma_i A_i\right)\left(\cos\theta - \sin\theta\, d\theta\right) - N_x \sin\theta + \left(N_y - w\right)\cos\theta = 0 \tag{2.74}$$

On neglecting flexural effects and fluid drag forces this becomes

$$T_{eff}\frac{d\theta}{ds} - w_{eff}\cos\theta - \left(\gamma_0 A_0 - \gamma_i A_i\right)\sin\theta d\theta = 0 \tag{2.75}$$

which compares with $T\,d\theta/ds - w\cos\theta = 0$, the equation of equilibrium for a simple catenary. Thus using the effective weight and effective tension, catenary solutions can be used for the static profiles of flexible risers subjected to self weight, pressure forces and steady internal flow giving results good enough for preliminary design. However with increasing complexity of risers and their loading, finite element analysis is used to find static profiles, though care has to be taken to overcome ill-conditioning due to the large difference in pipe axial and flexural stiffnesses.

The geometry, stresses, natural frequencies and dynamic response characteristics of flexible risers can be given by a modal decomposition method. Although not

necessarily being very accurate, such analysis can give useful prior knowledge for accurate finite element modelling. In essence, the mode shapes are determined through an eigenvalue analysis such as the Rayleigh-Ritz method. Substitution of these into the equation of dynamic equilibrium allows, with harmonic forcing and response, summation of responses up to the required mode giving the total deflection. Integration of the modal 'participation parameters' requires linearisation of the loading function which consists of dynamic wave force with structural and drag damping.

Frequency domain finite element analysis is rapid and can be applied to both regular and irregular waves. However, as mentioned above it does have shortcomings, involving approximations associated with linearisation of drag forces and other non-linearities such as change in wetted length of the riser with the passage of waves. Fully non-linear time domain analysis gives reliable results for problems also including sea-bed contact and material non-linearity. As this full analysis requires large amounts of time and computer storage space it is generally only used in such cases, the use of linear techniques giving good accuracy where time domain analysis is required.

Flexible pipe, especially where intended for dynamic application, may well have a bend stiffener to limit curvature in the vicinity of any more rigid connection. Sødahl (1991) includes a section on bend stiffener design.

Considering all possible extreme combinations of end force and force angle (difference in direction of pipe centre-line between top end of the bend stiffener and straight part of the riser) from stochastic wave modelling, the problem is reduced to finding a bending stiffness function while bearing in mind that the support moment is directly proportional to bending stiffener length. An initial design is chosen considering moment equilibrium of the bend stiffener alone (without adjacent riser part), with constant radius of curvature equal to the pipe critical value. The maximum tension and maximum force angle are taken as the design point and using the riser stiffness EI_r at the bend stiffener bottom end an equation for EI is found as a function of position along the stiffener (R_{cr} is the critical radius of curvature).

$$EI(s) = EI_r + 2T_{\max} R_{cr}^2 \sin^2\left(\frac{s}{2R_{cr}}\right) \tag{2.76}$$

With the given maximum force angle the minimum length of the stiffener (constant curvature) is prescribed.

A final design needs to be reached from this starting point. Using the initial result and now considering the initial part of the riser, e.g. 1.5m of it, next to the bend stiffener, curvatures for combinations of tension and angle along the chosen design line can be calculated, using a 'shooting method' to solve the two point boundary value problem. The rest of the riser, immediately adjacent to the initial part, is considered straight.

The curvatures calculated will turn out to be too large, exceeding the critical curvature in the bend stiffener close to the 'join' with the rest of the pipe. The initial design is too short and too stiff. Sødahl gives an iterative procedure to find a design radius of curvature and a design force while keeping the force angle fixed at the maximum, by optimising the effects of variations in force and radius of curvature while keeping the length of the stiffener to a minimum. Such effects are displayed graphically in the form of dimensionless design curves, giving design force and radius of curvature in terms of maximum force angle and a non-dimensional stiffness parameter. An example is given where the result is a reduced maximum force and an increased length of bend stiffener with maximum curvature reduced to the critical value at each end.

Consideration is given to the length of the riser part which is taken to be influenced by the bend stiffener. The effect this has on the design curves is shown in graphical form to diminish beyond a length of four fifths of a radius of curvature. (i.e. $S_r/R_{cr} = 0.8$) Thus it is safe to treat the rest of the riser beyond this initial part as straight for the purpose of bend stiffener design.

3 TENSILE ARMOUR STRESSES AND SLIP NEAR AN END FITTING

3.1 INTRODUCTION

Love's equilibrium equations are shown in the literature review to give analytical solutions only to simplified cases of thin rod loading, the more complicated wire rope analysis being reduced to that of axisymmetric loading or flexure at constant radius of curvature.

Many papers address the phenomenon of slip, which governs a flexible pipe's response to flexure. Slip is considered by some to be adequately measured by the consideration of axial slip along the strained helix, while others assume that a movement to a new geodesic curve is the controlling factor. Both curves are at least considered to be the limit curves for wire slip, the actual path probably being somewhere in between. Most such models are based on pipe sections away from any end fitting restraint, although an assumption of axial slip alone does allow the use of boundary conditions appropriate to end restraint of the wire.

The use of numerical analysis or finite element modelling to solve virtual work equations gives solutions based on the total pipe's behaviour, allowing results varying from global response to individual component stresses and displacements. Some such models are still for free field application, although complex structural modelling allows investigation of stresses at the end fitting, and the relative influence of the parameters affecting tensile armour wire behaviour. These results may be useful in guidance towards the formulation of analytical models.

The following is a description of an analytical method developed to address the problem of tensile armour wire behaviour in the region of an end fitting.

3.2 TENSILE ARMOUR WIRE ASSUMPTIONS

A tensile armour wire has a uniform rectangular cross-section (section A-A, Figure 3.1). In any cross-section, an axis drawn through the centre and perpendicular to the longer sides is coincident with the normal to the supporting cylindrical surfaces (Figure 3.1). In the initial unloaded state the centre line joining the centres of all cross-sections is a helix. The line of contact between the wire and the inner supporting cylinder surface is also a helix.

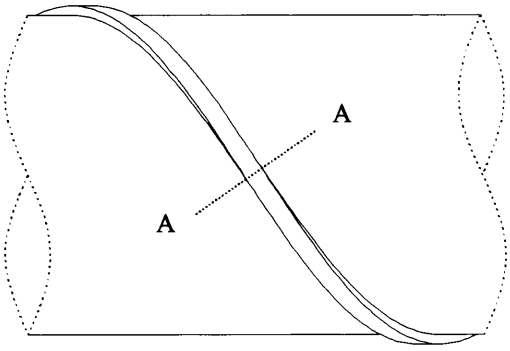

Section A – A

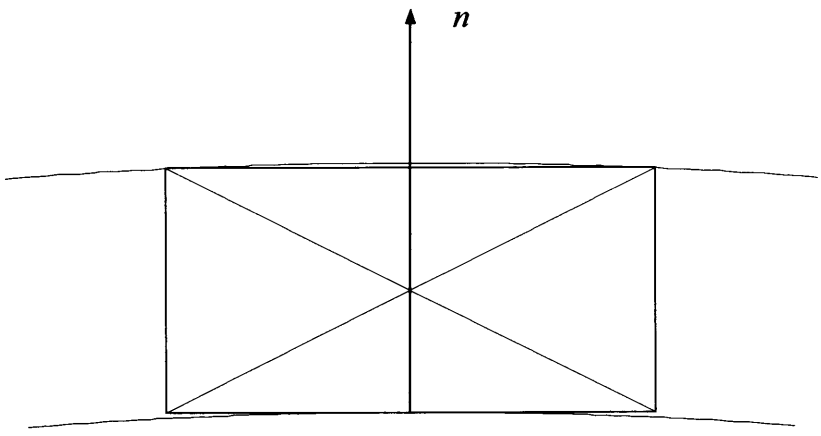

Figure 3.1 Right–hand helical tensile armour wire and cross-section.

The pipe cross-section is assumed to remain circular at all times, and due to the presence of pressure armour to provide smooth sufaces of constant radius for the tensile armour wires to move on. As the cylindrical pipe is stretched or bent, the wire moves away from the strained contact helix to a new position, with a new contact curve on the supporting surface. Wire and surface, on either side of the contact curve, have different strains. Wire cross-sections are assumed to remain plane and normal to the surface.

The new configuration of the wire centre line is what is required, and this can be thought of as resulting from a combination of two changes. Firstly, movement of the wire on the original cylindrical surface, and secondly, in the case of bending, an applied curvature.

The wire is assumed to slip between the surfaces in the absence of friction and to act independently of adjacent wires in the same layer. End restraint maintains the wire's original orientation at these points.

The new path of the single tensile armour tendon is taken to vary slightly from the initial helical path and to be described by the deviation through small angle $\alpha(s)$ from the initial helical angle α_0, with the boundary condition that $\alpha_{s=0} = 0$. The distribution of $\alpha(s)$ can be investigated by the minimisation of strip strain energies due to twist, bending and axial strain, within the constraints of the pipe loading. This is therefore an isoperimetric problem which can be solved using the Euler-Lagrange equation with a Lagrange multiplier.

3.3 WIRE STRAIN ENERGY

3.3.1 Strain Energy Integral

Elastic Strain Energy V_0 for the whole of a body is given in terms of stresses by the integral (Timoshenko, 1970, p. 246)

$$V_0 = \int\left(\frac{1}{2E}\left(\sigma_x{}^2 + \sigma_y{}^2 + \sigma_z{}^2\right) - \frac{\nu}{E}\left(\sigma_x\sigma_y + \sigma_y\sigma_z + \sigma_z\sigma_x\right) + \frac{1}{2G_1}\left(\tau_{xy}{}^2 + \tau_{yz}{}^2 + \tau_{zx}{}^2\right)\right)dV$$

In the case of a tensile armour wire the only significant stresses are the direct axial stress σ_z from wire tension and bending, and the shear stresses τ_{yz} and τ_{zx} due to twisting. This is based on neglecting shear strains γ_{yz} and γ_{zx} from bending due to the slenderness of the wire, and also neglecting γ_{xy} consistent with Prandtl's theory of torsion, presented by Timoshenko (1970, p. 293). Therefore the integral reduces to

$$V_0 = \int\left(\frac{1}{2E}\sigma_z{}^2 + \frac{1}{2G_1}\left(\tau_{yz}{}^2 + \tau_{zx}{}^2\right)\right)dV \qquad (3.1)$$

This can be expressed in terms of the individual strains as follows, beginning with the direct stress term.

3.3.2 Axial Stress Term

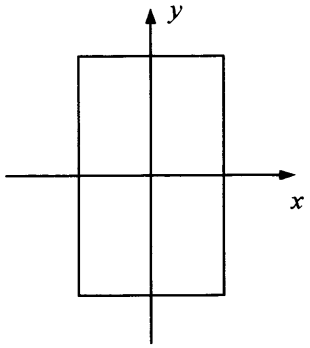

Figure 3.2 Rectangular Cross-Section.

Using simple beam theory as appropriate for a thin rod, the axial stress at any point in the wire is (Figure 3.2)

$$\sigma_z = \sigma_a + yE\Delta\kappa_n + xE\Delta\kappa_b \tag{3.2}$$

where x and y are as shown and $\Delta\kappa_b$ and $\Delta\kappa_n$ are the appropriate changes in curvature. As a result

$$\frac{1}{2E}\sigma_z^{\,2} = \frac{1}{2E}\left\{(E\varepsilon_a)^2 + (E\Delta\kappa_n)^2 y^2 + (E\Delta\kappa_b)^2 x^2 + 2\left(y\sigma_a E\Delta\kappa_n + x\sigma_a E\Delta\kappa_b + xyE^2\Delta\kappa_n\Delta\kappa_b\right)\right\} \tag{3.3}$$

Therefore for a wire of length L

$$\int \frac{1}{2E}\sigma_z^{\,2} dV = \int_0^L \int \left((E\varepsilon_a)^2 + (E\Delta\kappa_n)^2 y^2 + (E\Delta\kappa_b)^2 x^2\right) dA dz \tag{3.4}$$

as $\int ydA = \int xdA = \int xydA = 0$ for symmetrical cross-sections.

So finally, denoting the cross-section second moments of area about the principal axes by I_n and I_b,

$$\int \frac{1}{2E}\sigma_z^{\,2} dV = \frac{1}{2E}\int_0^L \left(A(E\varepsilon_a)^2 + I_n(E\Delta\kappa_n)^2 + I_b(E\Delta\kappa_b)^2\right) dz$$

$$= \tfrac{1}{2}\int_0^L \left(EA\varepsilon_a^{\,2} + EI_n(\Delta\kappa_n)^2 + EI_b(\Delta\kappa_b)^2\right) dz \tag{3.5}$$

3.3.3 Shear Stresses Term

The shear stresses included come only from changes in twist from the original twist and it is therefore easier to consider the work done by the twisting moment as the wire twists. The section polar moment of area cannot be used as the cross-section is

rectangular. For a rectangular section as shown in Figure 3.2 with sides of length A and B with $A < B$, the twisting moment is given by (Timoshenko, 1970, p. 313)

$$M_t = kG_1 \Delta\tau A^3 B$$

where $\Delta\tau$ is the change in twist per unit length of the wire and k is a factor dependent on the ratio B/A. Integrating this with respect to the change in twist gives the energy to be

$$\int_0^L \int M_t d(\Delta\tau) dz = \int_0^L \tfrac{1}{2} k G_1 A^3 B \Delta\tau^2 dz = \tfrac{1}{2} \int_0^L k_1 G_1 I_{\min} \Delta\tau^2 dz \qquad (3.6)$$

where $k_1 = 12k$ and $I_{\min}$ is the smaller of the two second moments of area I_n and I_b. Some values of k_1 are given in Table 3.1 below.

B/A	k_1
1	1.69
1.2	1.99
1.5	2.35
2	2.75
2.5	2.99
3	3.16
4	3.37
5	3.49
10	3.74
∞	4

Table 3.1 Values of k_1 for selected B/A ratios.

Hence the complete energy integral is

$$V_0 = \tfrac{1}{2} \int_0^L \left(EA\varepsilon_a^{\,2} + EI_n (\Delta\kappa_n)^2 + EI_b (\Delta\kappa_b)^2 + k_1 G_1 I_{\min} (\Delta\tau)^2 \right) dz \qquad (3.7)$$

3.4 AXI-SYMMETRIC LOADING WITHOUT FRICTION

The simplest pipe loading case involves axi-symmetric loading only, and no friction. Under such loading the pipe remains straight and is subjected to either tensile loading, twisting about the centre-line, or both. The pipe is considered to remain cylindrical with no change in the radius. Therefore the wire loading can be described by displacements of the far end compatible with the pipe loading, consisting of a displacement parallel to the pipe axis and a circumferential displacement.

The following sections cover wire kinematics and equilibrium, allowing the energy functional to be developed in terms of the small change in helical angle. With an appropriate constraint from the loading displacements the energy functional is minimized to find the distribution of the change in helical angle along the wire.

3.4.1 Wire Kinematics and Equilibrium

Pipe and Helix Geometry

The schematic in Figure 3.3 shows the essential geometry for a helical line of length L and helical angle α_0 on a cylindrical element of length L_p subjected to strain ε_p and twist defined by the number of turns ϕ_p per unit length. The element has been developed so as to show the original and strained helical lines as continuous lines and the cylinder strains have been grossly exaggerated to show the angle β between them. Cylinder radius and therefore line helical radius are assumed to remain constant.

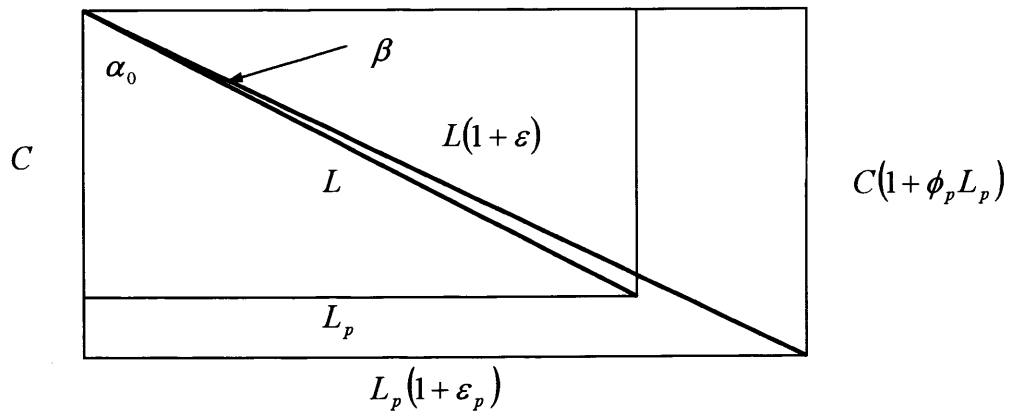

Figure 3.3 Schematic showing original and strained cylinder geometry.

Strained geometry

$$L^2(1+\varepsilon)^2 = C^2(1+\phi_p L_p)^2 + L_p{}^2(1+\varepsilon_p)^2 \tag{3.8}$$

Original geometry

$$L^2 = C^2 + L_p{}^2 \tag{3.9}$$

$$L_p = L\sin\alpha_0 \tag{3.10}$$

$$\tan\alpha_0 = \frac{L_p}{C} \tag{3.11}$$

Subtracting (3.9) from the strained geometry and using (3.10), to first order in the strains

$$L^2.2\varepsilon = C^2\left(2\phi_p L_p + (\phi_p L_p)^2\right) + L_p{}^2.2\varepsilon_p$$

$$\varepsilon = C^2\left(\frac{\phi_p \sin\alpha_0}{L} + \frac{\phi_p{}^2\sin^2\alpha_0}{2}\right) + \sin^2\alpha_0\varepsilon_p \tag{3.12}$$

For a more exact expression, using (3.11) and (3.10) in the strained geometry

$$L^2(1+\varepsilon)^2 = \frac{L_p{}^2}{\tan^2\alpha_0}(1+\phi_p L_p)^2 + L_p{}^2(1+\varepsilon_p)^2$$

$$L(1+\varepsilon) = L\sin\alpha_0\left(\left(\frac{1+\phi_p L_p}{\tan\alpha_0}\right)^2 + (1+\varepsilon_p)^2\right)^{1/2} \tag{3.13}$$

Finally the constant angle β is given by

$$\beta = \alpha_1 - \alpha_0 = \tan^{-1}\left(\frac{L_p(1+\varepsilon_p)}{C(1+\phi_p L_p)}\right) - \alpha_0 = \tan^{-1}\left(\tan\alpha_0\left(\frac{1+\varepsilon_p}{1+\phi_p L_p}\right)\right) - \alpha_0 \tag{3.14}$$

where α_1 is the helical angle of the strained helical line. Application of axial strain only to the element without any twist would leave C unaltered in the above geometry. Setting ϕ_p to zero simplifies the above expressions to

$$\varepsilon = \sin^2\alpha_0\varepsilon_p \qquad L(1+\varepsilon) = L\sin\alpha_0\left(\frac{1}{\tan^2\alpha_0} + (1+\varepsilon_p)^2\right)^{1/2}$$

$$\beta = \tan^{-1}\left(\tan\alpha_0(1+\varepsilon_p)\right) - \alpha_0$$

Tensile Armour Bending and Twist

Helical Wire

Figure 3.4 shows a right-handed helix and a short length of armour wire with rectangular cross-section. Curvature is represented by a vector in the direction of the axis of curvature and, because of the wire constraints, components of this give the wire twist τ and binormal curvature κ', as shown. These are known in terms of the wire centre line helical radius R and instantaneous helical angle $\alpha_0 + \alpha$.

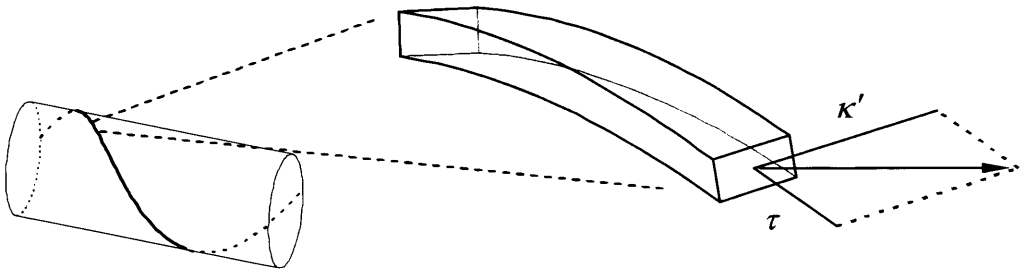

Figure 3.4 Right-hand helical strip section.

Wire initial twist and curvatures are

$$\kappa = 0 \qquad \kappa' = \frac{1}{R}\cos^2\alpha_0 \qquad \tau = \frac{1}{R}\cos\alpha_0 \sin\alpha_0 \tag{3.15}$$

For a new helix with helical angle $\alpha_0 + \alpha$ these become

$$\kappa = 0 \qquad \kappa' = \frac{1}{R}\cos^2(\alpha_0 + \alpha) \qquad \tau = \frac{1}{R}\cos(\alpha_0 + \alpha)\sin(\alpha_0 + \alpha) \tag{3.16}$$

Using double angle formulae and retaining only terms to first order in α, the binormal curvature and twist are

$$\kappa' = \frac{1}{R}\cos^2\alpha_0 - \frac{2\alpha}{R}\cos\alpha_0 \sin\alpha_0 \qquad \tau = \frac{1}{R}\cos\alpha_0 \sin\alpha_0 + \frac{\alpha}{R}\left(1 - 2\sin^2\alpha_0\right) \tag{3.17}$$

Wire with Small Departure from Helical Form

A helix is a specific geodesic on a cylindrical surface and therefore, at any point on the helix, its normal and the surface normal are parallel and the helix has no transverse curvature. A curved wire on a cylindrical surface, that is with transverse curvature, will at each point have its tangent concurrent with the tangent of a helix. This helix will indicate the components of curvature as shown above for the wire, while the curvature on the surface will be an additional normal curvature. Figures 3.5 and 3.6 show such a strip section and associated curvature components.

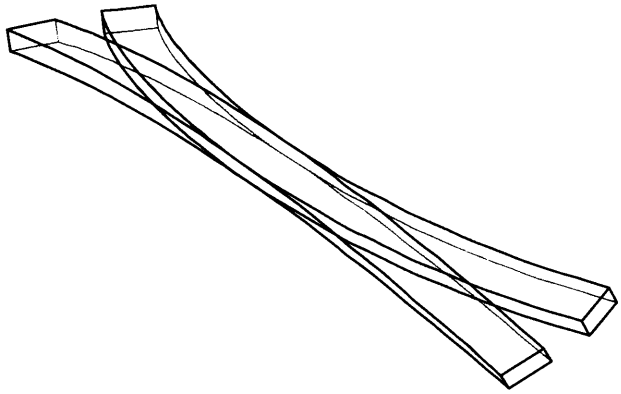

Figure 3.5 Curved strip and right-hand helical strip sections.

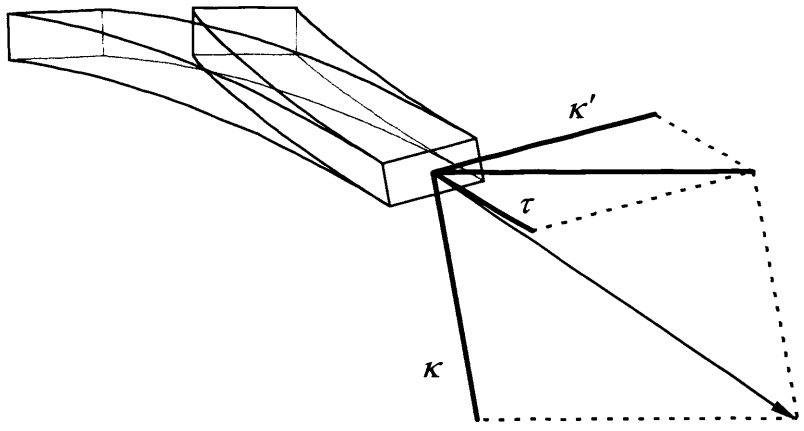

Figure 3.6 Strip section and curvatures.

The normal curvature leaves the helical components at the point unaltered and is given for a right-handed wire by

$$\kappa = -\frac{d\alpha}{ds} \tag{3.18}$$

Tensile Armour Tension

Equilibrium Equations

Wire tension for axial strain energy can be found using Love's thin rod equilibrium equations and standard constitutive relations from Hooke's Law. In the absence of friction, Love's equations are

$$\begin{aligned}
&\frac{dN}{ds} - N'\tau + T\kappa' + X = 0 && \frac{dG}{ds} - G'\tau + H\kappa' - N' = 0 \\
&\frac{dN'}{ds} - T\kappa + N\tau = 0 && \frac{dG'}{ds} - H\kappa + G\tau + N = 0 \\
&\frac{dT}{ds} - N\kappa' + N'\kappa = 0 && \frac{dH}{ds} - G\kappa' + G'\kappa + \Theta = 0
\end{aligned} \tag{3.19}$$

Substitution for shear stresses in the last (axial) force equilibrium equation gives

$$\begin{aligned}
&\frac{dT}{ds} + \frac{dG'}{ds}\kappa' - H\kappa\kappa' + G\tau\kappa' + \frac{dG}{ds}\kappa - G'\tau\kappa + H\kappa\kappa' = 0 \\
&\frac{dT}{ds} + \frac{dG'}{ds}\kappa' + \frac{dG}{ds}\kappa + \tau\left(G\kappa' - G'\kappa\right) = 0
\end{aligned} \tag{3.20}$$

As the initial curvatures κ_0 and κ_0' and the strip cross-section are constant, this simplifies further to

$$\frac{dT}{ds} + \frac{EI_2}{2}\frac{d}{ds}\left(\kappa'^2\right) + \frac{EI_1}{2}\frac{d}{ds}\left(\kappa^2\right) + \tau\left(G\kappa' - G'\kappa\right) = 0 \tag{3.21}$$

Application of the kinematic relations gives wire curvatures and twist and the respective moments to be

$$\kappa = -\frac{d\alpha}{ds} \qquad G = EI_1\left(-\frac{d\alpha}{ds}\right)$$

$$\kappa' = \frac{\cos^2\alpha_0}{R} - \frac{2\alpha}{R}\cos\alpha_0 \sin\alpha_0 \qquad G' = EI_2\left(-\frac{2\alpha}{R}\cos\alpha_0 \sin\alpha_0\right) \tag{3.22}$$

$$\tau = \frac{\cos\alpha_0 \sin\alpha_0}{R} + \frac{\alpha}{R}\left(1 - 2\sin^2\alpha_0\right) \qquad H = G_1 k_1 I_2\left(\frac{\alpha}{R}\left(1 - 2\sin^2\alpha_0\right)\right)$$

where G_1 is the shear modulus. Substitution of these into the tension equation and considering terms up to first order in α gives

$$T = \frac{2EI_2 + EI_1}{R^2}\cos^3\alpha_0 \sin\alpha_0\, \alpha + T_0$$

$$= A_1\alpha + T_0 \tag{3.23}$$

Tension Constant T_0

The angle β (Figure 3.3) describes a known path on the supporting cylinder, which is a new helix. The distribution of $(\beta - \alpha)$ represents a deviation of the wire from this known path (Figure 3.7) which must therefore lead to a change in arc length. This change will determine the overall level of tension in the wire. Although Love's differential equations have shown the dependence of the wire tension on the function α, the resulting constant of integration, tension T_0, is also dependent on α, to a much more significant degree.

There is an end restraint on the wire orientation but the total projection of the wire on the known path between its two ends must be constant and equal to $L + \Delta L$, where L is the original helical wire length and ΔL is the change in this length. This means that, for small α and β,

$$\int_0^L (1+\varepsilon_a)\cos(\beta-\alpha)ds = \int_0^L (1+\varepsilon_a)\left(1 - \frac{(\beta-\alpha)^2}{2}\right)ds = L + \Delta L \tag{3.24}$$

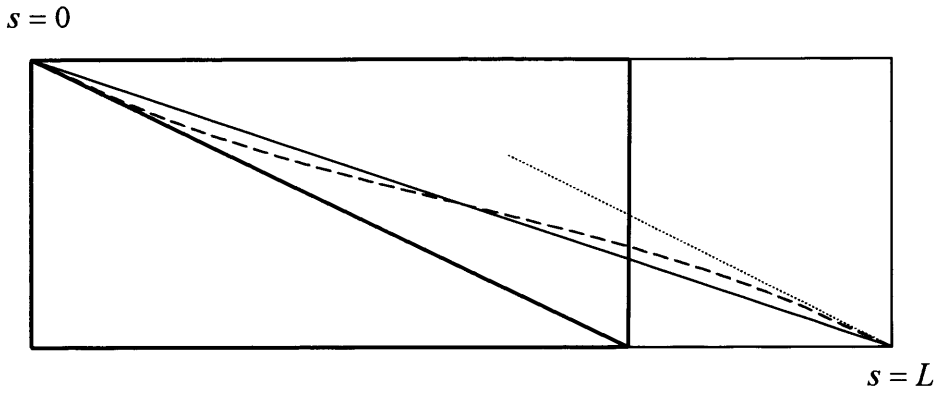

Figure 3.7 Developed cylindrical surface schematic showing strained original right-hand helix and strained wire (dashed).

Substituting using (3.23) for the axial strain from Love's equations,

$$\int_0^L \left(1+\frac{A_1}{EA}\alpha+\frac{T_0}{EA}\right)\cos(\beta-\alpha)ds = L+\Delta L$$

$$\Rightarrow \int_0^L \left(\frac{T_0}{EA}+\frac{A_1}{EA}\alpha-\frac{(\beta-\alpha)^2}{2}\right)ds = \Delta L \tag{3.25}$$

The change in length ΔL is simply (Figure 3.3)

$$\Delta L = L\varepsilon \tag{3.26}$$

Hence

$$\frac{T_0 L}{EA}+\int_0^L \left(\frac{A_1}{EA}\alpha-\frac{(\beta-\alpha)^2}{2}\right)ds = L\varepsilon$$

or,

$$T_0 = T_{00}+\frac{EA}{L}\int_0^L \left(\frac{(\beta-\alpha)^2}{2}-\frac{A_1}{EA}\alpha\right)ds \tag{3.27}$$

where T_{00} is $EA\varepsilon$.

Therefore wire tension is given by

$$T = T_{00} + A_1\alpha + \frac{EA}{L}\int_0^L \left(\frac{(\beta-\alpha)^2}{2} - \frac{A_1}{EA}\alpha \right) ds \tag{3.28}$$

Equation (3.28) shows that the wire tension has a significantly greater dependence on the average value of α^2 than it does on α, as the dimensionless ratio $A_1 : EA$ is typically of order 10^{-4}

Lateral Constraint

The end $s = L$ of the wire moves due to pipe axial strain and twist, and this movement must be matched by the total axial strain in the entire wire and its total circumferential displacement (see Figure 3.7). Calculation of the tension constant T_0 has made use of the axial wire constraint (3.24) which ensures the wire projection is correct, in other words that it is the correct length. The required lateral or orthogonal constraint, ensuring that the wire end is in the right place, is of the same form and is simply

$$\int_0^L (1+\varepsilon_a)\sin\alpha ds = C_1$$

or to first order in the small angle α

$$\int_0^L \alpha ds = C_1 \tag{3.29}$$

Constant C_1, by reference to Figure 3.3, is given by

$$C_1 = \int_0^L \beta(1+\varepsilon) ds$$

For small and constant β and ε this simplifies to

$$C_1 = \beta L \tag{3.30}$$

3.4.2 Energy Functional and Minimisation

Total strain energy for an armour wire length L, neglecting shear deformations, is

$$\tfrac{1}{2}\int_0^L \left(EA\varepsilon_a{}^2 + EI_1\kappa^2 + EI_2(\kappa' - \kappa_0')^2 + G_1k_1I_2(\tau - \tau_0)^2\right)ds \tag{3.31}$$

The strains involved in this expression have been discussed in the preceding section for a wire with the correct length and with consistent curvature and twist as defined by a deviation from a 'known path'. This description has included a lateral constraint at the far end of the wire. Inclusion of this constraint adds another term to the functional which will now have the form given below.

$$\tfrac{1}{2}\left(EA\varepsilon_a{}^2 + EI_1\kappa^2 + EI_2(\kappa' - \kappa_0')^2 + G_1k_1I_2(\tau - \tau_0)^2\right) + \lambda\alpha \tag{3.32}$$

To find the extremal function, the Euler-Lagrange equation in general is, for a functional F involving nth order differentials of the function $y(x)$ (Boas, 1983, p. 388),

$$\sum_{m=0}^{n}(-1)^m \frac{d^m}{dx^m}\left(\frac{\partial F}{\partial y^{(m)}}\right) = 0 \tag{3.33}$$

Here the functional for the Euler equation is of the form $F + \lambda G$ where F is the energy equation and λG reflects the constraint. The function to be found in this way will either be α or γ, depending on the pipe loading in question.

Functional Terms

Axial Strain Energy

The tension expression with expanded tension constant is (equation (3.28))

$$T = T_{00} + A_1\alpha + \frac{EA}{L}\int_0^L \left(\frac{(\beta-\alpha)^2}{2} - \frac{A_1}{EA}\alpha \right) ds$$

Substitution gives the axial strain contribution to the energy equation as

$$\int_0^L \tfrac{1}{2} EA\varepsilon_a{}^2 ds = \int_0^L \tfrac{1}{2} EA \left(\varepsilon + \frac{A_1}{EA}\alpha + \int_0^L \frac{1}{L}\left(\frac{(\beta-\alpha)^2}{2} - \frac{A_1}{EA}\alpha \right) ds \right)^2 ds$$

The terms in the strain expression are not all of the same order.[1] It is dominated by the strain ε and therefore to first order the contribution is

$$\int_0^L \tfrac{1}{2} EA \left(\varepsilon^2 + 2\varepsilon \left(\frac{A_1}{EA}\alpha + \int_0^L \frac{1}{L}\left(\frac{(\beta-\alpha)^2}{2} - \frac{A_1}{EA}\alpha \right) ds \right) \right) ds$$

As the inner integral in the double integral term is ultimately independent of s, the outer integral yields L, which cancels, giving

$$\int_0^L \tfrac{1}{2} EA \left(\varepsilon^2 + 2\varepsilon \left(\frac{(\beta-\alpha)^2}{2} \right) \right) ds \qquad (3.34)$$

[1] From Figure 3.3 β can be seen to be of the same order as α. From equations (3.12) and (3.14) the ratio of ε to β is close to unity for typical values of α_0. Therefore the respective orders of the terms in the strain expression are as follows.

$$o(\varepsilon) = o(\beta)$$
$$o\left(\frac{A_1}{EA}\alpha \right) = o\left(\beta \times 10^{-4} \right)$$
$$o\left(\frac{(\beta-\alpha)^2}{2} \right) = o(\beta^2)$$

Normal Bending Strain Energy

Initial wire normal bending is zero and using (3.18) the strain energy is

$$\int_0^L \tfrac{1}{2} EI_1 \kappa^2 ds = \tfrac{1}{2} EI_1 \int_0^L \left(-\frac{d\alpha}{ds} \right)^2 ds \tag{3.35}$$

Binormal Bending Strain Energy

Using (3.15) and (3.17) binormal bending strain energy is given by

$$\int_0^L \tfrac{1}{2} EI_2 (\kappa' - \kappa_0')^2 ds = \tfrac{1}{2} EI_2 \int_0^L \left(-\frac{2\alpha}{R} \cos\alpha_0 \sin\alpha_0 \right)^2 ds \tag{3.36}$$

Twisting Strain Energy

Similarly twisting strain energy is

$$\int_0^L \tfrac{1}{2} EI_2 (\tau - \tau_0)^2 ds = \tfrac{1}{2} G_1 k_1 I_2 \int_0^L \left(\frac{\alpha}{R} \left(1 - 2\sin^2 \alpha_0 \right) \right)^2 ds \tag{3.37}$$

Lateral Constraint

This has already been established as

$$\int_0^L \lambda \alpha ds \tag{3.38}$$

Minimisation of the Functional

Strain energies due to twist, curvature and axial strain have now all been expressed in terms of α, its first derivative, and constants associated with the original helix and the wire material and cross-section. The constraint has also been expressed in terms of α. The general Euler-Lagrange equation has already been introduced (equation (3.33)), but in this case the variable is only present up to the first derivative with respect to the independent arc length variable s and so the equation reduces to

$$\frac{\partial(F+\lambda G)}{\partial\alpha}-\frac{d}{ds}\left(\frac{\partial(F+\lambda G)}{\partial\alpha'}\right)=0 \tag{3.39}$$

Contributions from each term in the functional are as follows.

Axial Strain Energy

$$\int_0^L \tfrac{1}{2}EA\left(\left(\frac{T_{00}}{EA}\right)^2+2\left(\frac{T_{00}}{EA}\right)\left(\frac{(\beta-\alpha)^2}{2}\right)\right)ds$$

$$\begin{aligned}\frac{\partial}{\partial\alpha}&: \quad T_{00}(\alpha-\beta)\\ \frac{d}{ds}\left(\frac{\partial}{\partial\alpha'}\right)&: \quad 0\end{aligned} \tag{3.40}$$

Normal Bending Strain

$$\int_0^L \tfrac{1}{2}EI_1\kappa^2 ds=\tfrac{1}{2}EI_1\int_0^L\left(-\frac{d\alpha}{ds}\right)^2 ds$$

$$\begin{aligned}\frac{\partial}{\partial\alpha}&: \quad 0\\ \frac{d}{ds}\left(\frac{\partial}{\partial\alpha'}\right)&: \quad EI_1\left(\frac{d^2\alpha}{ds^2}\right)\end{aligned} \tag{3.41}$$

Binormal Bending Strain

$$\int_0^L \tfrac{1}{2}EI_2(\kappa'-\kappa_0')^2 ds=\tfrac{1}{2}EI_2\int_0^L\left(-\frac{2\alpha}{R}\cos\alpha_0\sin\alpha_0\right)^2 ds$$

$$\frac{\partial}{\partial \alpha}: \qquad \left(4\frac{EI_2}{R^2}\cos^2\alpha_0 \sin^2\alpha_0\right)\alpha$$

$$\frac{d}{ds}\left(\frac{\partial}{\partial \alpha'}\right): \quad 0 \tag{3.42}$$

Twisting Strain

$$\int_0^L \tfrac{1}{2} EI_2(\tau-\tau_0)^2 ds = \tfrac{1}{2} G_1 k_1 I_2 \int_0^L \left(\frac{\alpha}{R}\left(1-2\sin^2\alpha_0\right)\right)^2 ds$$

$$\frac{\partial}{\partial \alpha}: \qquad \left(\frac{G_1 k_1 I_2}{R^2}\left(1-2\sin^2\alpha_0\right)^2\right)\alpha$$

$$\frac{d}{ds}\left(\frac{\partial}{\partial \alpha'}\right): \quad 0 \tag{3.43}$$

Lateral Constraint

$$\int_0^L \lambda\alpha ds \qquad \frac{\partial}{\partial \alpha}: \quad \lambda \qquad \frac{d}{ds}\left(\frac{\partial}{\partial \alpha'}\right): \quad 0 \tag{3.44}$$

Summation and Differential Equation

Collection of the above terms (3.40) to (3.44) gives the following ordinary differential equation for the variable α.

$$EI_1\frac{d^2\alpha}{ds^2} - \left(T_{00} + 4\frac{EI_2}{R^2}\cos^2\alpha_0\sin^2\alpha_0 + \frac{G_1k_1I_2}{R^2}\left(1-2\sin^2\alpha_0\right)^2\right)\alpha = \lambda - T_{00}\beta$$

or

$$EI_1\frac{d^2\alpha}{ds^2} - T_1\alpha = \lambda - T_{00}\beta \tag{3.45}$$

3.4.3 Solution

This very simple second order differential equation (3.45) has solution

$$\alpha = Ae^{\mu s} + Be^{-\mu s} + C\,, \qquad \mu = \sqrt{\frac{T_1}{EI_1}}\,, \qquad C = \frac{T_{00}\beta - \lambda}{T_1}\,. \tag{3.46}$$

As expected the solution is symmetrical. However, for the purpose of investigating end effects, only one end, where $s = 0$, needs to be considered, the exponentially increasing component being irrelevant here. Therefore the solution, after application of the boundary condition $\alpha_{s=0} = 0$, is simply

$$\alpha = \frac{T_{00}\beta - \lambda}{T_1}\left(1 - e^{-\sqrt{\frac{T_1}{EI_1}}s}\right) \tag{3.47}$$

T_1 and EI_1 depend on the wire material, cross-section and helical radius, while T_{00}, β and λ are found from the geometry. In order to complete this solution, the multiplier λ and also the constant T_{00} need to be evaluated from the overall constraints. T_{00} has already been defined, in this case, as the tension that would exist in a helical wire stretched from the original helix to a new one as described by the pipe total stretch and twist, while λ is the constant which satisfies the lateral constraint

$$\int_0^L \frac{T_{00}\beta - \lambda}{T_1}\left(1 - e^{-\sqrt{\frac{T_1}{EI_1}}s}\right) ds = \int_0^L \beta ds \tag{3.48}$$

For the above condition the infinitesimal difference between wire axial strain and the strain in the new helix is ignored.

Completion of the Solution

The solution is developed as follows, the example being for a pipe under tension with no twist.

i) $$T_{00} = \frac{\varepsilon}{EA} \tag{3.49}$$

ii) $$\beta = \tan^{-1}\left(\tan\alpha_0\left(1+\varepsilon_p\right)\right) - \alpha_0 \tag{3.50}$$

iii) $$\int_0^L \frac{T_{00}\beta - \lambda}{T_1}\left(1 - e^{-\sqrt{\frac{T_1}{EI_1}}s}\right)ds = \int_0^L \beta ds$$

$$\frac{T_{00}\beta - \lambda}{T_1}\left(L + \sqrt{\frac{EI_1}{T_1}}\left(e^{-\sqrt{\frac{T_1}{EI_1}}L} - 1\right)\right) = \beta L$$

$$\lambda = T_{00}\beta - \frac{T_1\beta}{1 - \sqrt{\frac{EI_1}{L^2T_1}}\left(1 - e^{-\sqrt{\frac{T_1}{EI_1}}L}\right)} \tag{3.51}$$

Hence

$$\alpha = \frac{\beta}{1 - \sqrt{\frac{EI_1}{L^2T_1}}\left(1 - e^{-\sqrt{\frac{T_1}{EI_1}}L}\right)}\left(1 - e^{-\sqrt{\frac{T_1}{EI_1}}s}\right) \tag{3.52}$$

Example

An example result is given in Figure 3.8, showing change in helical angle and transverse curvature for a wire with initial helical angle 55 degrees and radius 52 mm, subjected to a pipe strain of 0.2%. Wire cross-section is 6mm by 3mm. The boundary layer nature of the response is clearly shown. The curvature at the end restraint causes a 6% increase in the maximum longitudinal strain.

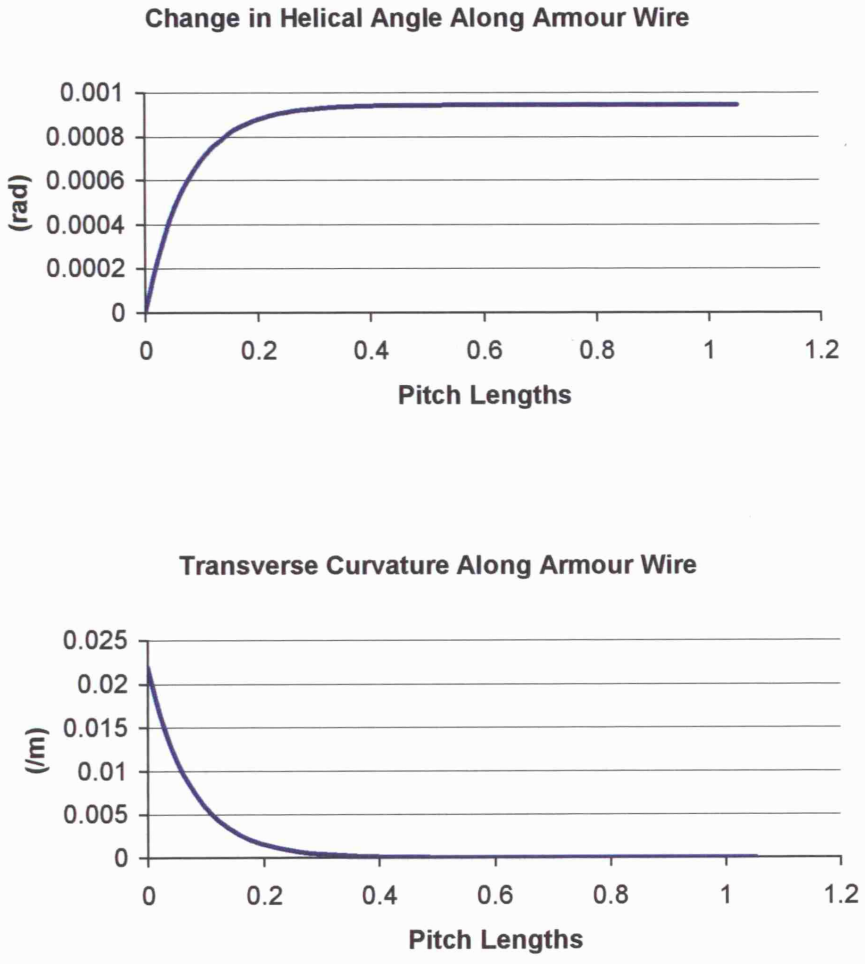

Figure 3.8 Graphs of armour wire change in helical angle and transverse curvature.

Non-Constant Tension Considerations

The solution developed is for a pipe under constant tension. For the case of a flexible riser in service the pipe tension and hence wire tension vary due to self weight, however the variation in tension with s is small compared to the initial level of tension at $s = 0$. Returning to the constant tension solution, the boundary layer nature of the wire response is shown in Figure 3.8. Further results for the same load case but using differing model lengths (see Figure 3.9) give the same boundary layer response, except for an unrealistically short length of one pitch length, showing that the response is independent of conditions several pitch lengths away from the end restraint. Hence, as the local variation in riser armour wire tension over the first few pitch lengths is negligible, a constant tension solution is considered to be suitable for examining the pipe boundary layer effect.

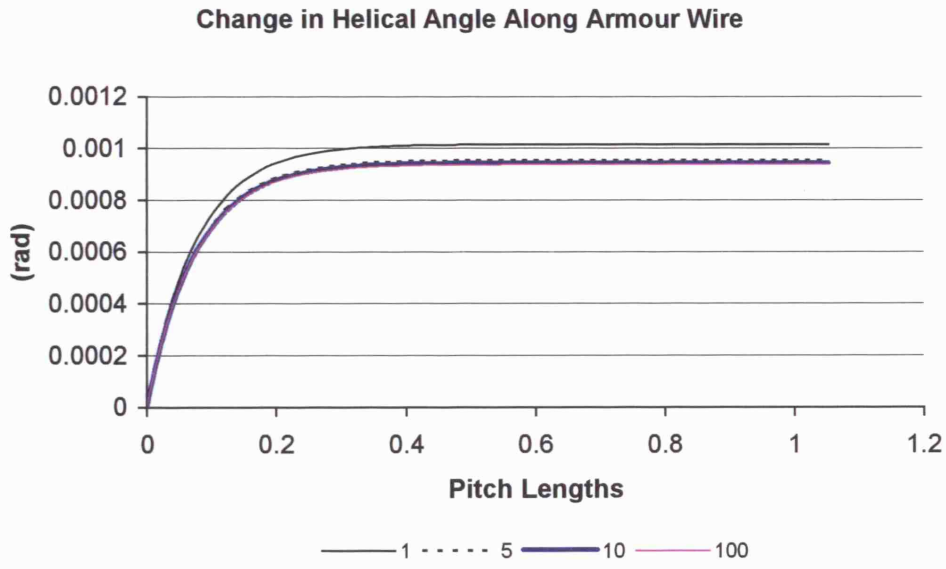

Figure 3.9 Effect of model length on result.

3.5 COMBINED FLEXURAL AND AXI-SYMMETRIC LOADING WITHOUT FRICTION

Typical flexible riser loading will involve bending as well as axial tension, while flexible pipe used for static flowlines may also be subjected to bending, particularly during installation. The model described in the preceding section, with constant pipe tension, will now be developed into a general model to include the effects of bending.

The pipe centre line is assumed to remain a plane curve and a general pipe curvature is described by

$$\frac{1}{\rho} = \mathrm{K}_p = Ze^{-ms} \tag{3.53}$$

This allows for an exponential decay typical to slender structures under tension applied at an angle, while also allowing for constant curvature cases where curvature is controlled. Pipe twist ϕ_p is set to zero.

3.5.1 Effects of Applied Bending

In the following analysis, pipe cross-sections are assumed to remain circular, and cylindrical layer cross-sections are assumed to remain plane. This second assumption does not apply to the helically wound armour which slides with respect to the supporting surfaces.

Applied Bending - Pipe

Consider a cylinder which is then bent by the curvature distribution given by (3.53) (see Figure 3.10). Local applied curvature is given by

$$K_p = \frac{1}{\rho - R\sin\theta} = \frac{1}{\rho} \cdot \frac{1}{\left(1 - \frac{R}{\rho}\sin\theta\right)} \tag{3.54}$$

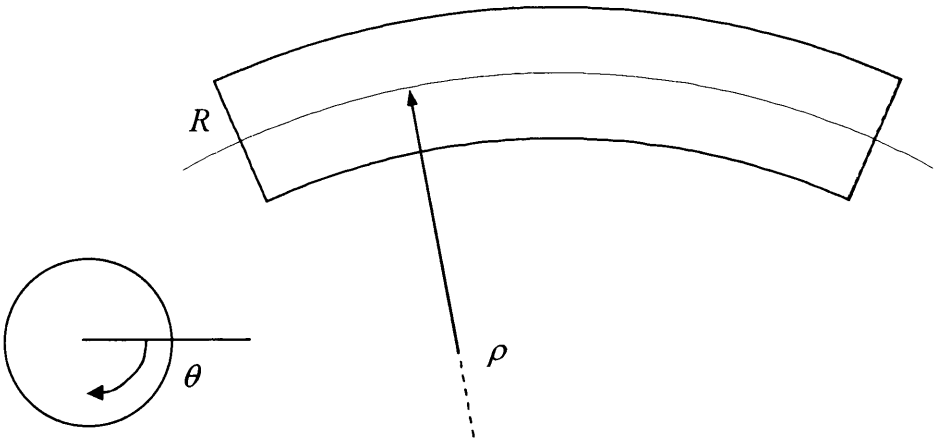

Figure 3.102 Bent cylinder parameters.

R is typically several centimetres or 0.075 – 0.15 m, while the radius of applied curvature is usually 1 m at worst and typically larger than this, especially for pipes of large radius. Hence (3.54) can be simplified by approximation to

$$K_p = \frac{1}{\rho}\left(1+\frac{R}{\rho}\sin\theta\right) \tag{3.55}$$

For small ratios of pipe radius to bending radius as mentioned above, this can be simplified further to the original centre line curvature. This simplifies the following expressions for the purpose of description of the model, inclusion of the full expression being a later refinement.

The curvature thus described is the applied curvature experienced by longitudinal lines on the toroid surface, lines parallel to the toroid axis.

Applied Bending – Loxodromic

Loxodromic curves cross longitudinal lines at a constant angle, and also cross sections at a constant angle. Therefore the applied curvature experienced by a loxodromic at, for example, angle α_0 to cross sections is always

$$K_{Lox} = K_p \sin \alpha_0 \tag{3.56}$$

Applied Bending – Strained Helix

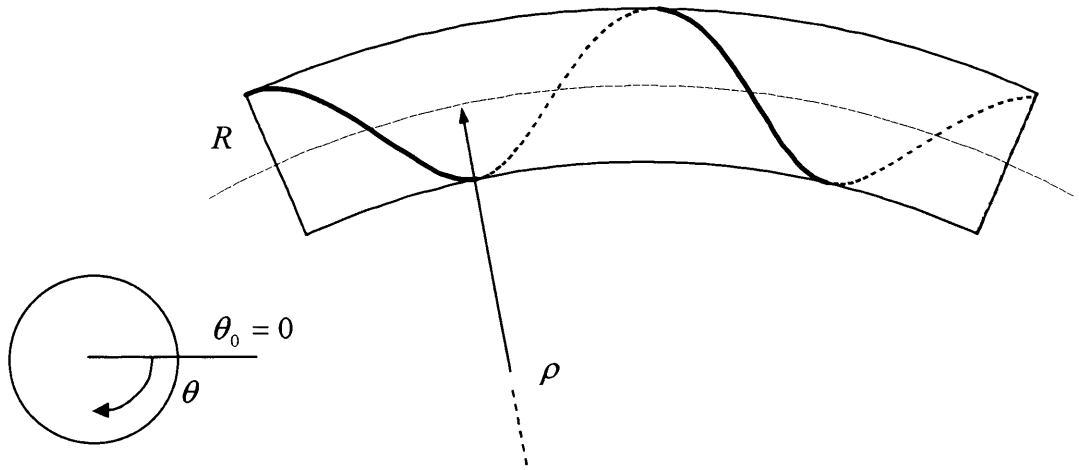

$$d\theta = (\cos\alpha_0 / R)ds = kds$$

Figure 3.11 Bent cylinder with strained helix.

Unlike a loxodromic curve, a curve following a strained helix (Figure 3.11) experiences further applied curvature due to strain of the toroidal surface, the difference being that original helices are strained with the surface but loxodromics are applied afterwards. In Section 3.1 the angle β was introduced and this angle can be used again in the description of the strained helix applied curvature. The global applied curvature is now

$$K_{SH} = K_p \sin(\alpha_0 + \beta(s)) \tag{3.57}$$

but there are additional components of curvature, firstly from changes in the original surface curvature experienced due to β, and secondly also from $d\beta/ds$, in the same way as in the axi-symmetric case.

Applied Bending – General Curve near a Strained Helix

The same applies for curves described by α as for strained helices described by β, *mutatis mutandis*.

Components of Applied Bending

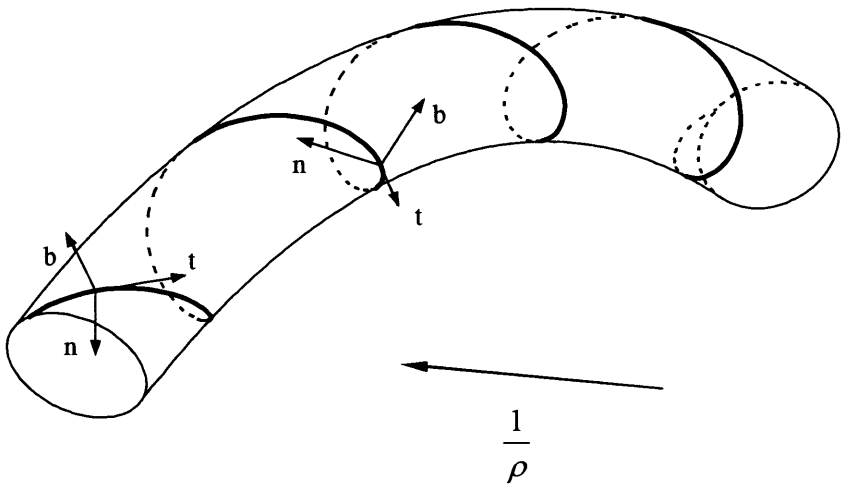

Figure 3.12. Right-hand helix with applied curvature.

As it is ultimately only the components of the applied curvature that are of interest rather than the actual total curvature, all that is needed to complete this applied curvature description is to split the global contribution into the relevant components. By considering the triads in Figure 3.12 for example, the degree of alignment of the surface normal, binormal and line tangent axes with the global applied curvature vector gives the appropriate components of curvature. Therefore, for the initially helical line shown in Figure 3.12, the complete components of applied curvature experienced are

$$\begin{aligned}
\Delta\kappa &= K_p \sin(\alpha_0 + \beta)\cos(ks + \theta_0) - \frac{d\beta}{ds} \\
\Delta\kappa' &= -K_p \sin^2(\alpha_0 + \beta)\sin(ks + \theta_0) - \frac{1}{R}\beta(1 - 2\sin^2\alpha_0) \\
\Delta\tau &= K_p \sin(\alpha_0 + \beta)\cos(\alpha_0 + \beta)\sin(ks + \theta_0) - \frac{2}{R}\beta\cos\alpha_0 \sin\alpha_0
\end{aligned} \tag{3.58}$$

where k and θ_0 are defined in Figure 3.11.

3.5.2 Wire Kinematics and Equilibrium

Pipe and Helix Geometry

When the pipe is stretched and bent the tensile armour wire moves to a new position. The contact curve of this new position on the cylinder is described by the variable α, which gives the orientation with respect to the loxodromic curve at angle α_0 to the centre line, starting at $s = 0$, which is being used as a datum.

A new variable is needed to account for the lateral displacement of the wire as the varying surface strain due to pipe curvature becomes highly significant to the wire tension. This is the sum of the small angle α and is defined by (3.59), and represents a deviation from the loxodromic curve at angle α_0.

$$\gamma(s) = \int_0^s \alpha ds_1 \tag{3.59}$$

Lateral Slip

Figure 3.3 showed original and strained cylinder geometry and defined the angle β for straight pipe analysis. Where flexure is involved β is now $\beta(s)$. Considering a small element of the strained helix on the surface (Figure 3.13),

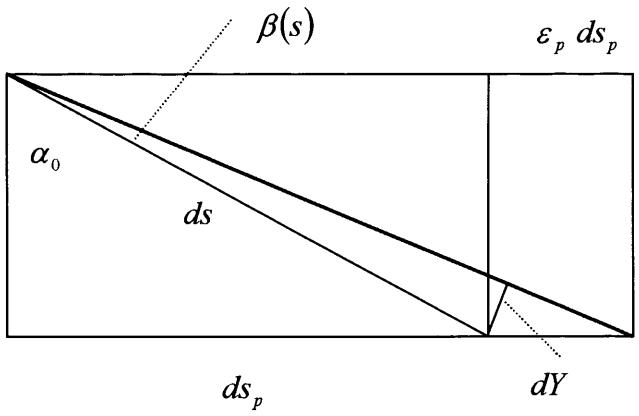

Figure 3.13 Element of strained helix.

$$dY = \varepsilon_p ds_p \cos\alpha_0 \qquad \left(\beta(s) = \frac{dY}{ds} = \varepsilon_p \sin\alpha_0 \cos\alpha_0\right)$$

$$Y(s) = \int_0^s \varepsilon_p ds_1 \sin\alpha_0 \cos\alpha_0 \tag{3.60}$$

$Y(s)$ is the surface movement in the lateral direction and, like the wire movement γ, this is also measured from the loxodromic or $\alpha = 0$ line which progresses uniformly along the surface in the pipe axial direction. Transverse slip is the difference between surface and wire lateral movements, and positive lateral slip is here defined as that leading to a clockwise movement of the wire about the cylinder axis with respect to the surface (Figure 3.14). Hence transverse slip S_l is given by

$$S_l(s) = Y(s) - \gamma(s) \tag{3.61}$$

and this corresponds to a deviation from a known path which is the strained original helix.

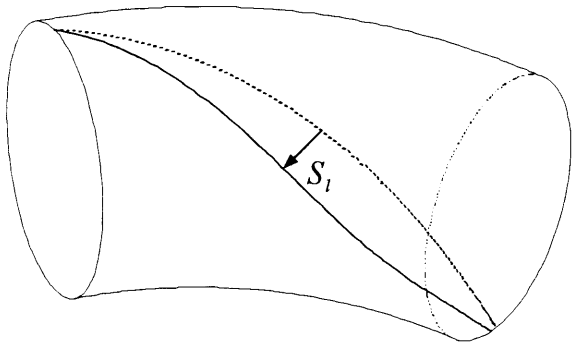

Dotted Line — Strained original helix
Full Line — Wire position

Figure 3.14 Lateral slip S_l for right-hand helix.

Tensile Armour Bending and Twist

Changes to the components of bending and twist are expressed in (3.58) for a strained helix. These can simply be repeated here for a line described by α but using the new variable γ, as follows.

$$\begin{aligned}
\Delta\kappa &= K_p \sin\left(\alpha_0 + \frac{d\gamma}{ds}\right)\cos(ks+\theta_0) - \frac{d^2\gamma}{ds^2} \\
\Delta\kappa' &= -K_p \sin^2\left(\alpha_0 + \frac{d\gamma}{ds}\right)\sin(ks+\theta_0) - \frac{1}{R}\frac{d\gamma}{ds}\left(1-2\sin^2\alpha_0\right) \\
\Delta\tau &= K_p \sin\left(\alpha_0 + \frac{d\gamma}{ds}\right)\cos\left(\alpha_0 + \frac{d\gamma}{ds}\right)\sin(ks+\theta_0) - \frac{2}{R}\frac{d\gamma}{ds}\cos\alpha_0 \sin\alpha_0
\end{aligned} \tag{3.62}$$

These components correspond to changes in normal and binormal bending and twist for a wire following the line described by α. For such a wire, allowed to slip axially and laterally from the original helix to follow this line, the position of the original arc length co-ordinate of the wire does not correspond to that of the same co-ordinate of the line, and the angle $(ks+\theta_0)$ is not quite the correct angle to use in (3.62). The error is however small, and also does not accumulate owing to its sinusoidal nature. The much more significant effects of this discrepancy will be discussed in the next section in the determination of the wire tension.

It can also be observed in (3.62) that terms involving the first derivative of γ are either dependent on the original cylindrical surface curvature or on the applied curvature. As a pipe's minimum bend radius is typically over 30 times its inner radius, the former is assumed to dominate and hence the expressions in (3.62) are conveniently simplified to

$$\begin{aligned}
\Delta\kappa &= K_p \sin\alpha_0 \cos(ks+\theta_0) - \frac{d^2\gamma}{ds^2} \\
\Delta\kappa' &= -K_p \sin^2\alpha_0 \sin(ks+\theta_0) - \frac{1}{R}\frac{d\gamma}{ds}\left(1-2\sin^2\alpha_0\right) \\
\Delta\tau &= K_p \sin\alpha_0 \cos\alpha_0 \sin(ks+\theta_0) - \frac{2}{R}\frac{d\gamma}{ds}\cos\alpha_0 \sin\alpha_0
\end{aligned} \tag{3.63}$$

Tensile Armour Tension

Equilibrium Equations

Application of Love's equations has already been shown to lead to (3.21), an expression for dT/ds. Using the above expressions, wire curvatures, twist and moments for substitution are

$$\kappa = -\frac{d^2\gamma}{ds^2} + K_p \sin\alpha_0 \cos(ks+\theta_0)$$

$$\kappa' = \frac{\cos^2\alpha_0}{R} - \frac{2}{R}\frac{d\gamma}{ds}\cos\alpha_0 \sin\alpha_0 - K_p \sin^2\alpha_0 \sin(ks+\theta_0)$$

$$\tau = \frac{\cos\alpha_0 \sin\alpha_0}{R} + \frac{1}{R}\frac{d\gamma}{ds}(1-2\sin^2\alpha_0) + K_p \sin\alpha_0 \cos\alpha_0 \sin(ks+\theta_0)$$

$$G = EI_1\left(-\frac{d^2\gamma}{ds^2} + K_p \sin\alpha_0 \cos(ks+\theta_0)\right)$$

$$G' = -EI_2\left(\frac{2}{R}\frac{d\gamma}{ds}\cos\alpha_0 \sin\alpha_0 + K_p \sin^2\alpha_0 \sin(ks+\theta_0)\right)$$

$$H = Gk_1 I_{\min}\left(\frac{1}{R}\frac{d\gamma}{ds}(1-2\sin^2\alpha_0) + K_p \sin\alpha_0 \cos\alpha_0 \sin(ks+\theta_0)\right)$$

(3.64)

Substitution and integration leads to an expression for the tension similar to (3.23), in that it is dominated by the constant of integration T_0 :-

$$T = \frac{2EI_2 + EI_1}{R^2}\cos^3\alpha_0 \sin\alpha_0 \frac{d\gamma}{ds} - \frac{EI_2}{R}\cos^2\alpha_0 \sin\alpha_0 \cdot K_p \sin(\theta+\theta_0)$$
$$- \frac{EI_1}{R^2}\cos^3\alpha_0 \sin\alpha_0 \int K_p \cos(\theta+\theta_0)ds + T_0$$

$$= A_1\frac{d\gamma}{ds} + f(K_p) + T_0 \qquad (3.65)$$

Tension Constant T_0

As described earlier in this section, $Y-\gamma$ represents a deviation from a known path and this leads to a change in arc length. The total projection of the wire on the known path must be constant, and this is influenced not only by orientation α but also by lateral displacement $Y-\gamma$ through strain of the surface due to applied curvature. Hence (3.24) is replaced by

$$\int_0^L (1+\varepsilon_a)\cos\left(\beta-\frac{d\gamma}{ds}\right)g(\gamma)ds = L+\Delta L \tag{3.66}$$

ΔL is given by the change in original path length due to axial strain and bending of the pipe, on the assumption that the adjacent layer cross-sections remain plane. Hence

$$\Delta L = L\varepsilon + \int_0^L RK_p \sin^2\alpha_0 \sin(ks+\theta_0)ds \tag{3.67}$$

Function $g(\gamma)$

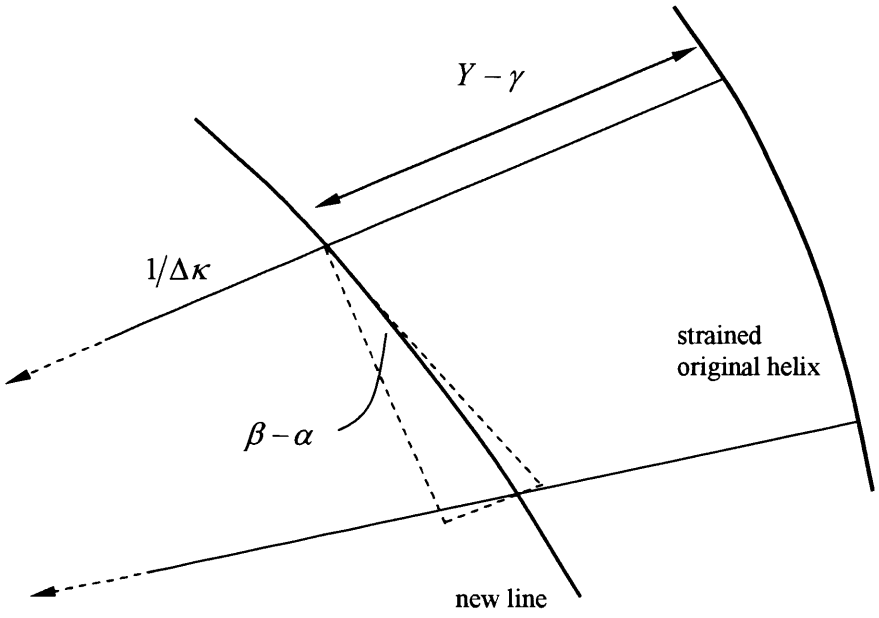

Figure 3.15 Projection of line on original helix due to curvature.

Lateral slip changes the required arc length but this can be more usefully viewed as an equal and opposite change in projection on the strained original helix. For an element of line as shown in Figure 3.15, its projection is reduced by the difference in orientation $\beta-\alpha$, but is also changed by its position with respect to the centre of lateral curvature. Assuming the distance along the radius of curvature can be approximated by the slip distance $Y-\gamma$, this component Δ of change in projection is, for small curvature $\Delta\kappa$ and small $Y-\gamma$,

$$\Delta \approx (Y-\gamma)/(1/\Delta\kappa) = \Delta\kappa(Y-\gamma) \tag{3.68}$$

Using the simplified form of the first of (3.58), this gives

$$g(\gamma) = 1+\left(K_p \sin\alpha_0 \cos(ks+\theta_0) - \frac{d\beta}{ds}\right)(Y-\gamma) \tag{3.69}$$

and as a result 3.66 can be replaced by

$$\int_0^L (1+\varepsilon_a)\left(1-\frac{(\beta-\gamma')^2}{2}\right)\left(1+\left(K_p \sin\alpha_0 \cos(ks+\theta_0)-\frac{d\beta}{ds}\right)(Y-\gamma)\right)ds = L+\Delta L \quad (3.70)$$

where $\gamma' = \frac{d\gamma}{ds}$.

In the same way as in Section 3.4.1, the tension (3.65) from Love's equations can be substituted to find the tension constant T_0, giving the following final expression for the wire tension (under constant applied tension).

$$T = A_1\gamma' + f(K_p) + T_{00}$$
$$+\frac{EA}{L}\int_0^L\left(\frac{(\beta-\gamma')^2}{2}-\left(K_p \sin\alpha_0 \cos(ks+\theta_0)-\frac{d\beta}{ds}\right)(Y-\gamma)-\frac{A_1}{EA}\gamma'-\frac{f(K_p)}{EA}\right)ds \quad (3.71)$$

where T_{00} is $EA\frac{\Delta L}{L}$ where ΔL is given by (3.67).

3.5.3 Energy Functional and Minimisation

Wire tension, curvatures and twist have now all been expressed in terms of the variable γ and its derivatives. Minimisation of the energy equation will yield γ, the integral from zero to s of the variable α. Hence no lateral constraint or therefore Lagrange multiplier is needed in the formulation, the constraint being applied through boundary conditions.

Functional Terms

Axial Strain Energy

The contribution of axial strain energy to the energy equation is, using (3.71),

$$\int_0^L \tfrac{1}{2} EA\varepsilon_a{}^2 ds = \tfrac{1}{2} EA \int_0^L \left(\varepsilon_{00} + \frac{A_1}{EA}\gamma' + \frac{f(K_p)}{EA} + \frac{1}{L}\int_0^L f_1(\gamma,\gamma',s)ds \right)^2 ds \qquad (3.72)$$

This can be expanded as follows for minimisation. [1]

---

[1] The Euler-Lagrange equation finds the function $y(x)$ which minimizes an expression of the form

$$I = \int_a^b F(x, y, y', ...)dx$$

This is achieved by taking the varied function $Y(x) = y(x) + \varepsilon\eta(x)$, where η is an arbitrary function and ε is a small parameter, substituting this into the expression for I so that it becomes $I(\varepsilon)$ and then setting

$$\left(\frac{dI}{d\varepsilon}\right)_{\varepsilon=0} = 0$$

In this way $y(x)$ will be the function to make $I(\varepsilon)$ stationary as $I(\varepsilon)$ is set not to vary with ε in the region of $\varepsilon = 0$, or where $Y(x) = y(x)$. For an expression I of the above form,

$$\left(\frac{dI}{d\varepsilon}\right)_{\varepsilon=0} = \int_a^b \left(\frac{\partial F}{\partial y}\eta(x) + \frac{\partial F}{\partial y'}\eta'(x) + ... \right) ds$$

Integrating the second and further terms in the brackets by parts and using the fact that $\eta(x)$, $\eta'(x)$ etc can be defined to be zero at a and b,

$$\int_a^b \left(\frac{\partial F}{\partial y} - \frac{d}{dx}\frac{\partial F}{\partial y'} + ... \right) \eta(x)ds = 0$$

As $\eta(x)$ is an arbitrary function, the expression inside the brackets must be zero and this is the Euler-Lagrange equation. (Boas, 1983, p. 388)

By the same token, if the function I is of the form

$$I = \left(\int_a^b F(x, y, y', ...)dx \right)^2 + \int_a^b G(x, y, y', ...)dx,$$

$$\int_0^L \tfrac{1}{2} EA\varepsilon_a{}^2 ds = \tfrac{1}{2} EA\int_0^L \left(\varepsilon_{00} + \frac{A_1}{EA}\gamma' + \frac{f(K_p)}{EA} \right)^2 ds$$

$$+ EA\int_0^L \left(\varepsilon_{00} + \frac{A_1}{EA}\gamma' + \frac{f(K_p)}{EA} \right)\left(\frac{1}{L}\int_0^L f_1(\gamma,\gamma',s)ds \right) ds$$

$$+ \tfrac{1}{2} EA\int_0^L \left(\frac{1}{L}\int_0^L f_1(\gamma,\gamma',s)ds \right)^2 ds \qquad (3.73)$$

Further energy terms are as below, which follow (3.35) – (3.37), augmented by the applied curvature.

Normal Bending Strain Energy

$$\int_0^L \tfrac{1}{2} EI_1\kappa^2 ds = \tfrac{1}{2} EI_1\int_0^L \left(-\frac{d^2\gamma}{ds^2} + K_p \sin\alpha_0 \cos(ks+\theta_0) \right)^2 ds \qquad (3.74)$$

Binormal Bending Strain Energy

$$\int_0^L \tfrac{1}{2} EI_2(\kappa' - \kappa_0')^2 ds = \tfrac{1}{2} EI_2\int_0^L \left(-\frac{2}{R}\frac{d\gamma}{ds}\cos\alpha_0 \sin\alpha_0 - K_p \sin^2\alpha_0 \sin(ks+\theta_0) \right)^2 ds \qquad (3.75)$$

Twisting Strain Energy

$$\int_0^L \tfrac{1}{2} G_1 k_1 I_2(\tau - \tau_0)^2 ds$$

$$= \tfrac{1}{2} G_1 k_1 I_2\int_0^L \left(\frac{1}{R}\frac{d\gamma}{ds}(1 - 2\sin^2\alpha_0) + K_p \sin\alpha_0 \cos\alpha_0 \sin(ks+\theta_0) \right)^2 ds \qquad (3.76)$$

$$\left(\frac{dI}{d\varepsilon}\right)_{\varepsilon=0} = 2\int_a^b F(x,y,y',...)dx.\int_a^b \left(\frac{\partial F}{\partial y}\eta(x) + \frac{\partial F}{\partial y'}\eta'(x) + ... \right) ds$$

$$+ \int_a^b \left(\frac{\partial G}{\partial y}\eta(x) + \frac{\partial G}{\partial y'}\eta'(x) + ... \right) ds$$

The first integral in the first expression involves the desired function only and no arbitrary additions and is hence a constant. In the subsequent formulation this constant can be stipulated for comparison later with the constant from the resulting function, and adjusted accordingly.

Minimisation of the Functional

The relevant form of the Euler-Lagrange Equation is now

$$\frac{\partial F}{\partial \gamma} - \frac{d}{ds}\left(\frac{\partial F}{\partial \gamma'}\right) + \frac{d^2}{ds^2}\left(\frac{\partial F}{\partial \gamma''}\right) = 0 \tag{3.77}$$

Contributions from each term in the functional are as follows.

Axial Strain

As the axial strain energy involves three separate terms they are dealt with in turn.

First Term

$$\tfrac{1}{2} EA \int_0^L \left(\varepsilon_{00} + \frac{A_1}{EA}\gamma' + \frac{f(K_p)}{EA} \right)^2 ds$$

$$\frac{\partial}{\partial \gamma}: \quad 0$$

$$\frac{d}{ds}\left(\frac{\partial}{\partial \gamma'}\right): \quad \frac{A_1^{\,2}}{EA}\gamma'' + \frac{A_1}{EA} f'(K_p)$$

$$\frac{d^2}{ds^2}\left(\frac{\partial}{\partial \gamma''}\right): \quad 0 \tag{3.78}$$

Second Term

$$EA \int_0^L \left(\varepsilon_{00} + \frac{A_1}{EA}\gamma' + \frac{f(K_p)}{EA} \right) \left(\frac{1}{L} \int_0^L f_1(\gamma, \gamma', s) ds \right) ds$$

$$= \frac{EA}{L} \int_0^L \left(\varepsilon_{00} + \frac{A_1}{EA}\gamma' + \frac{f(K_p)}{EA} \right) ds . \int_0^L f_1(\gamma, \gamma', s) ds$$

$$= \frac{EA}{L}(I_b \cdot I_a) \tag{3.79}$$

$$\begin{aligned}
&\frac{\partial}{\partial \gamma}: && \frac{EA}{L} I_b \left(K_p \sin \alpha_0 \cos(ks + \theta_0) - \frac{d\beta}{ds} \right) \\
&\frac{d}{ds}\left(\frac{\partial}{\partial \gamma'}\right): && \frac{EA}{L} I_b \left(\gamma'' - \frac{d\beta}{ds} \right) \\
&\frac{d^2}{ds^2}\left(\frac{\partial}{\partial \gamma''}\right): && 0
\end{aligned} \tag{3.80}$$

Third Term

$$EA \int_0^L \left(\frac{1}{L} \int_0^L f_1(\gamma, \gamma', s) ds \right)^2 ds$$

$$= \frac{EA}{L} \left(\int_0^L f_1(\gamma, \gamma', s) ds \right)^2$$

$$\begin{aligned}
&\frac{\partial}{\partial \gamma}: && \frac{EA}{L} I_a \left(K_p \sin \alpha_0 \cos(ks + \theta_0) - \frac{d\beta}{ds} \right) \\
&\frac{d}{ds}\left(\frac{\partial}{\partial \gamma'}\right): && \frac{EA}{L} I_a \left(\gamma'' - \frac{d\beta}{ds} \right) \\
&\frac{d^2}{ds^2}\left(\frac{\partial}{\partial \gamma''}\right): && 0
\end{aligned} \tag{3.81}$$

Normal Bending

$$\tfrac{1}{2} EI_1 \int_0^L \left(-\frac{d^2\gamma}{ds^2} + K_p \sin \alpha_0 \cos(ks + \theta_0) \right)^2 ds$$

$$\begin{aligned}
&\frac{\partial}{\partial \gamma}: && 0 \\
&\frac{d}{ds}\left(\frac{\partial}{\partial \gamma'}\right): && 0
\end{aligned}$$

$$\frac{d^2}{ds^2}\left(\frac{\partial}{\partial\gamma''}\right): \quad EI_1\left(\frac{d^4\gamma}{ds^4} - \sin\alpha_0 \cdot \frac{d^2}{ds^2}\left(K_p \cos(ks+\theta_0)\right)\right) \tag{3.82}$$

Binormal Bending

$$\tfrac{1}{2}EI_2\int_0^L\left(-\frac{2}{R}\frac{d\gamma}{ds}\cos\alpha_0 \sin\alpha_0 - K_p \sin^2\alpha_0 \sin\left(ks+\theta_0\right)\right)^2 ds$$

$$\frac{\partial}{\partial\gamma}: \quad 0$$

$$\frac{d}{ds}\left(\frac{\partial}{\partial\gamma'}\right): \quad EI_2\left(\frac{4}{R^2}\cos^2\alpha_0 \sin^2\alpha_0 \frac{d^2\gamma}{ds^2} + \frac{2}{R}\sin^3\alpha_0 \cos\alpha_0 \frac{d}{ds}\left(K_p \sin\left(ks+\theta_0\right)\right)\right)$$

$$\frac{d^2}{ds^2}\left(\frac{\partial}{\partial\gamma''}\right): \quad 0 \tag{3.83}$$

Twisting

$$\tfrac{1}{2}G_1k_1I_2\int_0^L\left(\frac{1}{R}\frac{d\gamma}{ds}\left(1-2\sin^2\alpha_0\right)+K_p \sin\alpha_0 \cos\alpha_0 \sin\left(ks+\theta_0\right)\right)^2 ds$$

$$\frac{\partial}{\partial\gamma}: \quad 0$$

$$\frac{d}{ds}\left(\frac{\partial}{\partial\gamma'}\right): \quad G_1k_1I_2\left(\frac{1}{R^2}\left(1-2\sin^2\alpha_0\right)^2 \frac{d^2\gamma}{ds^2}\right.$$

$$\left. + \frac{1}{R}\left(1-2\sin^2\alpha_0\right)\sin\alpha_0 \cos\alpha_0 \frac{d}{ds}\left(K_p \sin\left(ks+\theta_0\right)\right)\right)$$

$$\frac{d^2}{ds^2}\left(\frac{\partial}{\partial\gamma''}\right): \quad 0 \tag{3.84}$$

Differential Equation

Substituting all the terms from the above sections into (3.77), the following fourth order differential equation in γ results.

$$\begin{aligned}
&\frac{d^4\gamma}{ds^4}\cdot EI_1 \\
&-\frac{d^2\gamma}{ds^2}\cdot\left(\frac{EA}{L}(I_a+I_b)+\frac{A_1^{\,2}}{EA}+\frac{EI_2}{R^2}\left(4\cos^2\alpha_0\sin^2\alpha_0\right)+\frac{G_1k_1I_2}{R^2}\left(1-2\sin^2\alpha_0\right)^2\right) \\
&\qquad = EI_1\sin\alpha_0\cdot\frac{d^2}{ds^2}\left(K_p\cos(ks+\theta_0)\right) \\
&\qquad +EI_2\frac{2}{R}\sin^3\alpha_0\cos\alpha_0\frac{d}{ds}\left(K_p\sin(ks+\theta_0)\right) \\
&\qquad +\frac{G_1k_1I_2}{R}\left(1-2\sin^2\alpha_0\right)\sin\alpha_0\cos\alpha_0\frac{d}{ds}\left(K_p\sin(ks+\theta_0)\right) \\
&\qquad +\frac{A_1}{EA}f'(K_p) \\
&\qquad -\frac{EA}{L}(I_a+I_b)\sin\alpha_0K_p\cos(ks+\theta_0)
\end{aligned} \tag{3.85}$$

Introducing the new variable $\varphi=\frac{d^2\gamma}{ds^2}=\frac{d\alpha}{ds}$ and considering only significant terms[2], the left-hand side of (3.85) can be re-written as follows.

[2] The order of the terms in the φ coefficient is as follows.

$o\left(\frac{EA}{L}(I_a+I_b)\right)=o(EA\cdot\beta L\cdot K_p)$ (see (3.79) for I_a and I_b, and (3.65) for $f(K_p)$). L is the pipe length, K_p the applied curvature and β the change in helical angle on the supporting surface due to pipe axial strain.

$o(A_1)=o\left(\frac{EI}{R^2}\right)=o(EA\times10^{-4})$. (See 3.65 for A_1.) Hence $o\left(\frac{A_1^{\,2}}{EA}\right)=o(EA\times10^{-8})$.

$$EI_1 \frac{d^2\varphi}{ds^2}$$

$$-\left(\frac{EA}{L}(I_a + I_b) + \frac{EI_2}{R^2}\left(4\cos^2\alpha_0 \sin^2\alpha_0\right) + \frac{G_1 k_1 I_2}{R^2}\left(1 - 2\sin^2\alpha_0\right)^2\right)\varphi \tag{3.86}$$

Further substitution for the applied curvature from (3.53) and performance of the differentiations allows the right-hand side of (3.85) to be written as[3]

$$Ze^{-ms}\sin(ks+\theta_0)\left\{2mkEI_1 \sin\alpha_0\right.$$

$$\left. -m\left(EI_2 \frac{2}{R}\sin^3\alpha_0 \cos\alpha_0 + \frac{G_1 k_1 I_2}{R}\left(1 - 2\sin^2\alpha_0\right)\sin\alpha_0 \cos\alpha_0\right)\right\}$$

$$+Ze^{-ms}\cos(ks+\theta_0)\left\{EI_1 \sin\alpha_0\left(m^2 - k^2\right)\right.$$

$$+k\left(EI_2 \frac{2}{R}\sin^3\alpha_0 \cos\alpha_0 + \frac{G_1 k_1 I_2}{R}\left(1 - 2\sin^2\alpha_0\right)\sin\alpha_0 \cos\alpha_0\right)$$

$$\left. -\frac{EA}{L}(I_a + I_b)\sin\alpha_0\right\} \tag{3.87}$$

---

[3] Respective order of terms on the right-hand side is as follows.

$o\left(EI_1 \frac{d^2}{ds^2}(K_p)\right) = o\left(EI_1 \cdot K_p \cdot k^2\right)$ or $o\left(EI_1 \cdot K_p \cdot m^2\right)$ where $k = \frac{\cos\alpha_0}{R}$ and m is the constant governing the rate of decay of the applied curvature and is unlikely to be of an order greater than k.

Hence $o\left(EI_1 \frac{d^2}{ds^2}(K_p)\right) = o\left(EA \cdot K_p \times 10^{-4}\right)$.

Similarly $o\left(EI_2 \frac{d}{ds}(K_p)\right) = o\left(EA \cdot K_p \times 10^{-4}\right)$.

$o\left(\frac{A_1}{EA} f'(K_p)\right) = o\left(EA \cdot K_p \times 10^{-8}\right)$ (see (3.65) for $f(K_p)$).

$o\left(\frac{EA}{L}(I_a + I_b)K_p\right) = o\left(EA \cdot \beta L \cdot K_p^2\right)$.

Solution

This is a second order ordinary differential equation of the form

$$\frac{d^2\varphi}{ds^2} - A_2\varphi = B_2 e^{-ms}\sin(ks+\theta_0) + C_2 e^{-ms}\cos(ks+\theta_0) \tag{3.88}$$

In most cases the coefficient A_2 will be positive and so the solution given proceeds on this assumption. Integration of the solution for φ will give α.

$$\varphi_{C.F.} = A_3 e^{-\mu s} \tag{3.89}$$

where $\mu = \sqrt{A_2}$. Only a half solution is necessary as far-end characteristics are irrelevant.

$$\varphi_{P.I.} = B_3 e^{-ms}\sin(ks+\theta_0) + C_3 e^{-ms}\cos(ks+\theta_0) \tag{3.90}$$

Substituting into (3.96) and equating terms gives

$$B_2 = (m^2 - k^2)B_3 + 2mkC_3 - A_2B_3 = aB_3 + bC_3$$
$$C_2 = (m^2 - k^2)C_3 - 2mkB_3 - A_2C_3 = aC_3 - bB_3$$

which leads to

$$B_3 = \frac{aB_2 - bC_2}{a^2 + b^2}$$
$$C_3 = \frac{bB_2 + aC_2}{a^2 + b^2} \tag{3.91}$$

Hence φ can be written down with one unknown constant A_3 as

$$\varphi = A_3 e^{-\mu s} + B_3 e^{-ms}\sin(ks+\theta_0) + C_3 e^{-ms}\cos(ks+\theta_0) \tag{3.92}$$

Integrating once, α is

$$\alpha = A_4 e^{-\mu s} + B_4 e^{-ms}\sin(ks+\theta_0) + C_4 e^{-ms}\cos(ks+\theta_0) + D_4 \tag{3.93}$$

where

$$\begin{aligned} A_4 &= -\frac{A_3}{\mu} \\ B_4 &= \frac{1}{m^2+k^2}(kC_3 - mB_3) \\ C_4 &= \frac{-1}{m^2+k^2}(mC_3 + kB_3) \end{aligned} \tag{3.94}$$

The variable γ is also

$$\gamma = \int_0^s \alpha ds_1 = A_5\left(e^{-\mu s} - 1\right) + B_5 e^{-ms}\sin(ks+\theta_0) + C_5 e^{-ms}\cos(ks+\theta_0) + D_5 s + E_5 \tag{3.95}$$

where

$$\begin{aligned} A_5 &= -\frac{A_4}{\mu} \\ B_5 &= \frac{1}{m^2+k^2}(kC_4 - mB_4) \\ C_5 &= \frac{-1}{m^2+k^2}(mC_4 + kB_4) \\ D_5 &= D_4 \\ E_5 &= \frac{1}{m^2+k^2}\{B_4(k\cos\theta_0 + m\sin\theta_0) + C_4(m\cos\theta_0 - k\sin\theta_0)\} \end{aligned} \tag{3.96}$$

Boundary conditions are

$$\begin{aligned} \alpha_{s=0} &= 0 \\ \gamma_{s=L} &= Y(L) \qquad (S_l(L) = 0) \end{aligned} \tag{3.97}$$

From the first of (3.97),

$$D_4 = -(A_4 + B_4 \sin\theta_0 + C_4 \cos\theta_0) \tag{3.98}$$

and from the second

$$A_4 = -\mu A_5 = \frac{\mu\left(-Y + B_5 e^{-mL}\sin(kL+\theta_0) + C_5 e^{-mL}\cos(kL+\theta_0) + D_5 L + E_5\right)}{\left(e^{-\mu L} - 1\right)} \tag{3.99}$$

As D_5 is D_4, (3.98) and (3.99) are simultaneous equations in the remaining constants A_4 and D_4 required to complete the solutions for α and γ.

3.5.4 Example Normal Bending Moment Results

Consider a steel wire of 6mm x 3mm cross section and with an initial helical angle of 44°, on a cylinder of radius 12cm. This could represent a tensile armour wire in a 6 inch internal diameter flexible pipe. If the cylinder is bent to a small, gradually decaying radius of curvature ρ described by

$$\frac{1}{\rho} = -0.07 e^{-0.07z} \sin\left(\frac{1}{R\tan\alpha_0} z + \theta_0\right)$$

where z is measured along the pipe axis, and with the wire under tension caused by a pipe axial strain of 0.28%, the following results for transverse bending moment are obtained.

Wire restrained at neutral axis position.

Figures 3.16 and 3.17 show wire lateral curvature, the first showing the complete solution, the second breaking the solution down into its two component solutions and the applied curvature.

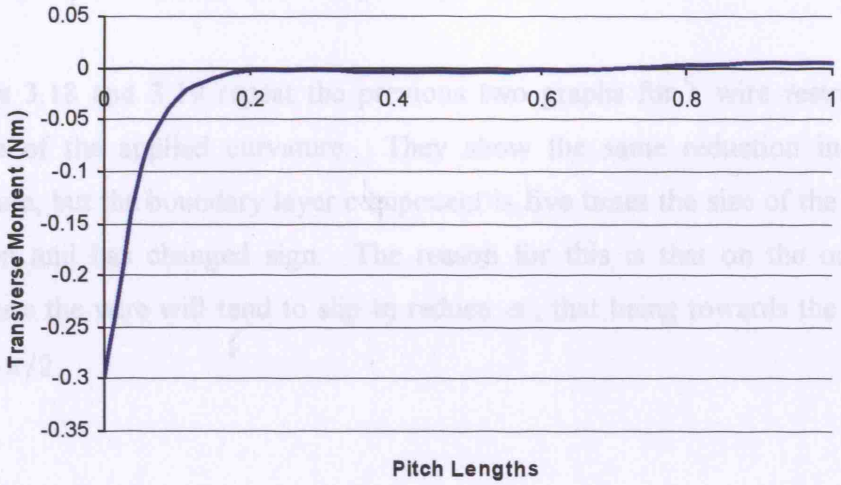

Figure 3.16 Transverse moment experienced by wire restrained at $\theta_0 = 0$.

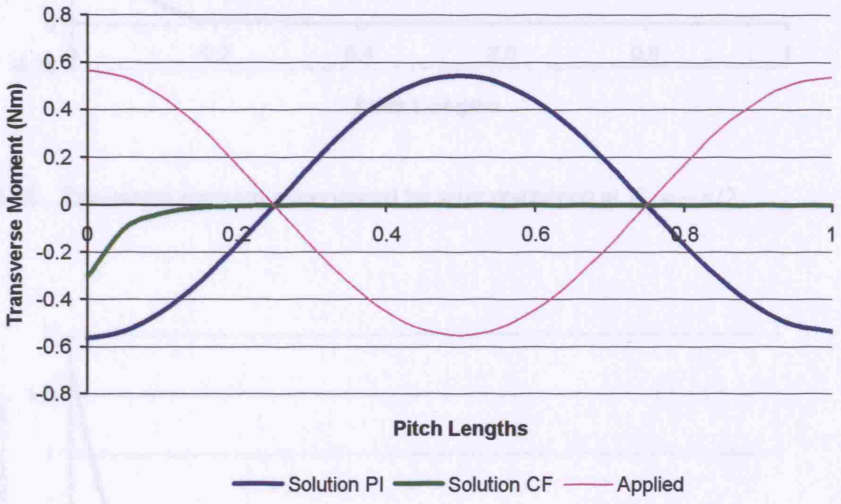

Figure 3.17 Transverse moment components, $\theta_0 = 0$.

The graphs show that the wire slips to eliminate lateral bending caused by the applied curvature along the pipe length. The maximum of the boundary layer component of the solution in this case stays close to the straight strained pipe value of 0.35 Nm.

Wire restrained at outside 'extreme fibre' position.

Figures 3.18 and 3.19 repeat the previous two graphs for a wire restrained on the outside of the applied curvature. They show the same reduction in the applied curvature, but the boundary layer component is five times the size of the straight pipe solution and has changed sign. The reason for this is that on the outside of the curvature the wire will tend to slip to reduce α, that being towards the geodesic for $\theta_0 = -\pi/2$.

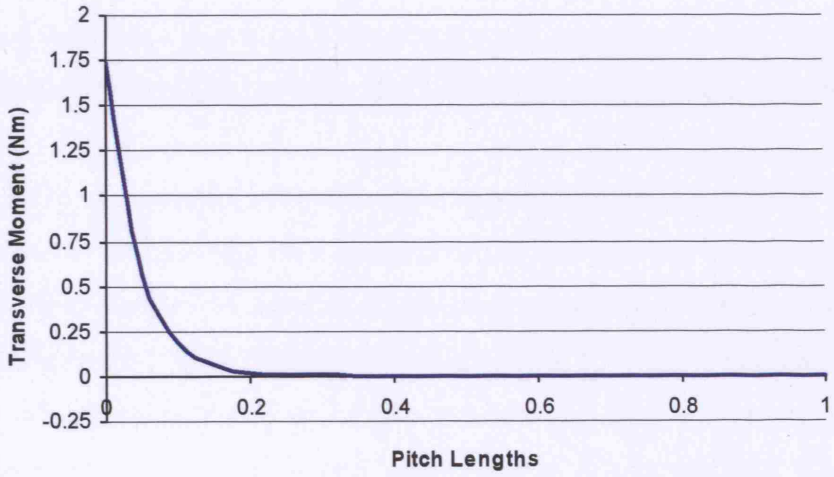

Figure 3.18 Transverse moment experienced by wire restrained at $\theta_0 = -\pi/2$.

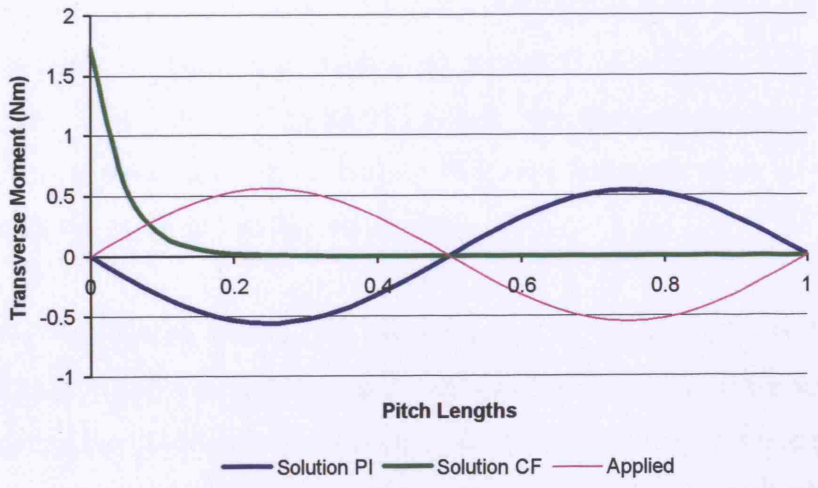

Figure 3.19 Transverse moment components, $\theta_0 = -\pi/2$.

3.5.5 Concluding Remarks

Equations (3.45) and (3.93) are two results for wire deviation from the initial helical angle, under axi-symmetric loading and under combined axial and flexural loading respectively. They constitute the analytical result arising from this tensile armour modelling study. It remains now to verify these expressions, which is the subject of the next chapter, before using them to complete the analysis of armour wire stresses and slip at and near to end fittings.

4 VERIFICATION OF STRESS MODELS

4.1 VERIFICATION OPTIONS

4.1.1 Physical Tests or Finite Element Modelling?

Two possibilities for finding an independent result for comparison with the analytical model described in Chapter 3 are either carrying out tests to provide measured data or implementing a second model using a finite element approach. A comparison with physical tests would be useful in order to examine the validity of of the mathematical model, whereas a numerical comparison might be a better way to check the solution to a detailed mathematical problem and so validate the analytical solution.

To carry out tests a test specimen either has to be constructed or obtained from elsewhere. Sufficiently long samples of flexible pipe are difficult to obtain and also difficult to handle. In order to attach strain gauges, part of the external sheath has to be removed but then replaced to maintain the twisting constraint. The test can be simplified by removal of all but one or a few of the tensile armour wires and perhaps some of the cylindrical layers, reducing the forces required when applying any loading. End restraint can be replicated by setting the whole of one end of the specimen in an epoxy filling between cylinders of sufficient diameter. Construction of a rig to hold the specimen as it is stretched and bent is also necessary.

Alternatively, a numerical modelling approach is possible using finite element analysis. Finite element packages include line elements such as beams and links which seem well suited to modelling thin rods, although there may be difficulty in applying the required twisting constraint.

For the verification carried out and presented in the rest of this chapter, the finite element approach was taken. The choice was based mainly on the success achieved in replicating the analytical solution for a plane wire bent under tension, a problem with strong similarities to the one under investigation. As an introduction to the chapter

some important aspects of finite element modelling using line elements are now presented.

4.1.2 Static Finite Element Modelling Basis

Minimum Total Potential Energy

The total potential energy of a system is the difference between the total strain energy and the work done by the external forces (Moaveni, 1999, p. 35). Finite element modelling makes use of the principle that for a system in equilibrium, the total potential energy is a minimum, therefore for any displacement the total potential energy is stationary.

To find the total strain energy for any element an approximation needs to be made of the element shape when loaded. For elements representing beams, where cross section dimensions are small compared to element length, the energy is dependent on bending, while for link elements it is assumed to be dependent only on axial strain. For beams used in frames where axial deformation is also considered, energy is dependent on both.

Stiffness Matrix

The deformed element shape is described using polynomials of the appropriate order and finding the coefficients in terms of the nodal values of the degrees of freedom. The result can then be rewritten in terms of these nodal values instead, leading to new coefficients, known as shape functions. In general, for a deformation variable v,

$$v = [\mathbf{S}]\{\mathbf{U}\} \tag{4.1}$$

where $[\mathbf{S}]$ is a single row matrix of shape functions and $\{\mathbf{U}\}$ is a single column matrix of nodal degrees of freedom (Moaveni, 1999, p. 131). These shape functions can be used to find elemental strain energy. For example, in the case of plane, isotropic beams, the bending strain energy is dependent on the second derivatives of the

deflection shape functions, represented by $[\mathbf{D}]$, squared, and can be written for an element length L as

$$\mathrm{E} = \frac{EI}{2}\int_0^L \{\mathbf{U}\}^T [\mathbf{D}]^T [\mathbf{D}]\{\mathbf{U}\}dx \tag{4.2}$$

In finding the minimum total potential energy this needs to be minimized with respect to all the degrees of freedom involved, yielding the stiffness matrix $[\mathbf{K}]$.

$$\frac{\partial \mathrm{E}}{\partial U_k} = EI\int_0^L [\mathbf{D}]^T [\mathbf{D}]dx\,\{\mathbf{U}\} = [\mathbf{K}]\{\mathbf{U}\} \tag{4.3}$$

This is the characteristic form of any elemental stiffness matrix, with $[\mathbf{D}]$ representing the required functions to give the strain needed when post multiplied by $\{\mathbf{U}\}$. By the same process, axial strain energy dependent on axial degrees of freedom can be added to the example given above.

To complete a solution, a global stiffness matrix is constructed from the individual element stiffness matrices, inverted, and used with a single column matrix of all applied loads to yield degrees of freedom values. This is a linear solution, in that the response is directly proportional to the loading (Cook, 1995, p. 25).

Stress-Stiffness Matrix

With slender structures, although the strains and rotations may remain small, axial and transverse equilibrium can not be uncoupled in this way. Stress stiffening is the stiffening of a structure due to its stress state (ANSYS, 2001), and takes into account the link between lateral displacements and axial strain. As a result, the stiffness matrix above needs to be augmented by the addition of a stress stiffness matrix, based on the following stress analysis taken from the ANSYS manual (ANSYS, 2001).

For a straight fibre or element of thin rod, length dS initially and ds after orthogonal movements u, v and w, with u in the axial direction, the axial strain is

$$\varepsilon_a = \frac{ds}{dS} - 1 = \sqrt{\left(1 + \frac{du}{dS}\right)^2 + \left(\frac{dv}{dS}\right)^2 + \left(\frac{dw}{dS}\right)^2} - 1 \tag{4.4}$$

As dS is dx due to the initial orientation, this is

$$\varepsilon_x = \sqrt{1 + 2\frac{\partial u}{\partial x} + \left(\frac{\partial u}{\partial x}\right)^2 + \left(\frac{\partial v}{\partial x}\right)^2 + \left(\frac{\partial w}{\partial x}\right)^2} - 1 \tag{4.5}$$

For small strains this is approximated with sufficient accuracy by

$$\varepsilon_x = \frac{\partial u}{\partial x} + \tfrac{1}{2}\left(\left(\frac{\partial u}{\partial x}\right)^2 + \left(\frac{\partial v}{\partial x}\right)^2 + \left(\frac{\partial w}{\partial x}\right)^2\right) \tag{4.6}$$

The stress stiffness matrix $[\mathbf{S}_i]$ can now be calculated using

$$[\mathbf{S}_i] = EA\varepsilon_i \int_0^L [\mathbf{G}_i]^T [\mathbf{G}_i] dx \tag{4.7}$$

(cf (4.3)), where $[\mathbf{G}_i]$ is a matrix of shape function derivatives and ε_i is the current axial strain. As shown by the subscripts i in (4.7), finding the solution has now become iterative as the stress stiffness matrix is dependent on the current stress state. Also in contrast to the linear solution, the response may no longer be directly proportional to the loading.

4.2 2D WIRE SOLUTIONS

4.2.1 Analytical solution for curvature

Figure 4.1 shows the centre line of a wire under tension T and with a prescribed end angle θ_1. Assuming constant cross section and constant material properties and ignoring wire axial strain, the following solution describes the wire geometry. This is a standard solution which can be found in several texts and is taken from Timoshenko (Timoshenko, 1941).

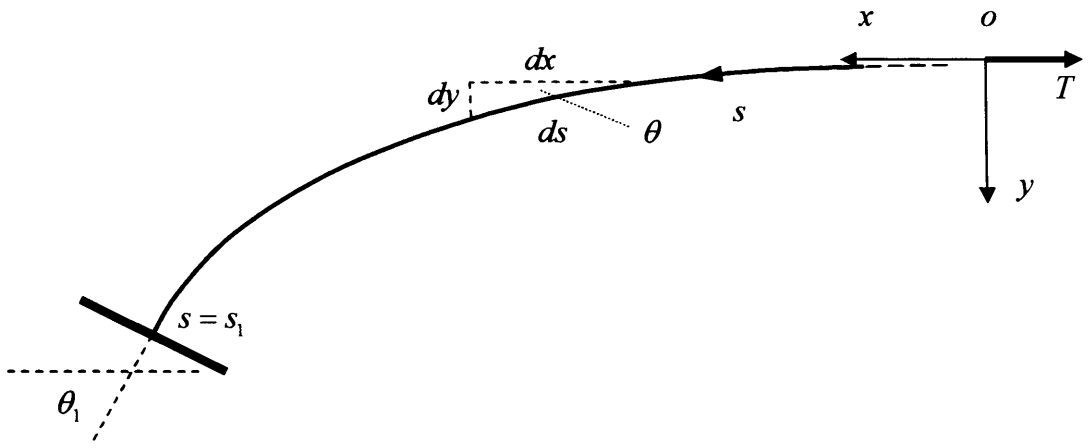

Figure 4.1 Wire centre line.

Moment equilibrium gives

$$M = Ty = EI\frac{d\theta}{ds} \tag{4.8}$$

Differentiating once and using $dy = ds\sin\theta$,

$$\frac{EI}{T}\frac{d^2\theta}{ds^2} = \frac{dy}{ds} = \sin\theta \tag{4.9}$$

Multiplying by $\frac{d\theta}{ds}$, integrating with respect to s and putting $k^2 = \frac{T}{EI}$,

$$\tfrac{1}{2}\left(\frac{d\theta}{ds}\right)^2 = -k^2\cos\theta + C \tag{4.10}$$

The boundary conditions are

$$\begin{aligned} &\text{at } s = -\infty \text{ :-} \quad \theta = 0,\ \frac{d\theta}{ds} = 0 \\ &\text{at } s = s_1 \text{ :-} \quad \theta = \theta_1 \end{aligned} \tag{4.11}$$

The first of (4.11) gives $C = k^2$, and

$$\frac{d\theta}{ds} = k\sqrt{2}\sqrt{1-\cos\theta} \qquad \left(\frac{d\theta}{ds} \text{ always +ve }\right) \tag{4.12}$$

Integration of the above expression and of expressions given by the substitutions $dx = ds\cos\theta$ and $dy = ds\sin\theta$, and using the second of (4.11), gives the following relations between s, x and y coordinates and the angle θ.

$$s - s_1 = \frac{1}{k}\ln\left(\frac{\tan\frac{\theta}{4}}{\tan\frac{\theta_1}{4}}\right)$$

$$x - x_1 = \frac{1}{k}\ln\left(\frac{\tan\frac{\theta}{4}}{\tan\frac{\theta_1}{4}}\right) + \frac{2}{k}\left(\cos\frac{\theta}{2} - \cos\frac{\theta_1}{2}\right)$$

$$y = \frac{\sqrt{2}}{k}\sqrt{1-\cos\theta} \tag{4.13}$$

Rearrangement of the first of (4.13) gives

$$\theta = 4\tan^{-1}\left(\tan\frac{\theta_1}{4}e^{k(s-s_1)}\right) \qquad s \le s_1 \tag{4.14}$$

Numerical Example

As an example, consider a steel wire not dissimilar to flexible pipe tensile armour wires, but of circular cross section with diameter 5mm. This has a cross sectional area of $1.96\text{x}10^{-5}$ m^2 and second moment of area $3.07\text{x}10^{-11}$ m^4. Assume Young's Modulus of the material to be $2.1\text{x}10^{11}$ MPa. If the prescribed tension and end angle are 250N and 0.04 rad respectively, then the characteristic constant k is 6.23 m^{-1} and the profile of the first half metre of the strained wire is as shown in Figure 4.2, where the fixed end is at the origin. Axial stress in the wire due to the tension is 12.7 MPa while the maximum bending stress from simple beam theory is 210 MPa.

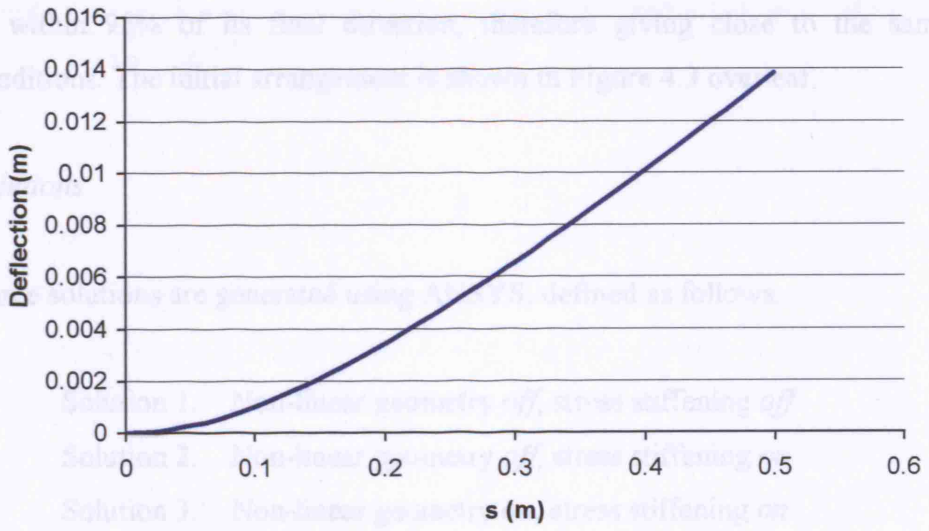

Figure 4.2 Deflected wire profile, analytical solution.

4.2.2 Construction of ANSYS model

As beam elements are naturally expected to have cross-sectional dimensions rather smaller than their length, they are well suited to representing a length of wire. Replication of the problem shown in the previous section can be achieved by setting

up a number of nodes in a straight line and creating two-noded beam elements between them. The prescribed tension and end angle can be created by application of suitable longitudinal and lateral forces at one end while restraining the other end against all displacements and rotations.

Model for Comparison

A series of beam elements with the same cross section and material characteristics as in the previous section can be used to compare with the example shown in Figure 4.2. The first half metre of wire is represented by twenty elements, each straight, 2.5 cm long and aligned in a straight line. The loading is replicated by fixing one end, node 1, against all displacements and rotations and applying forces parallel and perpendicular to the element axes at the other end, node 21. The forces used are 249.8 N in the axial direction and 10 N laterally. These combine to give 250 N tension at an angle of 0.4 rad at the far end where, according to the analytical solution, the wire has straightened to within 95% of its final direction, therefore giving close to the same loading conditions. The initial arrangement is shown in Figure 4.3 overleaf.

Solutions

Three solutions are generated using ANSYS, defined as follows.

Solution 1. Non-linear geometry *off*, stress stiffening *off*
Solution 2. Non-linear geometry *off*, stress stiffening *on*
Solution 3. Non-linear geometry *on*, stress stiffening *on*

Running a linear analysis (Solution 1) of the above model fails to capture the significance of the tension, with moments only calculated using the initial geometry, the structure being analysed as a beam rather than a beam-tie. Hence the wire deflection is completely overstated (Figure 4.4). If stress-stiffening is included (Solution 2), then the corrective moment from the tension is accounted for but the displacements are incorrect as the axial component comes simply from accumulated strains in the axial direction given by the initial geometry (Figure 4.5). Only when non-linear geometry and stress stiffening are both included does the correct solution

appear (Solution 3), with displacements allowing for the rotation of the wire. Figure 4.6 shows a comparison of the full non-linear geometry and stress stiffening solution with the analytical profile. Tension, moment and deflection results from all four solutions are compared in Table 4.1

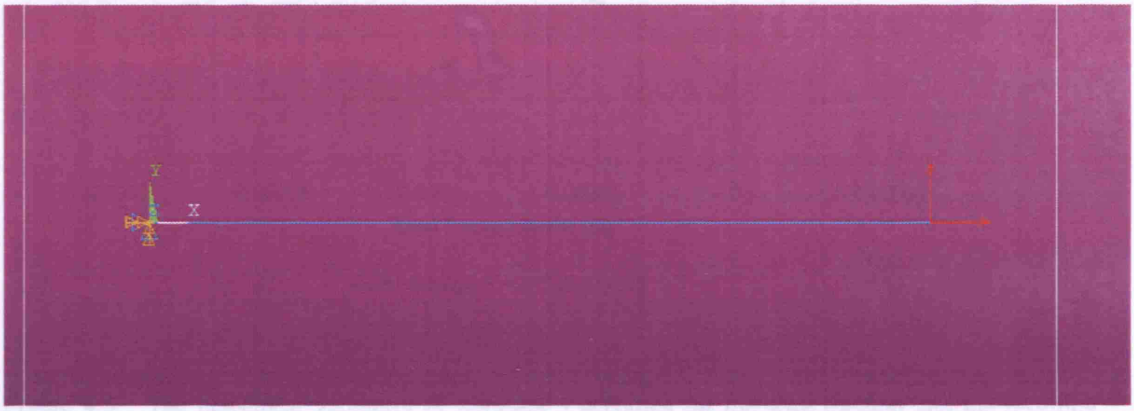

Figure 4.3 ANSYS extract showing initial arrangement of elements, fixed at the origin (left hand side) and with forces applied at the far end.

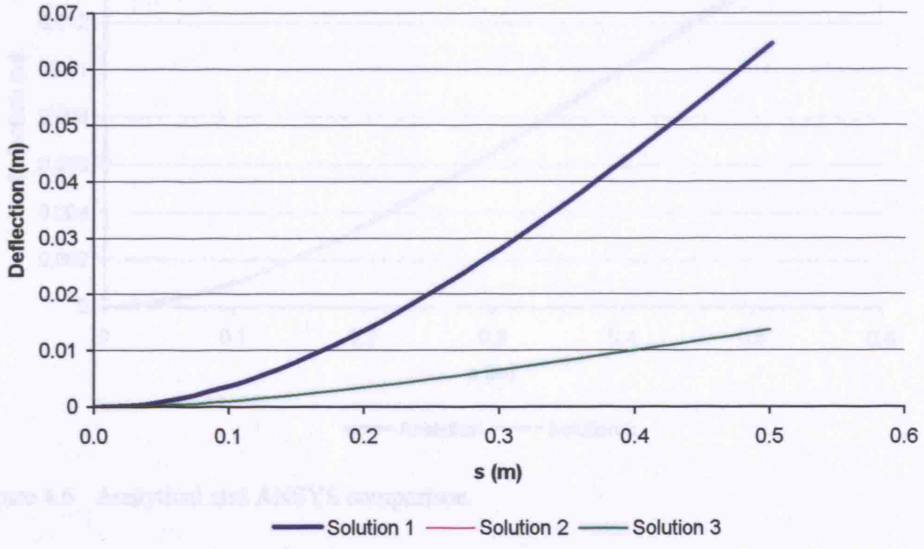

Figure 4.4 Three ANSYS solutions, clearly showing the unsuitability of Solution 1. Solutions 2 and 3 appear identical at this scale.

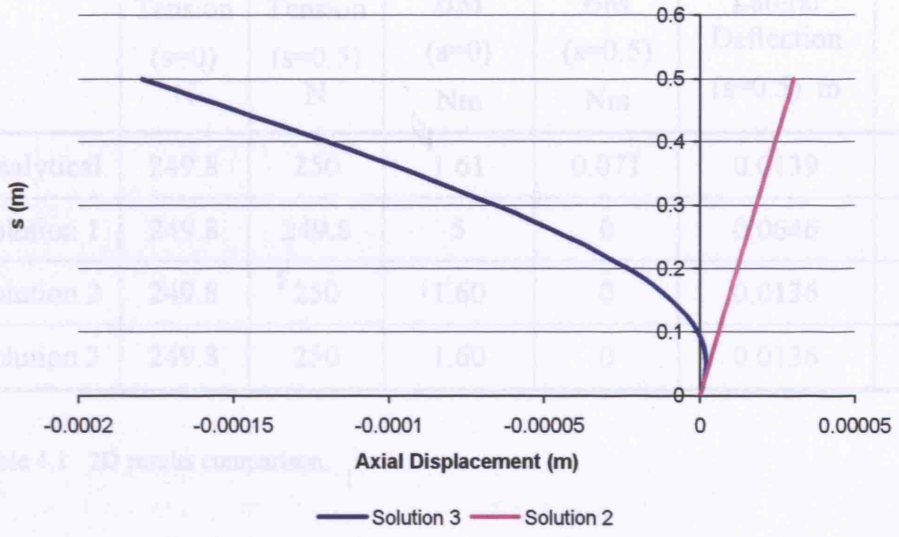

Figure 4.5 The non-linear geometry of Solution 3 accounts for the wire rotation and the resulting shortening in the initial axial direction.

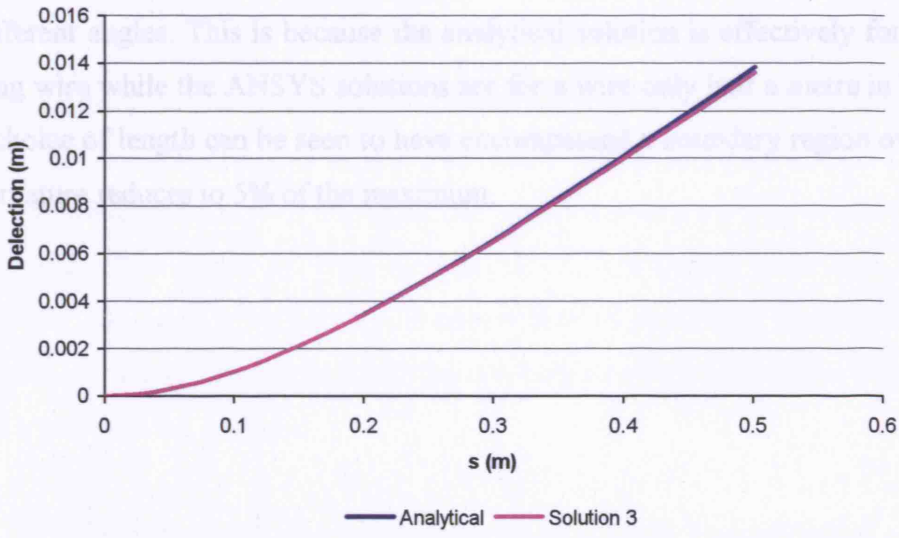

Figure 4.6 Analytical and ANSYS comparison.

	Tension (s=0) N	Tension (s=0.5) N	BM (s=0) Nm	BM (s=0.5) Nm	Lateral Deflection (s=0.5) m	Axial Deflection (s=0.5) m
Analytical	249.8	250	1.61	0.071	0.0139	-2.19×10^{-4}
Solution 1	249.8	249.8	5	0	0.0646	3.03×10^{-5}
Solution 2	249.8	250	1.60	0	0.0136	3.03×10^{-5}
Solution 3	249.8	250	1.60	0	0.0136	-1.79×10^{-4}

Table 4.1 2D results comparison.

4.2.3 Conclusion from 2D Analysis

Solution 3 from the above set of solutions clearly captures the behaviour of a wire under tension with a prescribed end angle. Discrepancy between this solution and the analytical one is simply due to axial strain and application of the tension at slightly different angles. This is because the analytical solution is effectively for an infinitely long wire while the ANSYS solutions are for a wire only half a metre in length. Such a choice of length can be seen to have encompassed a boundary region over which the curvature reduces to 5% of the maximum.

4.3 STRAIGHT PIPE SOLUTIONS

4.3.1 Tensile Armour Example

For the test cases used in this section and in the following curved pipe section, an example tensile armour wire is used with characteristics as set out in Table 4.2. The cross section is rectangular.

E	210 GPa
ν	0.3
Cross section	6 mm x 3 mm
Radius	0.12 m
Helical angle α_0	43.7°

Table 4.2 Example tensile armour wire characteristics.

4.3.2 Construction of ANSYS model

The approach to constructing ANSYS models representing individual helical armour wires on straight pipes is similar to that used for the two dimensional comparison in the previous section, with the important addition that a radial constraint needs to be imposed. The nodes for each element are now arranged in a helix rather than a straight line, and it is also more convenient to apply the loading by specifying displacements at both the first and the last nodes as these are the boundary conditions used to define the analysis.

In the case of a straight pipe, a radial constraint is easily represented by a spar element (which only has translational degrees of freedom) placed between each node and a corresponding 'shadow' node on the cylinder axis (Figure 4.7). Such an element is ideal as, if sufficiently stiff, it will not allow displacement in its original axial direction and it does not present any shear forces or moments. As a result, nodes have freedom to move in the original nodal plane tangent to the cylindrical surface.

The only characteristic not adequately represented by this modelling is the twisting constraint from the surrounding layers on wires with a rectangular cross section. This will lead to some discrepancy in the results.

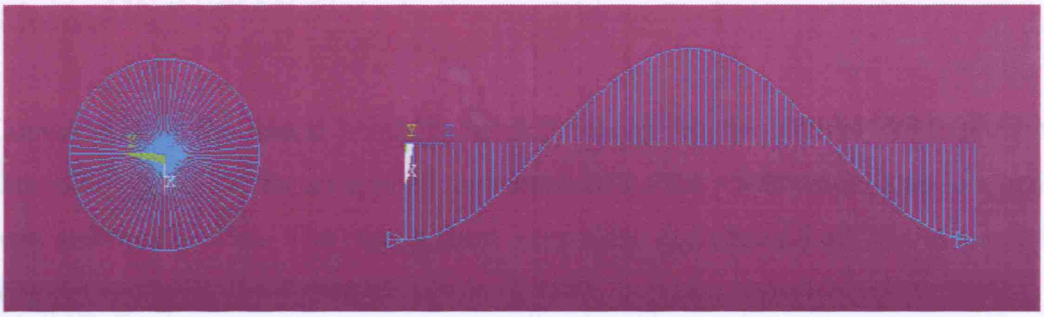

Figure 4.7 Arrangement of ANSYS elements for pipe axial loading.

Model for Comparison

A series of 73 nodes is arranged along a helix with radius 12 cm (Table 4.2), equally spaced and covering one pitch length. The spacing between nodes in the direction of the cylinder axis is 1 cm, which gives a helical angle of 43.7°, a good representation of typical flexible pipe helical armour configurations. As a result the helical wire is modelled by an arrangement of 72 beam elements, each 1.45 cm long. For flexible pipe tensile armour modelling the element cross section should be rectangular and a cross section 6 mm by 3 mm is used. An example with the circular cross section from the 2D case is also examined as the difference in the analytical and numerical twisting constraints should not be so critical. Element material characteristics are kept as in the two dimensional case.

A second series of 73 nodes is arranged equally spaced 1 cm apart along the cylinder axis. These nodes are constrained not to move perpendicular to the axis. The radial constraint to the helix is provided by spar elements of the same material and cross sectional area as the beam elements positioned radially between each helix node and the corresponding axis node.

To apply loading, nodes 1 and 73 in the helical arrangement are fixed against all rotations. Both nodes are moved a prescribed equal but opposite distance in the pipe axial direction while circumferential displacements are kept to zero. The radial constraint is already provided by the central spar.

Solutions

Comparison of the lateral bending moment results for the circular cross section is shown in Figure 4.8, for an applied pipe strain of 0.28%. This would lead to a helical wire strain of 0.13%. The results show very close correlation both in the maximum moment and in its decay rate.

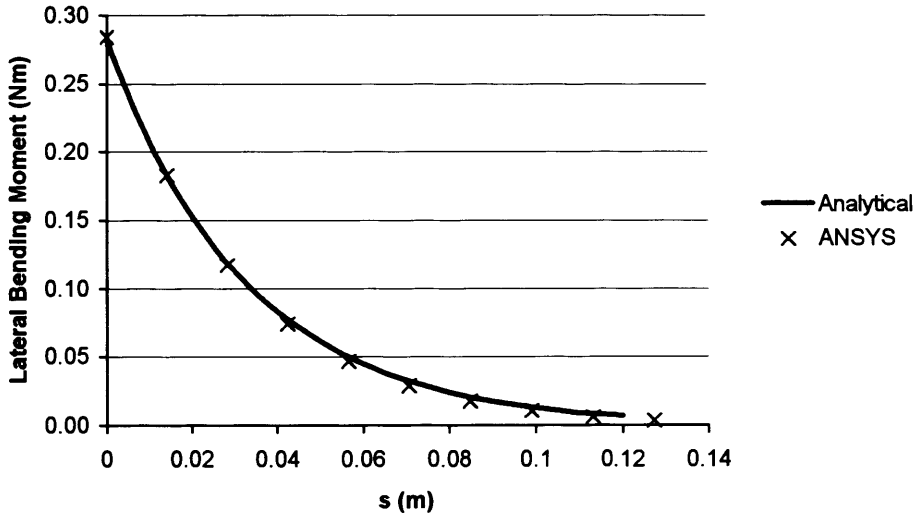

Figure 4.8 Transverse bending moment over boundary region (circular cross section).

The same comparison for the rectangular cross section case is shown in Figure 4.9. Here the maximum values agree well but the ANSYS result suggests a slightly faster decay rate than does the analytical result, with the bending moment becoming negative.

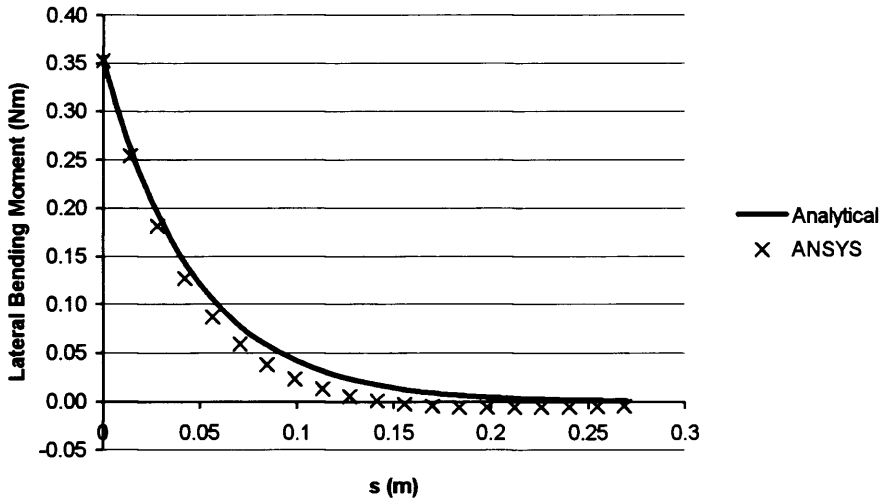

Figure 4.9 Transverse bending moment over boundary region (rectangular cross section).

Owing to the end restraint the wire is being bent laterally, or about the surface normal, while due to the stretching of the helix it is also being straightened about the cylinder axis. Rather than undergoing two such changes in curvature, a wire with no twisting constraint will twist, relieving both bending requirements simultaneously. Using the ANSYS nodal rotations directly, combining the global output to find rotations about the surface normal gives the ANSYS equivalent of the variable α, defining the path of the wire on the surface. Figure 4.10 shows a comparison between this and the analytical result, showing close agreement regarding the wire position and confirming that the ANSYS result has allowed the wire to twist.

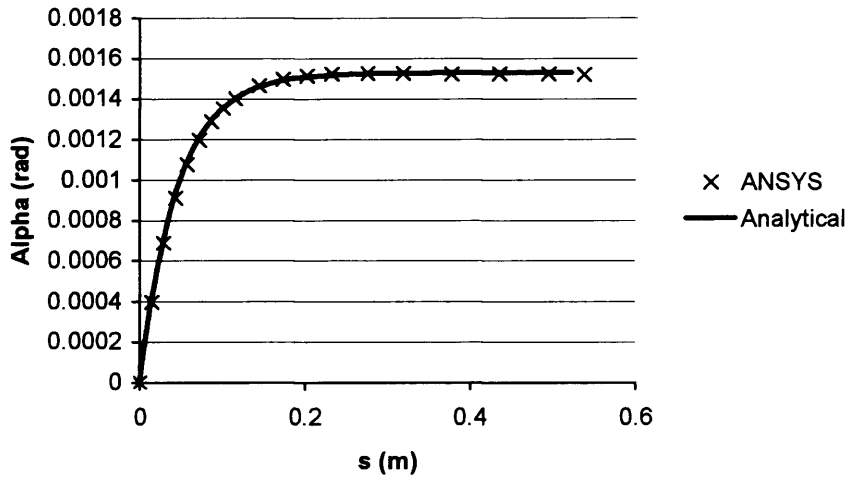

Figure 4.10 Wire rotation about the surface normal (rectangular cross section).

Returning to the circular cross section case, the ANSYS result can be seen to decay slightly faster than the analytical one for the same reason. The analytical constraint on the twist in this case is less realistic as, in the absence of friction, there is no mechanical restriction on rotation. The tendency to twist to relieve curvature will also be less in this case than for the rectangular cross section, there being no imbalance in the cross section.

Wire tension results for the rectangular case are shown in Table 4.3, showing good agreement. The difference of about one percent is due to a slight reduction in radius in the ANSYS case. The very small increase in tension away from the end restraint in the analytical results is also shown by the ANSYS model.

Helical wire (all s)	5051.94 N
Analytical (s=0)	5051.94 N
Analytical (s=0.5)	5052.41 N
ANSYS (s=0)	4998.1 N
ANSYS (s=0.5)	4998.4 N

Table 4.3 Tension results.

4.3.3 Variation in Pipe Strain

The tension levels shown correspond to 280 MPa stress, which is a typical operating stress for the material, and so the pipe strain considered is near the maximum limit. The maximum bending moment response as pipe strain is increased from zero through to 0.28 % is shown in Figure 4.11. The analytical and ANSYS results are in good agreement, showing the same non-linearity of the response.

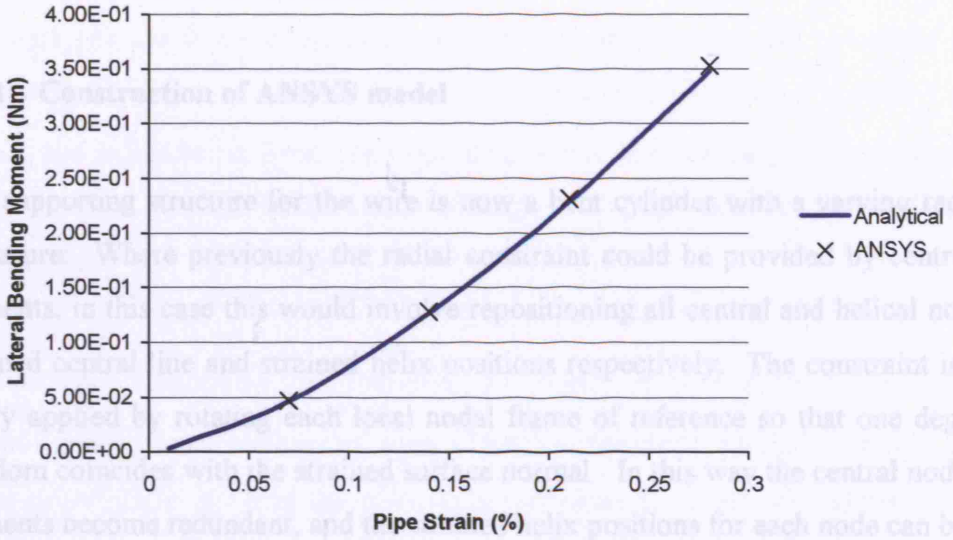

Figure 4.11 Transverse bending moment for range of pipe strains.

4.3.4 Conclusion from Straight Pipe Analysis

The case study carried out shows very good agreement between the ANSYS model and the analytical solution for maximum lateral bending moment at the wire termination. Results for the wire path on the cylinder surface are also very close, with discrepancies in the lateral bending moment distribution being accounted for by a lack of twisting constraint in the ANSYS model. Differences in the wire tension are not significant.

4.4 CURVED PIPE SOLUTIONS

4.4.1 Construction of ANSYS model

The supporting structure for the wire is now a bent cylinder with a varying radius of curvature. Where previously the radial constraint could be provided by central link elements, in this case this would involve repositioning all central and helical nodes to strained central line and strained helix positions respectively. The constraint is more easily applied by rotating each local nodal frame of reference so that one degree of freedom coincides with the strained surface normal. In this way the central nodes and elements become redundant, and the strained helix positions for each node can be used to locate the tangent plane on which the node is allowed to move. Hence loading is provided by fixing the first helix node against all displacements and rotations, moving all other nodes in the direction of the strained surface normals, and giving the last node the required displacements to remain in position with respect to the end cross section.

The loading is now dependent on the direction and amount of applied curvature. The direction is controlled by the displacements rather than by alteration of ν_0 as in the analytical model. It is also possible to model a straight pipe scenario in this way and make a comparison with the central spar model of the previous section.

Model Input Data

New input required for the flexural loading models is the rotations for each nodal frame of reference and the perpendicular distance from the initial nodal locations to the tangent planes. The rotations used are three successive Euler angles which rotate the local frame to coincide with the strained surface normal, the strained helix tangent and a third axis to complete the triad, this being in the direction of lateral slip.

The strained pipe configuration consists first of an axial strain and then of a plane curvature of the strained pipe axis due to applied tension and prescribed end angle, in the same way as in Figure 4.1.

Strained helix nodal locations can be constructed from the geometry of the strained pipe axis and plane cross sections perpendicular to it as follows. A point on the unstrained helix can be defined by its two cylindrical coordinates z (axial) and ϕ (polar), the radius being fixed, the z coordinate also defining the pipe cross section on which the node lies. An axial strain to the pipe axis simply alters the z coordinate to a new one, z_1.

Application of a curvature distribution κ_p to the pipe centre line causes the centre line to move and the cross sections to rotate. The direction of curvature is controlled by an initial polar angle ϕ_0[1] and the new nodal positions in terms of a global cartesian coordinate system can be written as (see Figure 4.12)

$$X = X_{CL} + R\sin(\phi+\phi_0)\cos\theta_{CL}\sin\phi_0 + R\cos(\phi+\phi_0)\cos\phi_0$$

$$Y = Y_{CL} + R\sin(\phi+\phi_0)\cos\theta_{CL}\cos\phi_0 - R\cos(\phi+\phi_0)\sin\phi_0$$

$$Z = Z_{CL} - R\sin(\phi+\phi_0)\sin\theta_{CL} \qquad (4.15)$$

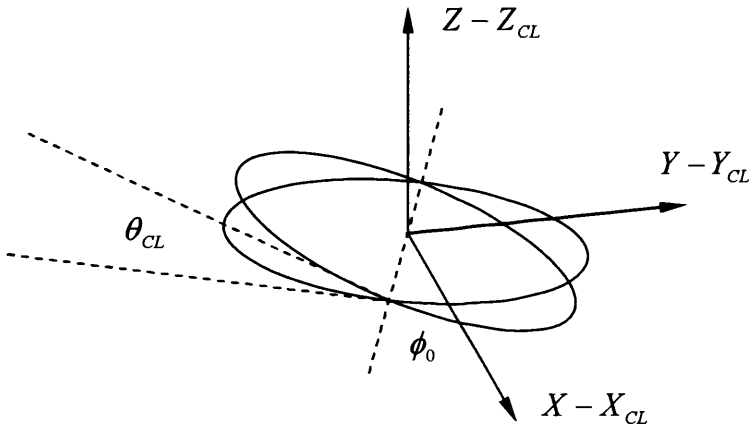

Figure 4.12 Rotated pipe cross section definitions. Pipe radius is R.

[1] The initial ANSYS helix is defined only once in the global cartesian system (X,Y,Z). ϕ_0 therefore coincides with θ_0 in the analytical model, where the plane of curvature is fixed and the wire end is rotated.

The first term in the expressions (4.15) is the centre line coordinate, the second is the nodal projection parallel to the slope and the third is the nodal projection perpendicular to the slope.

A tangent vector to the strained helix in (4.15) is conveniently found by differentiation with respect to the strained axial coordinate z_1. Relationships are as follows (see Figure 4.13).

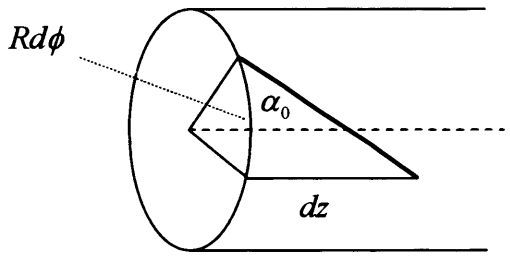

Figure 4.13 Differential element of unstrained helix showing relationship $\phi(z)$.

$$\frac{d\phi}{dz} = \frac{1}{R\tan\alpha_0}, \qquad \frac{d\phi}{dz_1} = \frac{1}{R\tan\alpha_0(1+\varepsilon_p)} \tag{4.16}$$

$$\frac{d\theta_{CL}}{dz_1} = k\sqrt{2}\sqrt{1-\cos(\theta_1-\theta_{CL})} \qquad \text{(from 4.12)} \tag{4.17}$$

$$\frac{dX}{dz_1} = \sin\theta_{CL}\sin\phi_0 + R\sin\phi_0\left\{\cos\theta_{CL}\cos(\phi+\phi_0)\frac{1}{R\tan\alpha_0(1+\varepsilon_p)}\right.$$
$$\left. -\sin(\phi+\phi_0)\sin\theta_{CL}k\sqrt{2}\sqrt{1-\cos(\theta_1-\theta_{CL})}\right\}$$
$$-R\cos\phi_0\sin(\phi+\phi_0)\frac{1}{R\tan\alpha_0(1+\varepsilon_p)} \tag{4.18}$$

$\frac{dY}{dz_1}$ follows, replacing $\sin\phi_0$ with $\cos\phi_0$ and $\cos\phi_0$ with $-\sin\phi_0$ in 4.18 (see (4.8)).

$$\frac{dZ}{dz_1} = \cos\theta_{CL} - R\left\{\sin(\phi+\phi_0)\cos\theta_{CL}\, k\sqrt{2}\sqrt{1-\cos(\theta_1-\theta_{CL})}\right.$$
$$\left. + \sin\theta_{CL}\cos(\phi+\phi_0)\frac{1}{R\tan\alpha_0(1+\varepsilon_p)}\right\} \qquad (4.19)$$

The above X, Y and Z differentials with respect to z_1 are the X, Y and Z components of a tangent vector. Division of these terms by the modulus is necessary to find the unit tangent as z_1 is not a natural coordinate of the wire.

The unit surface normal at each node is found by extrapolation of the line through it from the centre line point with the same z_1 coordinate. The third vector of the unit triad, in the (binormal) direction of lateral slip, follows from the vector product of the tangent with the normal, in that order, so that the normal, binormal and tangent vectors form a right-handed set. This set of vectors can be evaluated at each node to find the Euler angles and the displacement required to find the tangent plane.

Euler Angles

One method employed by ANSYS to change from one set of axes to another is the use of sequential Euler angles applied about the instantaneous z, x and y axes in turn. These are shown in Figure 4.14 and the resulting expressions show how the Euler angles are found.

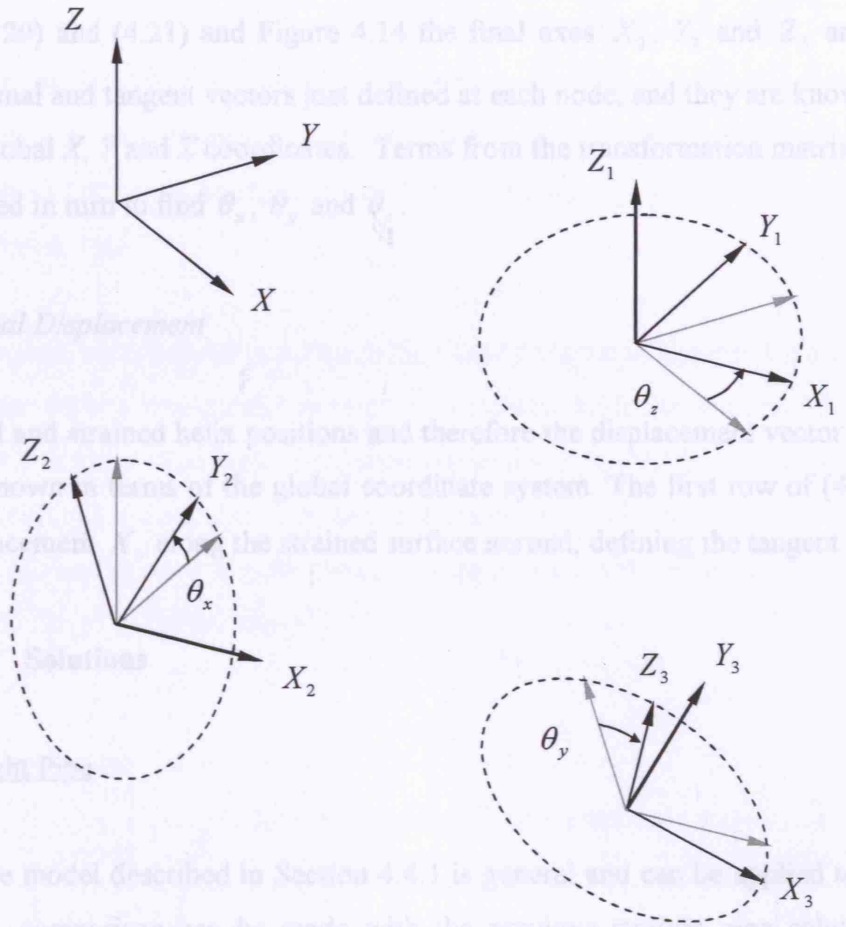

Figure 4.14 Sequential Euler angles.

$$
\begin{aligned}
Z_1 &= Z & X_2 &= X_1 & Y_3 &= Y_2 \\
X_1 &= X\cos\theta_z + Y\sin\theta_z & Y_2 &= Y_1\cos\theta_x + Z_1\sin\theta_x & Z_3 &= Z_2\cos\theta_y + X_2\sin\theta_y \\
Y_1 &= Y\cos\theta_z - X\sin\theta_z & Z_2 &= Z_1\cos\theta_x - Y_1\sin\theta_x & X_3 &= X_2\cos\theta_y - Z_2\sin\theta_y
\end{aligned}
\tag{4.20}
$$

$$
\begin{pmatrix} X_3 \\ Y_3 \\ Z_3 \end{pmatrix} =
\begin{pmatrix}
\cos\theta_y\cos\theta_z & \sin\theta_x\sin\theta_y\cos\theta_z & -\cos\theta_x\sin\theta_y \\
-\sin\theta_x\sin\theta_y\sin\theta_z & +\cos\theta_y\sin\theta_z & \\
-\cos\theta_x\sin\theta_z & \cos\theta_x\cos\theta_z & \sin\theta_x \\
\sin\theta_y\cos\theta_z & -\sin\theta_x\cos\theta_y\cos\theta_z & \\
+\sin\theta_x\sin\theta_y\sin\theta_z & +\sin\theta_y\sin\theta_z & \cos\theta_x\cos\theta_y
\end{pmatrix}
\begin{pmatrix} X \\ Y \\ Z \end{pmatrix}
\tag{4.21}
$$

In (4.20) and (4.21) and Figure 4.14 the final axes X_3, Y_3 and Z_3 are the normal, binormal and tangent vectors just defined at each node, and they are known in terms of the global X, Y and Z coordinates. Terms from the transformation matrix in (4.21) can be used in turn to find θ_x, θ_y and θ_z.

Normal Displacement

Initial and strained helix positions and therefore the displacement vector for each node are known in terms of the global coordinate system. The first row of (4.21) gives the displacement X_3 along the strained surface normal, defining the tangent plane.

4.4.2 Solutions

Straight Pipe

As the model described in Section 4.4.1 is general and can be applied to straight pipe cases, comparison can be made with the previous straight pipe solutions. Lateral bending moments are shown in Figure 4.15.

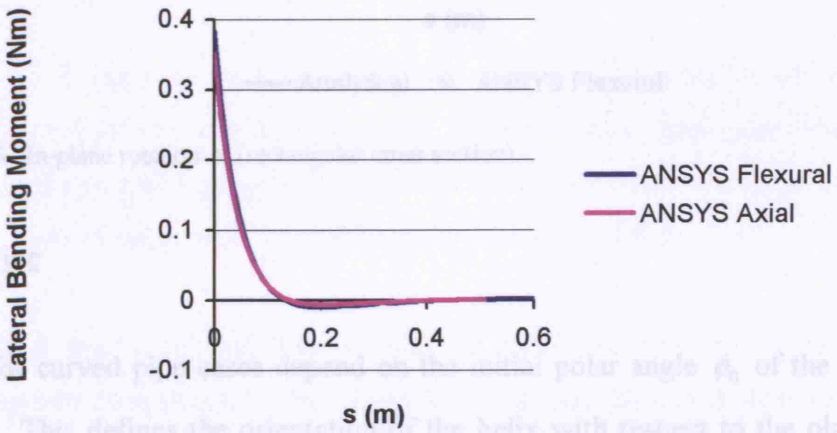

Figure 4.15 Comparison of the two ANSYS models, straight case bending moments (rectangular cross section).

The models display good agreement, although the maximum bending moment value in the flexural model case is 0.38 Nm compared with 0.35 Nm. This is attributable to the lack of in-plane rotational constraint at the far end in the flexural model, and also to the tangent plane association in the flexural model with the strained helix rather than the original one.

Agreement with the analytical model is already shown in Figures 4.9 and 4.10. Figure 4.16 shows the analytical variable α compared with the normal rotation from the ANSYS models. The lack of twisting constraint in the ANSYS models is responsible for the slight differences, this being because twist will make lateral bending easier while increasing very slightly the energy associated with change in binormal curvature due to change in helical angle.

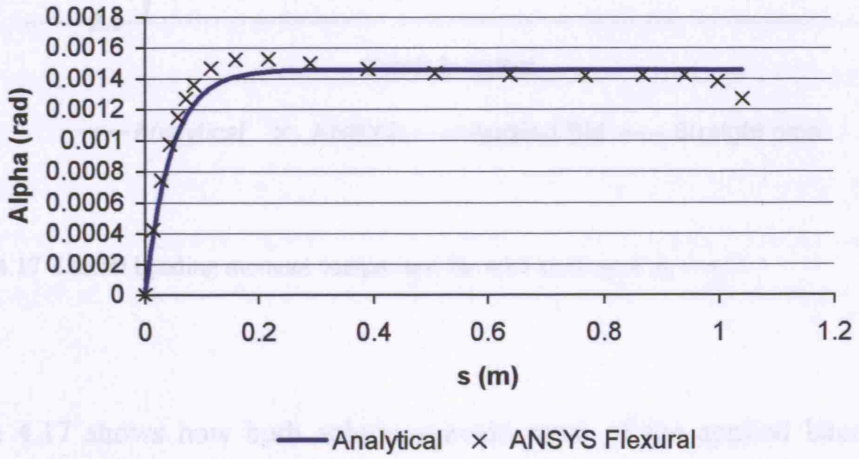

Figure 4.16 In-plane rotation α (rectangular cross section).

Curved Pipe

Results for curved pipe cases depend on the initial polar angle ϕ_0 of the wire at the restraint. This defines the orientation of the helix with respect to the plane of pipe curvature, with $\phi_0 = 0$ being opposite the pipe neutral axis position and $\phi_0 = \pi/2$ being on the inside (compressive side) of the curvature (see Figure 4.12). The example result shown in Figure 4.17 is for the same pipe as in the previous cases with a small amount of applied curvature in addition, this being at an almost constant radius

of curvature of 20 m. The figure gives the lateral curvature from the ANSYS flexural model and compares it with the analytical result. Also given is the original result for the strained pipe without curvature and the applied lateral bending moment. ϕ_0 is $\pi/2$ so the wire end is constrained at the 'extreme fibre' position on the compressive side.

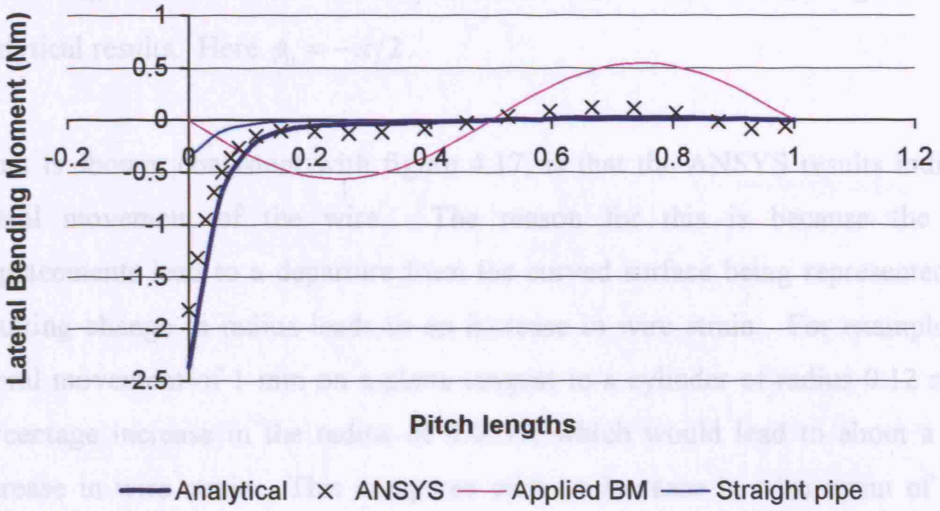

Figure 4.17 Lateral bending moment comparison for wire starting at $\phi_0 = \pi/2$.

Figure 4.17 shows how both solutions avoid most of the applied lateral curvature along the length of the wire at the expense of an increased maximum lateral bending moment at the restraint, suggesting that the wire tends to move towards the surface geodesic. This effect is more pronounced in the analytical case.

Values for α can be inferred from the ANSYS nodal rotation output by subtraction of the appropriate component of the centre line rotation. However if these results are then used via summation to find γ, there is a shortfall in the total and $Y - \gamma$ at the far end of the wire is not zero as it should be to be consistent with the applied boundary conditions.

In view of the fact that the ANSYS displacements are likely to be more reliable than the rotations, a better approach is to find γ directly and then to find α from the changes in γ. To do this, the ANSYS output displacements can be subtracted from the input displacements, which are to the strained helix, and lateral components taken to find $Y-\gamma$. As Y is also known fom integration of the angle β, γ is easily extracted, and a value for α can be found from the differences in γ between each node. Figures 4.18 and 4.19 show these results for α and γ together with the analytical results. Here $\phi_0 = -\pi/2$.

What is shown, consistent with figure 4.17, is that the ANSYS results indicate less lateral movement of the wire. The reason for this is because the ANSYS displacements lead to a departure from the curved surface being represented and the resulting change in radius leads to an increase in wire strain. For example a small lateral movement of 1 mm on a plane tangent to a cylinder of radius 0.12 m gives a percentage increase in the radius of 0.0035, which would lead to about a 0.002 % increase in wire strain. This compares with an increase in wire strain of 0.0012% associated with an angle α of 0.005 rad, showing that the additional strain energy introduced by the tangent plane approximation to the surface is of the same order as the energies associated with α, and will therefore impinge on the results.

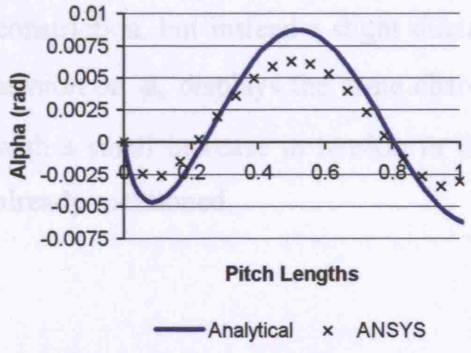

Figure 4.18 Normal rotation.

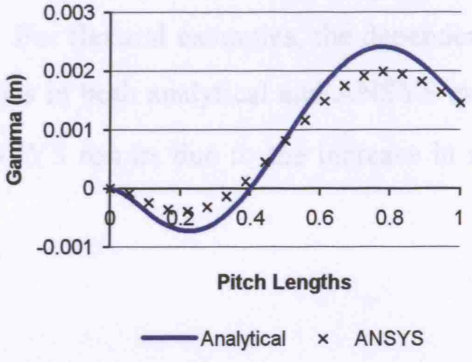

Figure 4.19 Lateral displacement.

The bending moment at the end fitting as a function of polar angle ϕ_0 is shown in Figure 4.20. The magnification shown by ANSYS for $\phi_0 = \pi/2$ is also shown for all ϕ_0, and there is a slight 'phase shift' between the analytical and ANSYS relationships, but the characteristic dependence on ϕ_0 is the same.

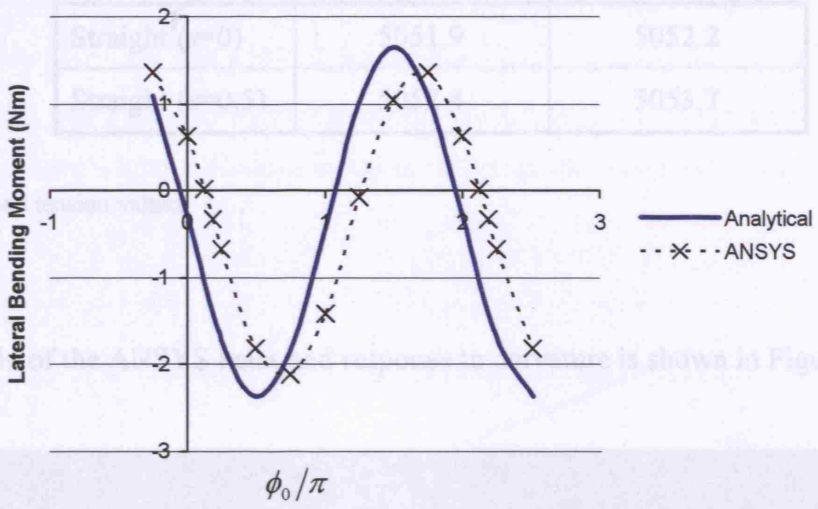

Figure 4.20 End moment as a function of restraint polar angle with repect to plane of curvature.

Finally a comparison of end tension values is shown in Table 4.4. The ANSYS flexural model returns a straight pipe tension very slightly greater than the analytical result, in accordance with the new restraint which makes sure that there is no radial constriction, but instead a slight dilatation. For flexural examples, the dependence of tension on ϕ_0 displays the same charcteristics in both analytical and ANSYS models, with a small increase in tension in the ANSYS results due to the increase in radius already mentioned.

ϕ_0	Analytical (N)	ANSYS (N)
0	4785.5	4869.3
$\pi/2$	4911.0	4965.4
π	5038.7	5042.3
$3\pi/2$	4913.1	4944.5
Straight (s=0)	5051.9	5052.2
Straight (s=0.5)	5052.4	5053.7

Table 4.4 End tension values.

An example of the ANSYS helix and response to curvature is shown in Figure 4.21.

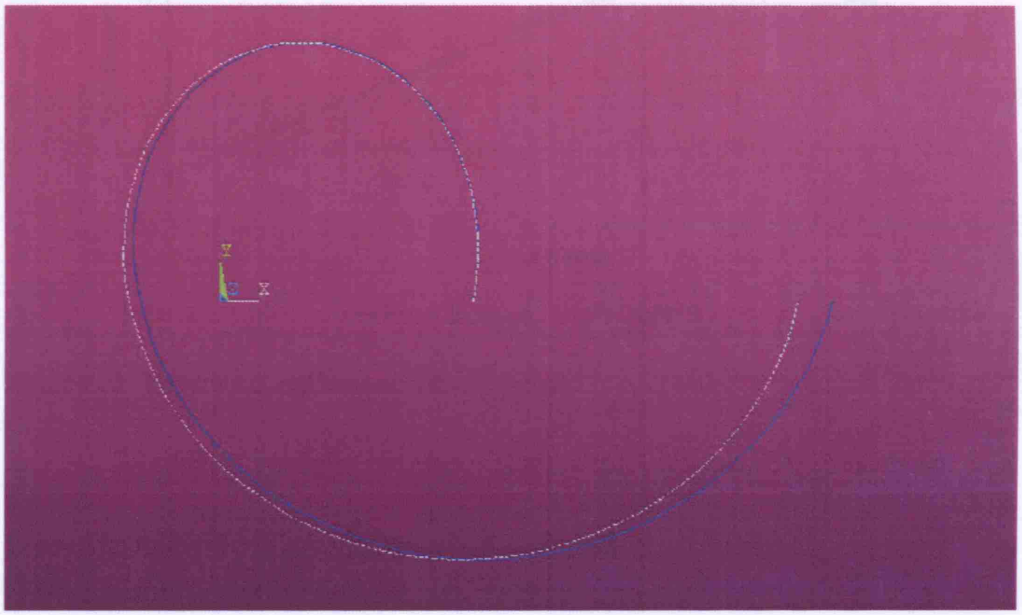

Figure 4.21 Initial helix and response to curvature $(\phi_0 = \pi/2)$.

4.4.3 Variation in Applied Curvature

The end moment is due to a combination of pipe tension and pipe bending, with the ANSYS response to tension very similar to the analytical one but with some difference in magnitude between the responses to curvature. Figure 4.22 shows a comparison of end moment results as the amount of curvature applied is varied, with the tension level remaining constant and ϕ_0 also constant at $-\pi/2$. The comparison indicates that as the curvature increases, the ANSYS result shows less tendency for the wire to move, thus reducing the variation in end moment when compared to the analytical result. This is consistent with the increase in radius affecting the previous results.

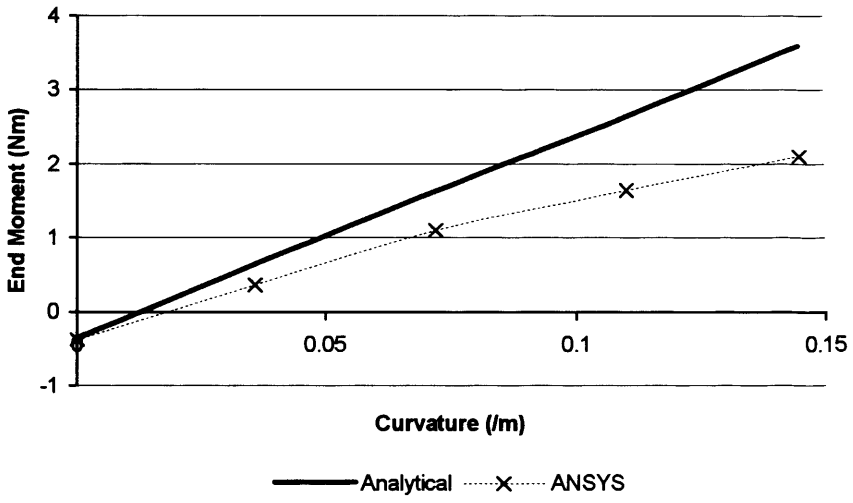

Figure 4.22 Variation in end moment with curvature.

4.4.4 Conclusion from Curved Pipe Analysis

Linking the ANSYS input data to the strained helix in order to define toroidal surface tangent planes does not define the problem perfectly, although to use any other tangent planes, adopted after the results from the analytical model, would reduce the independence of the verification. Where there is lateral movement of the wire, as happens more in the flexural cases, the departure of the wire from the cylinder surface is more pronounced and the solution becomes the solution to a slightly different problem, in other words of a wire sliding on a cylinder with a polygonal cross section

rather than a circular one. However, the essential characteristics displayed by both the analytical and the ANSYS models are very similar and indicate that the wire tends to move towards the surface geodesic, this being at a greater 'helical' angle on the inside of the curvature than on the outside.

The analytical solution has been more successful than the ANSYS one in allowing for movement along the circumference of the cylinder. The tangential directions used by ANSYS are not updated during the analysis, whereas use of the variables α and γ avoids this difficulty in the analytical solution. This provides further confirmation that using the angle α as a fundamental variable was a good choice for description of the problem which has allowed the pursuit of a more valuable closed-form solution.

4.5 VERIFICATION CONCLUSIONS

As the problem under consideration is that of a thin rod under tension, if a finite element model is to be used it must include a non-linear geometry capability, thereby being able to account for the effects on equilibrium of any deformation of the structure.

Using such a capability, ANSYS is able to model accurately a two dimensional wire with prescribed tension and end angle problem, indicating its suitability for further thin rod analysis. However difficulties with implementing a model for flexible pipe tensile armour include maintaining radial and twisting constraints on the wire.

For problems where wire movement is essentially in the pipe axial direction, and the wire cross section is axisymmetric, these difficulties are reduced in significance. ANSYS results for such cases agree well with the analytical model and provide the first indication that the analytical model is correct. Introduction of a rectangular cross section causes the expected difference between analytical and ANSYS normal bending moments, but the wire centre line paths in both models remain the same, as do the maximum bending moments. Furthermore, as the level of pipe strain is varied the response of both models is the same.

For flexural cases which involve greater lateral slip, accurate definition of the problem of a wire sliding on a bent cylindrical surface using finite element analysis is more difficult. This is because for the elements used it was possible to define degrees of freedom in terms of cartesian coordinates only. Close approximation can be achieved by allowing certain points of the wire to move on planes tangent to the surface, although this will lead to increases in radius on the outside of curvature and increases or decreases on the inside.

Given this discrepancy in the analytical and ANSYS models, the results from ANSYS lend good support to the analytical model by showing the same type of straightening in response to the applied curvature. This is clear from the lateral bending moment distribution and in particular from the end moment distribution around the pipe circumference at the restraint and its response to increase in curvature.

In conclusion, the ANSYS modelling has returned results consistent with the analytical answers, giving good support to the analytical model which is now available for case studies and parameter surveys.

5 ENGINEERING APPLICATIONS

5.1 INTRODUCTION

The analysis presented in Chapter 3 provides the opportunity to assess flexible pipe tensile armour behaviour under the influence of end restraint. The models developed reduce the problem of wire response to loading to the determination of a single variable from which wire orientation and wire position can be found, allowing wire stresses and also wire slip to be predicted.

Stresses caused by wire local bending increase the maximum longitudinal stresses experienced, and this is of interest from a fatigue point of view and also regarding maximum loading. Slip may also be of interest from a fretting fatigue point of view although this is not a primary aim of the modelling as it is frictionless, and aimed at dynamic flexible pipe designed with features to reduce wear between layers. What is of interest regarding slip is whether or not inter-wire gaps are closed and if so, what impact this has on the validity of the model. Both stresses and slip provide answers which may be assessed against those of other analyses.

The chapter begins with the selection of typical pipe parameter ranges within which the reported model studies are carried out. Calculation of stresses and slip from the model results is explained, together with the assessment of inter-wire gap closure due to rotation and relative lateral motion. There then follow applications of the axi-symmetric and flexural models, including analysis of the expressions obtained, typical results and parametric surveys.

5.2 TYPICAL FLEXIBLE PIPE PARAMETER VALUES

Some flexible pipe parameter ranges significant to tensile armour analysis are listed in Table 5.1, covering variations in the helical geometry and wire cross-section and material.

Pipe Bore	2" - 16" (51mm – 406mm)
Tensile Armour Helix Radius	45 mm – 235 mm
Tensile Armour Helical Angle	30° – 60°
Wire Height	3.5 mm – 4 mm
Wire Width	6 mm – 10 mm
Wire UTS	750 – 1000 MPa

Table 5.1 Flexible pipe tensile armour parameter ranges.

Pipe loading for axial cases is based on applied tension up to a damaging pull[1] at which a wire yield stress of 0.5 (0.67) times the UTS is reached. Flexible pipe is normally operated at up to about one quarter or one fifth of this level of tension.

Pipe bending for flexural cases is up to but not exceeding a minimum radius of curvature dependent on the pipe bore. Calculation of the minimum radius is shown in Section 5.5.

[1] Damaging pull refers to the level of tension at which first yield occurs, therefore leading to permanent deformation of the pipe structure.

5.3 STRESSES AND SLIP

5.3.1 Increase in Maximum Longitudinal Stress

Axial stress σ_a in the tensile armour due to tension is taken to be uniformly distributed over the cross-section, while longitudinal stresses σ_b due to bending are found using the simple beam theory equations 5.1 (standard notation).

$$\frac{M}{I} = \frac{\sigma}{y} = \frac{E}{R} \tag{5.1}$$

Hence maximum stress due to bending is, for a rectangular cross-section with sides A and B, A<B,

$$(\sigma_b)_{\max} = \frac{E}{2}\left(|\kappa_n|B + |\Delta\kappa_b|A\right)_{\max}$$

$$= \frac{E}{2}\left(\left|K_p \sin\alpha_0 \cos(ks+\theta_0) - \frac{d\alpha}{ds}\right|B + \left|K_p \sin^2\alpha_0 \sin(ks+\theta_0) + \frac{2}{R}\alpha\cos\alpha_0 \sin\alpha_0\right|A\right)_{\max} \tag{5.2}$$

The maximum value will usually occur at the end restraint although in some cases, where there is only a small change in wire orientation, it may occur elsewhere. Such maxima will be small compared to those dominated by normal bending at the end fitting.

5.3.2 Slip

Axial Slip

Axial slip is obtained by comparing wire axial extension and extension of the original path on the surface. As wire tension results are largely independent of s this will be dominated by the surface strain due to pipe curvature. Surface bending strain is

$$\varepsilon_s = -\frac{R}{\rho_0} e^{-ms} \sin(ks + \theta_0) \tag{5.3}$$

Defining positive slip as wire movement in the positive s direction with respect to the surface, axial slip S_a is therefore

$$S_a(s) = \frac{R}{\rho_0} \int_0^s e^{-mx} \sin(kx + \theta_0) dx \sin^2 \alpha_0 \tag{5.4}$$

Transverse Slip

Transverse slip is the difference between surface and wire lateral movements and is therefore dependent on wire movement γ and also on the total surface strain, as set out in Section 3.5.1.

Surface movement is (from (3.68))

$$\Delta_s(s) = \left\{ \varepsilon_1 s - \int_0^s \frac{R}{\rho_0} e^{-mx} \sin(kx + \theta_0) dx \right\} \sin \alpha_0 \cos \alpha_0 \tag{5.5}$$

where ε_1 is the surface strain due to pipe tension. Zero total strain would lead to zero displacement, and this coincides with the loxodromic curve at angle α_0 to the centre line.

Wire movement is γ, also measured from the loxodromic or $\alpha = 0$ line. Hence transverse slip is given by

$$S_t(s) = \left\{ \varepsilon_1 s - \int_0^s \frac{R}{\rho_0} e^{-mx} \sin(kx + \theta_0)\, dx \right\} \sin\alpha_0 \cos\alpha_0 - \gamma(s) \tag{5.6}$$

5.3.3 Inter-Wire Gaps

Flexible pipe tensile armour wires are wound with a small gap between adjacent wires in the same layer. If this were not the case, even a small amount of bending would cause wires to be packed too closely together, compromising the flexibility of the pipe and leading to a disruption of the structure if wires were pushed out of position. These gaps are opened and closed when the pipe is bent, due to a combination of wire normal rotation and differential movement across the supporting surfaces.

Wire Rotation

Decrease in helical angle will cause wires to be forced closer together, as the circumferential cross-section of each wire increases. The change in space available for adjacent gaps due to wire rotation α is (Figure 5.1)

$$\begin{aligned} \Delta g &= w(\sin(\alpha_0 + \alpha) - \sin\alpha_0)\sin\alpha_0 \\ &= w\alpha \sin\alpha_0 \cos\alpha_0 \end{aligned} \tag{5.7}$$

for small α.

The full change in the wire cross-sections on any circumferential cross-section could be compared with the layer circumference to assess whether or not any free space remains. However, consideration of the perpendicular gap between wires allows individual wire contact to be assessed by combining any changes due to rotation with the potentially greater changes due to lateral slip.

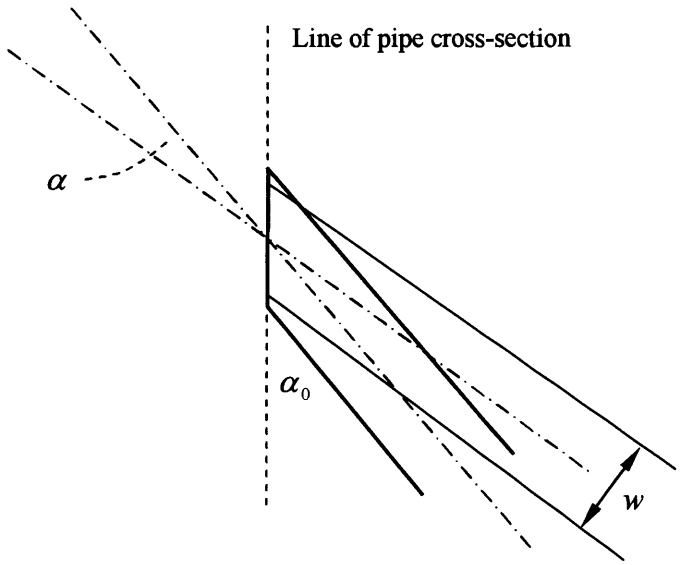

Figure 5.1 Cross-section change due to wire normal rotation (α exaggerated).

Wire Lateral Slip

The models developed have provided a result for wire lateral slip in terms of the polar position of the wire end restraint θ_0 and of the position along the wire s. For comparison of lateral slip, a perpendicular variable x should be used (see Figure 5.2). As x increases from its origin, defined by initial values s_0 and θ_{00}, the corresponding individual wire values of s and θ_0 change, with the following proportionalities.

$$s = \frac{x}{\tan\alpha_0} + s_0 = k_2 x + s_0$$

$$\theta_0 = -\frac{x}{R\sin\alpha_0} + \theta_{00} = k_3 x + \theta_{00} \qquad (5.8)$$

Hence the function $(Y - \gamma)$ can be rewritten as a function of x rather than of s (see (5.9) and (5.10)), and evaluated for each wire to indicate relative movement for comparison with the average space available. Differentiation of the function with respect to the new variable x could be carried out and compared with the initial gap

size, although this requires lengthy evaluation as the constants in (5.10) are also functions of θ_0.

$$Y = \varepsilon_1 \cos\alpha_0 \sin\alpha_0 (k_2 x + s_0)$$
$$-\frac{RZ_p \cos\alpha_0 \sin\alpha_0}{m^2 + k^2}\{-m(e^{-m(k_2 x+s_0)} \sin(k_4 x + ks_0 + \theta_{00}) - \sin(k_3 x + \theta_{00}))$$
$$-k(e^{-m(k_2 x+s_0)} \cos(k_4 x + ks_0 + \theta_{00}) - \cos(k_3 x + \theta_{00}))\} \qquad (5.9)$$

where $k_4 = kk_2 + k_3$

$$\gamma = A(k_2 x + s_0) + \frac{B}{\mu}(e^{-\mu(k_2 x+s_0)} - 1) + \frac{1}{m^2 + k^2}\{$$
$$+(kC - mD)(e^{-\mu(k_2 x+s_0)} \sin(k_4 x + ks_0 + \theta_{00}) - \sin(k_3 x + \theta_0))$$
$$-(mC + kD)(e^{-\mu(k_2 x+s_0)} \cos(k_4 x + ks_0 + \theta_{00}) - \cos(k_3 x + \theta_0))\} \qquad (5.10)$$

with $A(\theta_0), B(\theta_0), C(\theta_0)$ and $D(\theta_0)$.

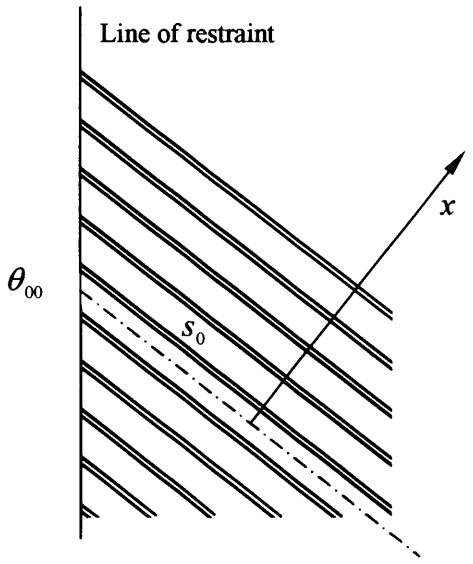

Figure 5.2 Tensile armour near end fitting, showing perpendicular variable x.

5.4 APPLICATION OF AXIAL MODEL

5.4.1 Analysis of Result

Large Pipe Radius R

As the pipe radius is increased towards infinity, the cylinder surface in the region of a wire termination becomes more and more flat. For large R, solution (3.46) reduces to

$$EI_1 \frac{d^2\alpha}{ds^2} - T_{00}\alpha = \lambda - T_{00}\beta \tag{5.11}$$

This leads to a decay rate in the solution of $\sqrt{T_{00}/EI_1}$, which is the same as in the standard result obtained by the two dimensional analysis of a wire under tension at a prescribed angle. The angle is

$$\alpha = \frac{\beta}{1 - \sqrt{\frac{EI_1}{L^2 T_{00}}}\left(1 - e^{-\sqrt{\frac{T_{00}}{EI_1}}L}\right)}\left(1 - e^{-\sqrt{\frac{T_{00}}{EI_1}}s}\right)$$

As the two dimensional analysis is for a semi-infinite wire, this reduces further to the standard result

$$\alpha = \beta\left(1 - e^{-k_0 s}\right), \qquad k_0^{\,2} = T_{00}/EI_1 \tag{5.12}$$

Tensile Armour Cross-Section Aspect Ratio w/h

As the ratio w/h increases it is of interest to see whether or not this results in an increase in the bending stresses at the end fitting. From simple beam theory,

$$\sigma_{\max} = \frac{EY}{R_1} = \frac{E}{2} w \left| \frac{d\alpha}{ds} \right| \tag{5.13}$$

where the curvature is given by

$$\left| \frac{d\alpha}{ds} \right| = \frac{k\beta}{1 - \sqrt{\frac{1}{kL^2}}\left(1 - e^{-kL}\right)}, \qquad k = \sqrt{\frac{T_1}{EI_1}} \tag{5.14}$$

For practical cases of flexible pipe in operation, length $L >> 1$, and therefore the maximum stress is

$$\sigma_{\max} = \frac{E}{2} wk\beta \tag{5.15}$$

Examining the characteristic constant k for dependence on w,

$$T_1 = Ehw\varepsilon_{00} + \frac{Eh^3 w}{3R^2}\cos^2\alpha_0 \sin^2\alpha_0 + \frac{Gk_1 h^3 w}{12R^2}\left(1 - 2\sin^2\alpha_0\right)^2 \tag{5.16}$$

$$EI_1 = \frac{Ehw^3}{12}$$

Constant k_1 reduces gradually as w/h increases, being a measure of effectiveness of the cross-section shear forces in resisting twist. For flexible pipe helical angles the twisting term does not contribute significantly to T_1, being zero for a helical angle of $\pi/4$. Hence k is inversely proportional to w, therefore the maximum bending stress at the end fitting is independent of the width of the armour wire and hence of the cross-section aspect ratio.

5.4.2 Stress Increase at End Fitting

The significance of the increase in maximum axial stress due to local bending can be shown by examining the proportional increase over the direct axial stress due to pipe

tension. Typical parameter values have been set out in Table 5.1, and significance can be tested by variation across the ranges shown. Initial parameter values are set out in Table 5.2 below.

Pipe Bore	8″ (200 mm)
Helix Radius	0.12 m
Helical Angle	45°
Wire Height	3 mm
Wire Width	6 mm
Wire UTS	1 GPa
Wire Young's Modulus	2.1×10^{11} Pa
Wire Poisson Ratio	0.3
Pipe Length	10 lay lengths

Table 5.2 Initial parameter values.

The ratio of bending stress to direct stress, σ_b/σ_a, against the ratio of direct axial stress to yield stress, σ_a/σ_y, is shown in Figure 5.3 (where sb/sa is σ_b/σ_a) for typical values of helical angle α_0. The ratio is seen to vary between 2% and 14%, although over the practical operating range up to $\sigma_a/\sigma_y \approx 1/4$ this is reduced to between 2% and 7%.

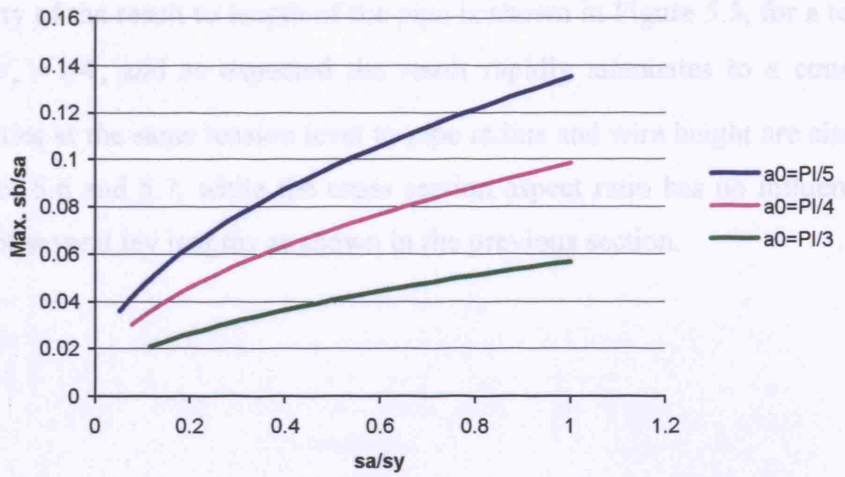

Figure 5.3 Proportional increase in tensile armour axial stress at end fitting.

An example of contributions to bending stress from normal and binormal bending is shown in Figure 5.4 which indicates that the overall increase in maximum axial stress due to end fitting restraint is about three quarters of the indicated ratio σ_b/σ_a, binormal bending being present away from the restraint due to change in helical angle. Therefore over the entire range of tension the maximum increase in wire axial stress due to end fitting restraint is 10%. This is for a helical angle of $\pi/5$, which corresponds to the natural pressure equilibrium helical angle. For wires with a higher helical angle and which are therefore aligned closer to the pipe axis, the stress increase at the end fitting is less pronounced.

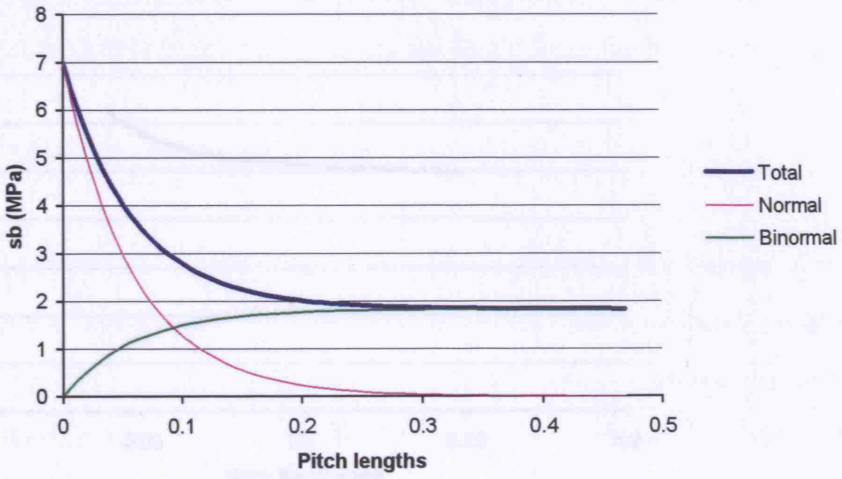

Figure 5.4 Contributions to bending strain.

Sensitivity of the result to length of the pipe is shown in Figure 5.5, for a tension level of $\sigma_a/\sigma_y = 1/4$, and as expected the result rapidly attenuates to a constant value. Sensitivities at the same tension level to pipe radius and wire height are also presented in Figures 5.6 and 5.7, while the cross section aspect ratio has no influence for pipe lengths of several lay lengths as shown in the previous section.

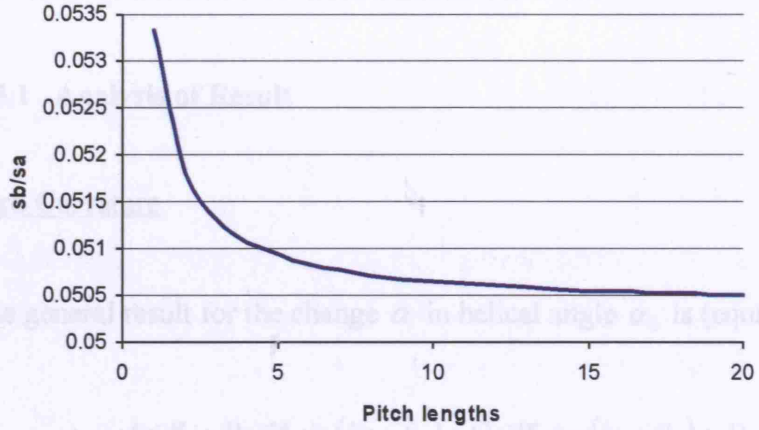

Figure 5.5 Sensitivity of *sb/sa* to model length.

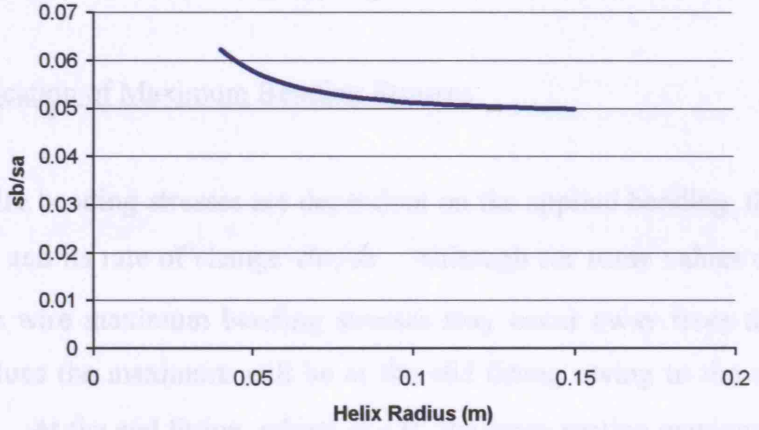

Figure 5.6 Sensitivity of *sb/sa* to armour wire helical radius.

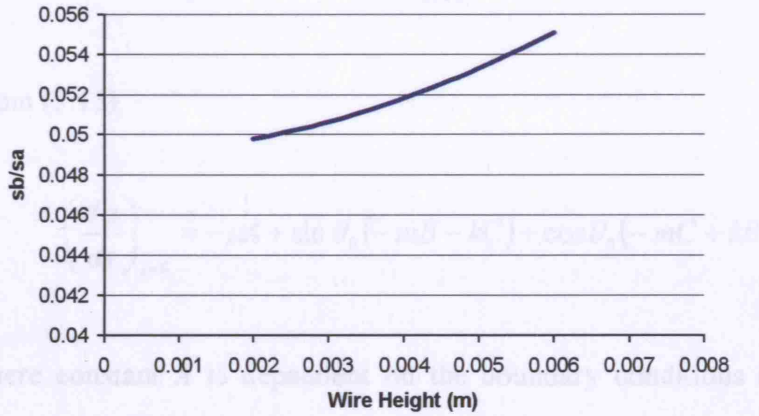

Figure 5.7 Sensitivity of *sb/sa* to armour wire height.

5.5 APPLICATION OF FLEXURAL MODEL

5.5.1 Analysis of Result

Zero Curvature

The general result for the change α in helical angle α_0 is (equation 3.93)

$$\alpha = Ae^{-\mu s} + Be^{-ms}\sin(ks+\theta_0) + Ce^{-ms}\cos(ks+\theta_0) + D \tag{5.17}$$

For zero curvature the general result reduces immediately to the axial solution, as B and C are zero and the remaining constants are found from the boundary conditions.

Location of Maximum Bending Stresses

Wire bending stresses are dependent on the applied bending, the change in orientation α and its rate of change $d\alpha/ds$. Although for some values of initial polar angle θ_0 the wire maximum bending stresses may occur away from the end fitting, for other values the maximum will be at the end fitting owing to the wire's initial orientation α_0. At the end fitting, where $\alpha = 0$, the cross-section maximum bending stresses are

$$\sigma_b = \frac{Ew}{2}\left(K_w\cos\theta_0 - \left(\frac{d\alpha}{ds}\right)_{s=0}\right) + \frac{Eh}{2}K_w\sin\alpha_0\sin\theta_0 \tag{5.18}$$

From (5.15),

$$\left(\frac{d\alpha}{ds}\right)_{s=0} = -\mu A + \sin\theta_0(-mB - kC) + \cos\theta_0(-mC + kB) \tag{5.19}$$

where constant A is dependent on the boundary conditions and hence also on θ_0. From condition $\alpha_{s=0} = 0$, (5.17) can be rewritten

$$\alpha = -A\left(1-e^{-\mu s}\right)+B\left(e^{-ms}\sin\left(ks+\theta_0\right)-\sin\theta_0\right)+C\left(e^{-ms}\cos\left(ks+\theta_0\right)-\cos\theta_0\right)$$

and after integration, from condition $\gamma_{s=L} = Y(L)$,

$$-A\left(L+\frac{1}{\mu}\left(e^{-\mu L}-1\right)\right) = Y(L)-B\left(\frac{1}{m^2+k^2}\left(-m\sin\theta_0-k\cos\theta_0\right)-L\sin\theta_0\right)$$
$$-C\left(\frac{1}{m^2+k^2}\left(-m\cos\theta_0+k\sin\theta_0\right)-L\cos\theta_0\right) \qquad (5.20)$$

Therefore for large L, constant A is given by the approximation

$$-A \approx B\sin\theta_0 + C\cos\theta_0 \qquad (5.21)$$

Now differentiating (5.18) with respect to θ_0 and putting this equal to zero,

$$0 = -\mu\left(B\cos\theta_0 - C\sin\theta_0\right)-\cos\theta_0\left(-mB-kC\right)+\sin\theta_0\left(-mC+kB\right)$$
$$-K_w\left(\sin\theta_0-\frac{h}{w}\sin\alpha_0\cos\theta_0\right) \qquad (5.22)$$

$$\tan\theta_0 = \frac{\mu B - mB - kC - K_w\dfrac{h}{w}\sin\alpha_0}{\mu C - mC + kB - K_w} \qquad (5.23)$$

Solving expression (5.23) for θ_0 gives a close approximation to the positions on the circumference at the end fitting at which the armour wires are subjected to the greatest bending strains. For typical riser cases the result is consistently close to $7\pi/12$ (and $-5\pi/12$), in other words near, though not exactly at, the equivalent 'extreme fibre' positions at $\pm\pi/2$.

5.5.2 Stress Increases at End Fitting

Taking a 6″ bore base case riser with characteristics as set out in Table 5.3, sensitivity of the local bending stresses to various parameters can be assessed as in Section 5.3. The riser loading is dependent on the applied tension and on the magnitude and rate of decay of the applied curvature. Results for the proportion of stress increase for two tension levels and two curvature levels are presented in Figure 5.8.

The tensions are chosen to be one fifth and one tenth respectively of the damaging pull tension, leading to pipe strains of $\varepsilon_p = 0.001$ and $\varepsilon_p = 0.0005$. The curvatures are based on the locking radius of the pipe. A maximum curvature based on 1.5 times the minimum bend radius would give a curvature of 0.4 m^{-1}, an upper bound level. The levels chosen are therefore less than this, being 0.22 and 0.11 m^{-1}. The decay rate is set at unity, giving for the 0.22 m^{-1} cases the following wire curvature.

$$K_w = 0.22e^{-s} \sin \alpha_0 \tag{5.24}$$

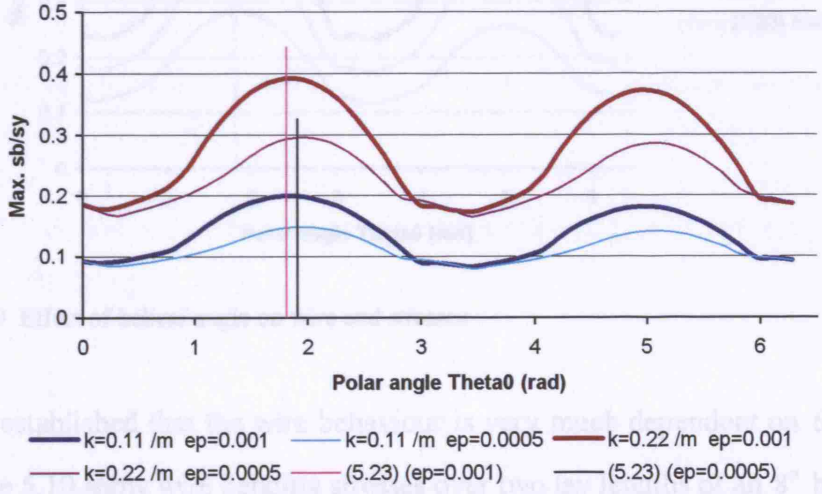

Figure 5.8 Example stress increases at end fitting for 6 inch I.D. pipe.

Figure 5.8 shows firstly that the prediction by (5.23) of the polar location for the maximum bending stress is a good approximation, while wires with end restraint near the neutral axis positions are not unduly stressed by the restraint, with maximum bending occurring elsewhere along the pipe. The response to curvature is linear, with

a doubling of the curvature leading to a doubling of the maximum stress. The response to tension is also significant, highlighting the 'extreme fibre' locations where the wire change in orientation is greater.

There is a significant variation in maximum σ_b/σ_a with helical angle α_0, as also shown in the axial case. Maintaining the curvature at the 0.22 m^{-1} level and altering pipe strain to keep the pipe tension at the same level, Figure 5.9 shows this variation. The sensitivity is reversed from the axial case, with the highest helical angle showing the greatest stresses. This is because a wire aligned straighter along the pipe axis experiences more bending per unit length from the applied bending than one wrapped more circumferentially. Hence the 'neutral angle' shows a better response to applied bending.

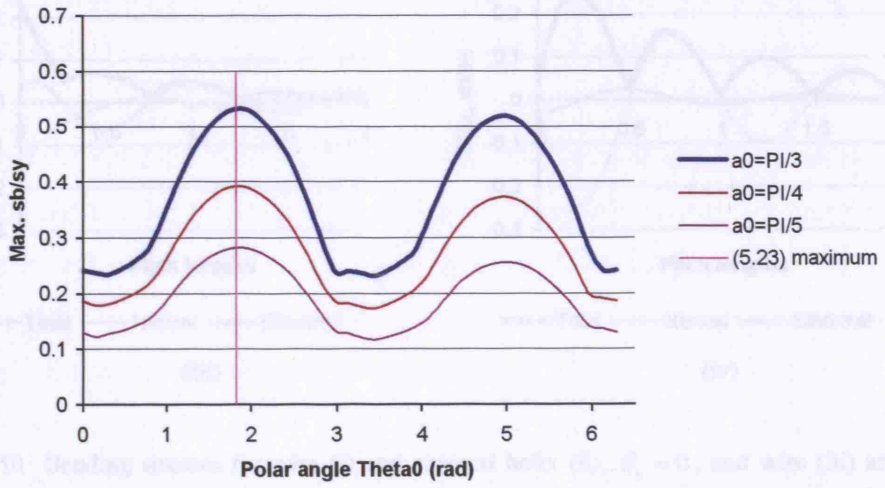

Figure 5.9 Effect of helical angle on wire end stresses.

Having established that the wire behaviour is very much dependent on θ_0, the graphs in Figure 5.10 show wire bending stresses over two lay lengths of an 8″ bore pipe with helical angle $\pi/5$, for neutral axis and 'extreme fibre' values 0 and $\pi/2$ respectively of θ_0. Bending stresses that would be experienced on the strained helix are also presented for comparison. What is shown is that the wire moves to reduce lateral bending where possible at the expense of an increase in binormal bending, but that

overall bending strains are reduced. Stresses at the end fitting may be increased as a result as already discussed.

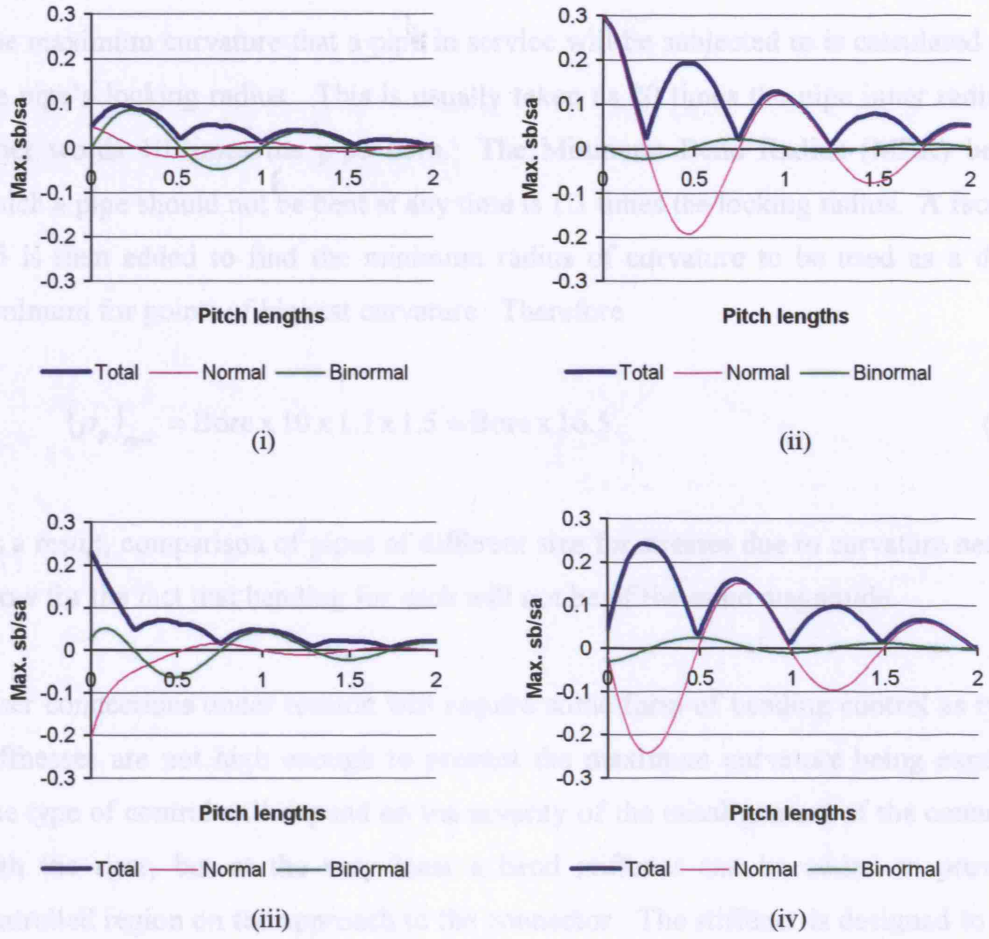

Figure 5.10 Bending stresses for wire (i) and strained helix (ii), $\theta_0 = 0$, and wire (iii) and strained helix (iv), $\theta_0 = \pi/2$.

5.5.3 Effect of Pipe Diameter and Wire Dimensions on Wire Stresses

Maximum Curvature

The maximum curvature that a pipe in service will be subjected to is calculated using the pipe's locking radius. This is usually taken as 20 times the pipe inner radius, in other words 10 times the pipe bore. The Minimum Bend Radius (MBR) beyond which a pipe should not be bent at any time is 1.1 times the locking radius. A factor of 0.5 is then added to find the minimum radius of curvature to be used as a design minimum for points of highest curvature. Therefore

$$(\rho_p)_{max} = \text{Bore} \times 10 \times 1.1 \times 1.5 = \text{Bore} \times 16.5 \tag{5.25}$$

As a result, comparison of pipes of different size for stresses due to curvature needs to allow for the fact that bending for each will not be of the same magnitude.

Riser connections under tension will require some form of bending control as typical stiffnesses are not high enough to prevent the maximum curvature being exceeded. The type of control will depend on the severity of the misalignment of the connection with the riser, but at the very least a bend stiffener can be added to provide a controlled region on the approach to the connector. The stiffener is designed to avoid the maximum curvature at any point along the approach, and while the curvature profile may vary quite sharply in this region, an exponentially decaying profile is adopted here to capture the basic attenuation of curvature experienced by the riser.

Typical pipe values for the decay constant k (5.12) at one fifth of the damaging pull tension range from about 1.5 to 4.5 m^{-1}, increasing as bore diminishes. The chosen decay rate can not exceed these values as this would represent a decrease in pipe stiffness. Therefore a decay constant of 1 m^{-1} is used in the following analysis, increasing where possible to 3 m^{-1}, the analysis being of pipe response to certain conditions of bending rather than of solutions to a particular design case.

Comparison of Stresses for 2 inch – 16 inch Bore Pipes

Using the maximum allowable curvature as a basis, wire end bending stresses for certain wire cross-section dimensions are presented in Figure 5.11 which shows graphs of stress ratio σ_b/σ_y against pipe bore. The wire initial polar angle is kept at $\pi/2$ in view of the results in the previous sections. Helical angle and pipe strain are kept constant at $\pi/4$ and 0.001 respectively.

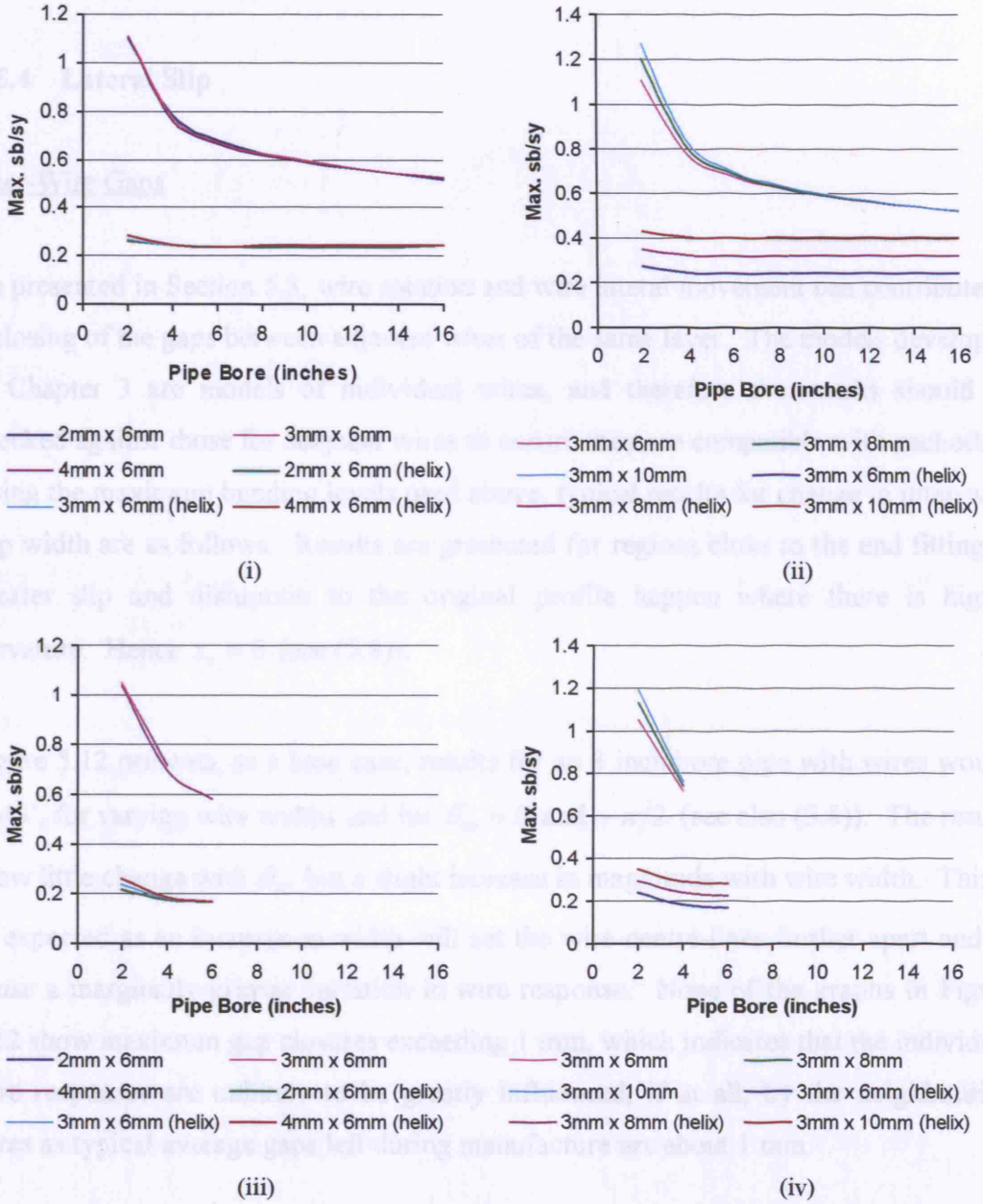

Figure 5.11 Bending stresses at maximum curvature, for exponential decay rates of 1 /m (i and ii) and 3 /m (iii and iv, applicable only to smaller bore pipes).

The graphs suggest that the wire cross-section has little effect on the bending stresses, apart from when the pipe has a small internal diameter of the order of 4 inches or less in which cases an increased wire width leads to increased stresses. However for such pipes of small diameter the calculated minimum bending radius seems to lead to higher than acceptable levels of bending stress. A higher decay rate (3 m^{-1}) reduces these stress levels slightly – this is as a result of the quicker reduction in curvature along the riser and hence less change in orientation of the wires. The bending stresses in all cases exceed those on the strained helix, as already noted for $\theta_0 = \pi/2$.

5.5.4 Lateral Slip

Inter-Wire Gaps

As presented in Section 5.3, wire rotation and wire lateral movement can contribute to a closing of the gaps between adjacent wires of the same layer. The models developed in Chapter 3 are models of individual wires, and therefore the results should be checked against those for adajcent wires to ensure they are compatible with eachother. Using the maximum bending levels used above, typical results for change in inter-wire gap width are as follows. Results are presented for regions close to the end fitting as greater slip and disruption to the original profile happen where there is higher curvature. Hence $s_0 = 0$ (see (5.8)).

Figure 5.12 presents, as a base case, results for an 8 inch bore pipe with wires wound at 45°, for varying wire widths and for $\theta_{00} = 0$ and $-\pi/2$ (see also (5.8)). The results show little change with θ_{00} but a slight increase in magnitude with wire width. This is as expected as an increase in width will set the wire centre-lines further apart and so cause a marginally greater variation in wire response. None of the graphs in Figure 5.12 show maximum gap closures exceeding 1 mm, which indicates that the individual wire responses are unlikely to be greatly influenced, if at all, by the neighbouring wires as typical average gaps left during manufacture are about 1 mm.

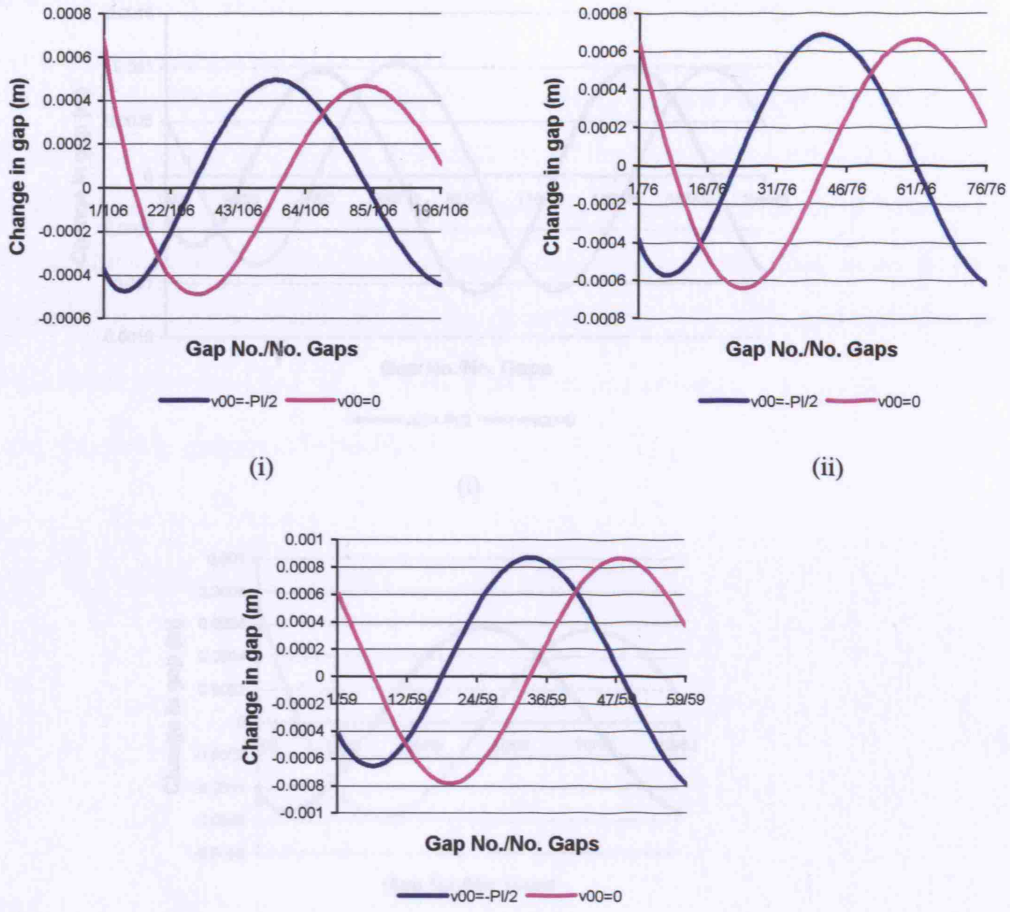

Figure 5.12 Inter-wire gap changes for 8 inch riser, wire cross-section 3 mm x 4 mm (i), 6 mm (ii) and 8 mm (iii).

Results for pipes of different bore are very similar to those in Figure 5.12, bearing in mind that the maximum curvature changes with the bore. Results for different helical angle though show some variation, and are presented for an 8 inch bore pipe in Figure 5.13, where helical angle is set at $\pi/3$ or $\pi/5$, with pipe strain altered to maintain constant pipe tension. The result for the larger angle and hence more axially wound wires shows a gap closure exceeding 1 mm in parts and this indicates a possibility of interference between wires. While this may modify the wire response given by the model, it also indicates that wires wound in this way may be forced out of position when the pipe is bent to high curvatures, thus damaging the integrity of the pipe.

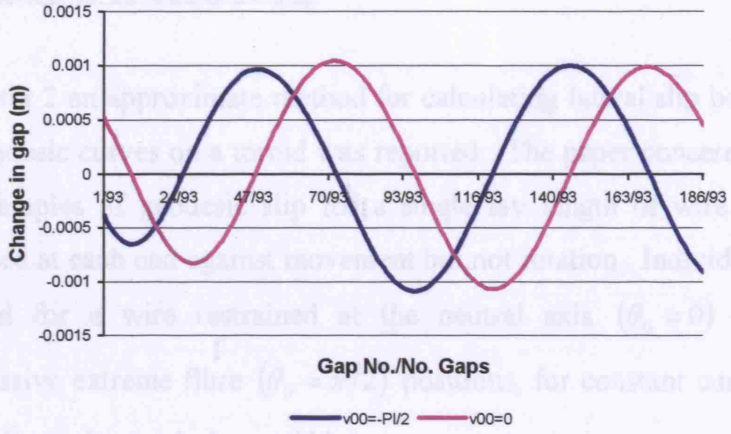

(i)

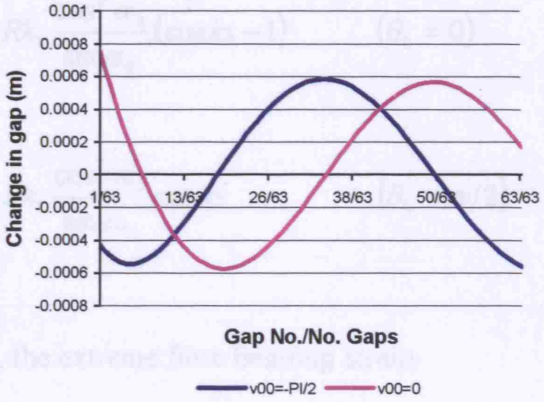

(ii)

Figure 5.13 Inter-wire gap changes for 8 inch riser, wire cross-section 3 mm x 6 mm, helical angle $\pi/3$ (i) and $\pi/5$ (ii).

Transverse Slip vs Geodesic Slip

In chapter 2 an approximate method for calculating lateral slip between strained helix and geodesic curves on a toroid was reported. The paper concerned (Out, 1997) gave two examples of geodesic slip for a single lay length of wire on a bent cylinder, restrained at each end against movement but not rotation. Individual expressions were obtained for a wire restrained at the neutral axis $(\theta_0 = 0)$ and on the inside, compressive extreme fibre $(\theta_0 = \pi/2)$ positions, for constant curvature. From these, lateral slip to the geodesic would be

$$S_{t,g} = 3Rk_1 \frac{\cos^2 \alpha_0}{\sin \alpha_0}(\cos ks - 1) \qquad (\theta_0 = 0) \tag{5.26}$$

$$S_{t,g} = 3Rk_1 \frac{\cos^2 \alpha_0}{\sin \alpha_0} \cos ks \qquad (\theta_0 = \pi/2) \tag{5.27}$$

where k_1 is $\frac{R}{\rho}$, the extreme fibre bending strain.

For the example, k_1 is set at 0.1. It is interesting to compare expressions (5.26) and (5.27) with the analytical result (5.6) for wire transverse slip with the appropriate constant curvature and a sufficient amount of additional pipe strain to ensure the wire remains in tension. Figures 5.14 and 5.15 show this comparison.

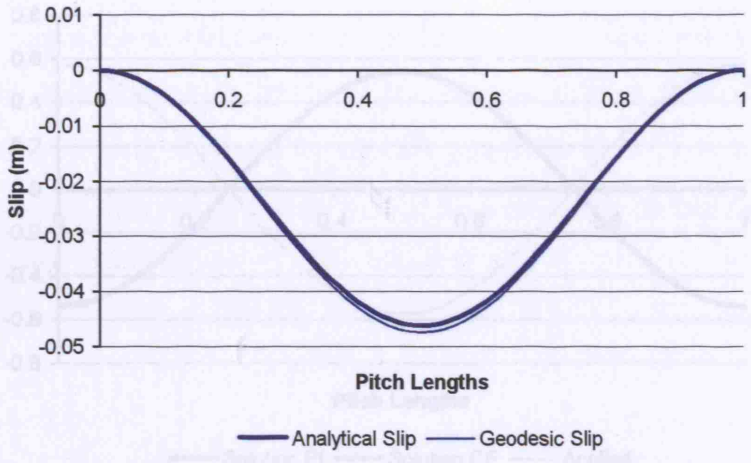

Figure 5.14 Analytical solution slip against geodesic slip, $(\theta_0 = 0)$.

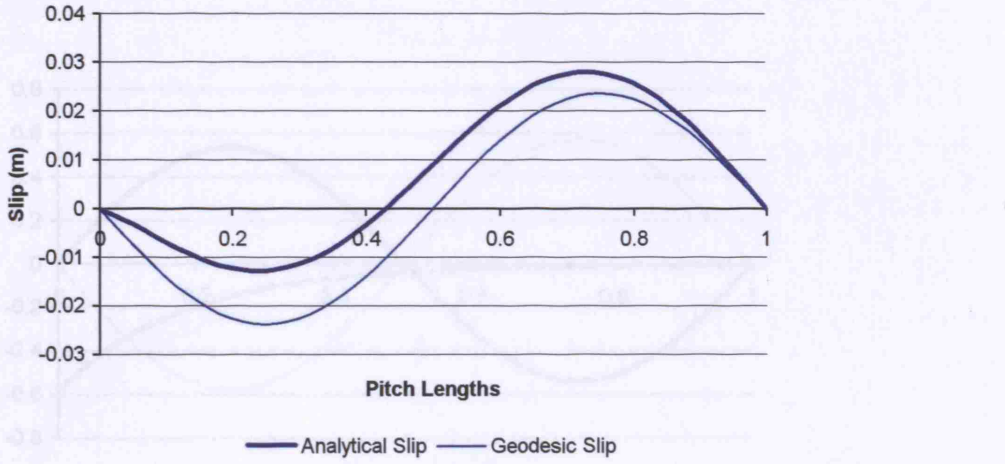

Figure 5.15 Analytical solution slip against geodesic slip, $(\theta_0 = \pi/2)$.

When restrained at the neutral axis position, the wire moves very close to the geodesic curve. When restrained on the inside of the curvature the wire moves towards the geodesic but does not get as close. For $\theta_0 = 0$, the wire's initial orientation is in the same direction as the geodesic and so the assumption that it will take a geodesic path is reasonable, however for the other case the geodesic orientation at the restraint is not the same. Therefore the wire must bend if it is to follow the geodesic and such an assumption is less reasonable. This is shown in Figures 5.16 and 5.17 by the components of the analytical solutions for the wire curvature.

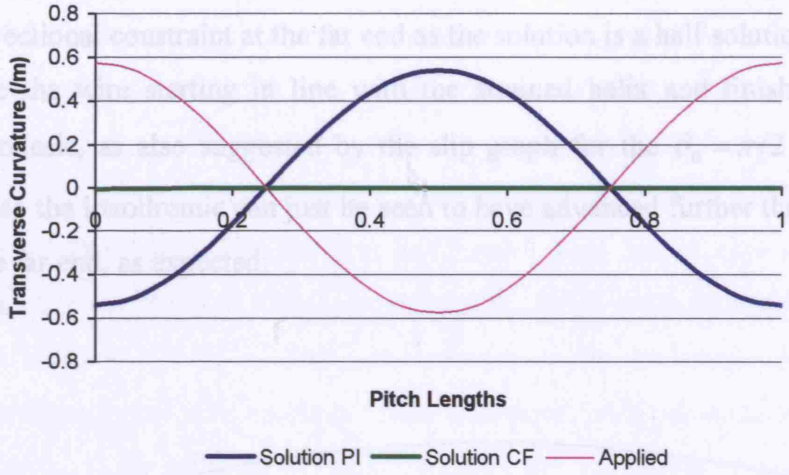

Figure 5.16 Analytical solution curvature components, $(\theta_0 = 0)$.

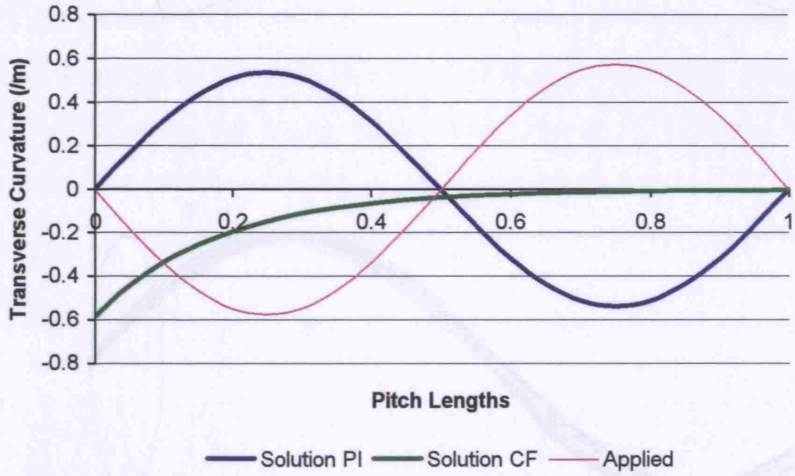

Figure 5.17 Analytical solution curvature components, $(\theta_0 = \pi/2)$.

Figure 5.18 overleaf shows a comparison between strained helix, loxodromic, wire solution and geodesic curves for restraint at the tensile extreme fibre position, $(\theta_0 = -\pi/2)$. The side-on view shows the strained helix advancing first in the axial direction from the left-hand side, followed by the loxodromic, the wire solution and the geodesic, in that order. The strained helix, wire solution and geodesic all have the same start and end points, but the loxodromic is defined by the initial helical angle and start point only and therefore does not pass through the same end point. The wire is

restrained in the strained helix direction at the start although there is no such directional constraint at the far end as the solution is a half solution. It is interesting to see the wire starting in line with the strained helix and finishing in line with the geodesic, as also suggested by the slip graph for the $\theta_0 = \pi/2$ case in figure 5.15. Also the loxodromic can just be seen to have advanced further than the other curves at the far end, as expected.

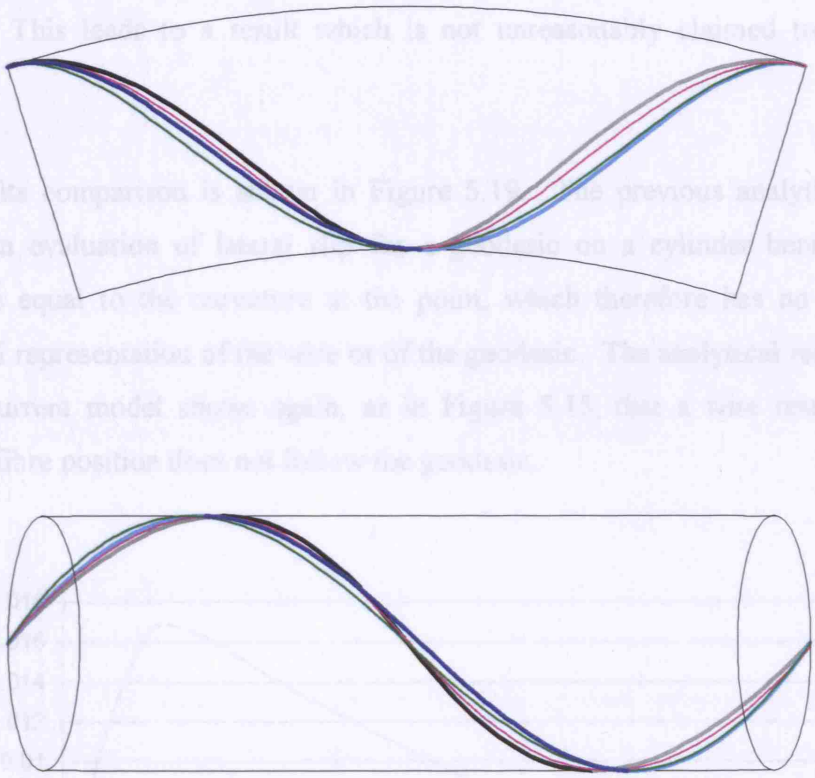

Figure 5.18 Constant curvature toroid showing strained helix, loxodromic, wire solution and geodesic, viewed from beside and below.

A further comparison with a geodesic can also be made using a result from Saevik (1993). Here numerical and so-called analytical results were presented for armour wire transverse slip in a particular test case involving a short length of 8 inch bore pipe, and it is of interest to compare these results with the result from the new analytical model. The model is 2.5 pitch lengths long, with curvature varying linearly from 0.25 to zero over the first half pitch. This can be approximated by a rapidly decaying curvature in the analytical model. Wire cross-section is 3 mm x 6 mm and the lay angle is 25°. The wire restraint is on the tensile side of the pipe, but significantly the wire end is not fully restrained, being able to rotate about the surface normal. This leads to a result which is not unreasonably claimed to represent a geodesic.

The results comparison is shown in Figure 5.19. The previous analytical result is simply an evaluation of lateral slip for a geodesic on a cylinder bent at constant curvature equal to the curvature at the point, which therefore has no value as an analytical representation of the wire or of the geodesic. The analytical result provided by the current model shows again, as in Figure 5.15, that a wire restrained at an extreme fibre position does not follow the geodesic.

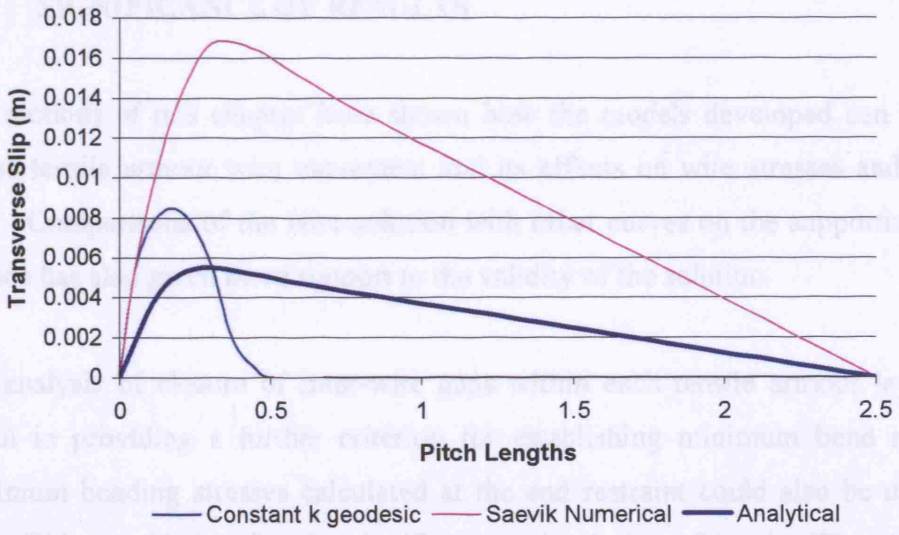

Figure 5.19 Transverse slip and geodesic slip comparison.

An ANSYS version modelling the restrained wire, over one pitch length only, is also presented in Figure 5.20 together with a single pitch analytical solution for comparison, showing good agreement within the limitations of the ANSYS model.

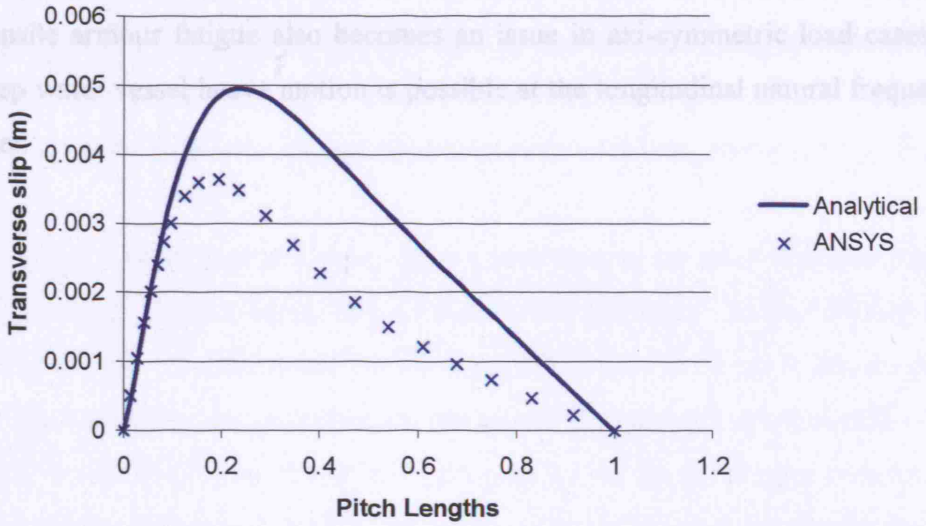

Figure 5.20 Analytical and ANSYS comparison over single pitch length.

5.6 SIGNIFICANCE OF RESULTS

The sections of this chapter have shown how the models developed can be used to assess tensile armour wire movement and its effects on wire stresses and inter-wire gaps. Comparisons of the wire solution with other curves on the supporting cylinder surface has also given more support to the validity of the solution.

The analysis of closure of inter-wire gaps within each tensile armour layer can be useful in providing a further criterion for establishing minimum bend radii. The maximum bending stresses calculated at the end restraint could also be used in this way. This would therefore be significant to the design of bend stiffeners and bend restrictors, and also to pipe reeling.

The results for stress increases at end restraints are readily applicable to fatigue analysis if used together with analyses of riser response to environmental loading. In this respect both the axi-symmetric and the combined axial and flexural load models are useful. Riser tensile armour fatigue due to flexure in response to environmentally induced motions is of high importance, particularly if the conditions inside the pipe annulus are corrosive due to either H_2S or CO_2 permeation or sea-water ingress. Tensile armour fatigue also becomes an issue in axi-symmetric load cases where in deep water vessel heave motion is possible at the longitudinal natural frequency of the riser.

6 CONCLUSIONS AND FURTHER WORK

6.1 CONCLUSIONS

The aim of the work has been to evaluate the effect of end restraint on flexible pipe tensile armour. Tensile armour is helically wound in the unloaded state and its behaviour under loading is characterized by slip on restraining cylindrical or toroidal surfaces. Flexible pipe tensile armour has a rectangular cross section and this tends to control twist while encouraging movement across the smooth supporting surfaces.

In previous work slip has either been considered as an axial slip along the strained original path or as a lateral slip to the surface geodesic. In the vicinity of the end fitting the geodesic is not compatible with the restraint but there is also no guarantee at all that the wires are restrained to remain on the strained original path. Hence the work has set out to find the position adopted by the tensile armour between these two limit curves and to evaluate its significance in terms of stress increase in the vicinity of the end fitting.

A solution has been found in the absence of friction and this provides a new limiting curve which indicates the ideal location towards which tensile armour will attempt to move. Solutions have been achieved for flexible pipe under axi-symmetric loading and loading including simultaneous tension and bending with a non-constant radius of curvature as appropriate for flexible riser applications.

These solutions are found by minimisation of strain energy due to tension, bending and twist. The energies involved are all able to be expressed in terms of a change in helical angle and its rate of change per unit length of wire, with wire twisting with respect to its supporting surfaces prevented. Pipe radius is assumed constant due to the presence of an interlocking pressure armour layer.

6.1.1 Axi-symmetric Cases

The simplest case involves axi-symmetric loading. The effect of the end restraint is to keep the tensile armour oriented in its original direction thus causing a transition or boundary layer over which there is lateral bending of the wire. Beyond this region which is typically less than half a pitch length along the wire, the wire assumes a new helical form. Longitudinal stresses as a result of the local lateral bending can cause an overall increase in longitudinal stress of up to 10%, this being dependent on the level of tension and on the initial helical angle, but not on the wire cross-section aspect ratio.

The response to tension is slightly non-linear, with stresses increasing faster with greater tension.

6.1.2 Flexural Cases

For dynamic flexible risers an exponentially decaying curvature distribution is used to represent controlled curvature over the end region. The result shows the same type of boundary layer solution, with the wire moving to reduce tension and lateral bending away from the end restraint. As in the axi-symmetric case, this involves a tendency to move towards the geodesic on the surface, and because the difference between the original and geodesic orientations at the restraint is greatest near the 'extreme fibre' positions, this causes greater lateral bending stresses here than opposite the neutral axis.

This is in contrast to previous suggestions, usually based on the fact that there is a greater amount of applied lateral bending at the neutral axis. In most cases of failure due to bending, tensile armour failures near end fittings are observed to be opposite the neutral axis, but these are generally due to fretting fatigue as this location corresponds to greatest slip. Wire rope failures also display the same characteristics. However in the case of dynamic risers fretting is less likely to be an issue than reciprocating stresses due to local bending at the end fitting.

In a pipe fatigue test reported by Saevik (Saevik, 1993), primary failure was observed to be due to fretting fatigue in the inner layer of tensile armour. Secondary failure was observed in the outer layer of tensile armour and this was located at the end fitting 'on the tensile side of the pipe relative to the global bending moment'. Although this failure was caused by an increase in stress due to the primary failures, this failure location is in agreement with the analytical results obtained here.

6.2 FURTHER WORK

The models already developed can easily be extended to look at further cases of pipe loading. When pipe is manufactured and reeled, armour layer wires are subjected to a high degree of bending which may result in the presence of compressive axial forces and in a sinusoidal rather than hyperbolic solution.

Secondly, curvature controls for risers may involve sections of pipe under different conditions to those imposed by a bend stiffener. They may for example provide an initial section of straight pipe, followed by a region of curvature that is reasonably constant (except over the transitions to zero or low curvature) to achieve the correct pipe orientation. The resulting piecewise configuration can easily be modelled by the method developed using separate models with compatible boundary conditions where they join.

An alternative can be to use a more sensitive function to indicate the applied curvature in the model. For example, curvature distributions over end regions with a bend stiffener can be represented by functions of the form

$$K_p = Z_p\, e^{-(as)^n} / \left(b(1+cs)\right) \tag{6.1}$$

examples of which are shown in Figure 6.1 where $a = 1$, $n = 8$, $b = 4$ and c is either zero or 0.25.

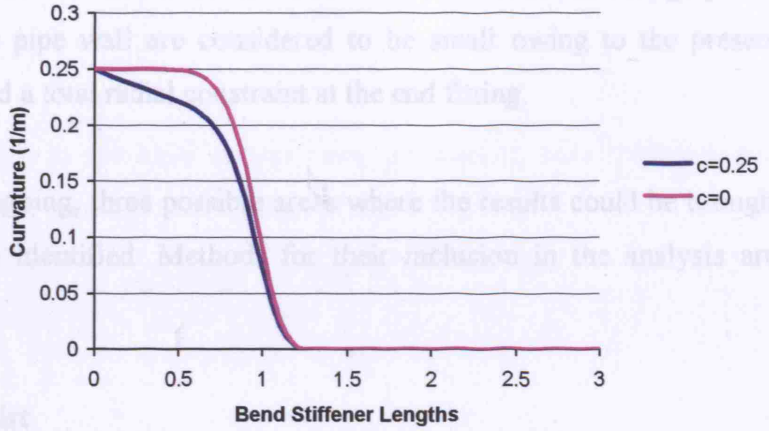

Figure 6.1 Applied curvature distributions near end fitting.

In the work so far, the stresses obtained are for a wire with no frictional resistance which is also restrained completely against twist relative to the supporting surfaces. This means that the results for slip are upper bound values, conservative in that they give the maximum values, and the same also for some of the stresses at the end fitting in the flexural model case.

Axial slip is very unlikely to be affected by friction owing to the high tension gradients that would be created in the tensile armour. Lateral slip may be more easily suppressed owing to small lateral curvature, but here again resistive forces may be beyond the supporting surface interfaces although they may be enhanced by high external hydrostatic pressure.

If the supporting surfaces are deemed to be compliant in the face of frictional forces, then they may also be considered to provide a less than perfect restraint against twisting. Twisting of the wire with respect to the supporting surfaces provides an opportunity for lateral bending to be relieved by the wire's natural and comparatively high binormal curvature, at the expense of work done against the surfaces and some twisting strain energy.

Changes in radius due to constriction under tension or due to high pressure differential across the pipe wall are considered to be small owing to the presence of pressure armour and a total radial constraint at the end fitting.

In the foregoing, three possible areas where the results could be brought into question have been identified. Methods for their inclusion in the analysis are suggested as follows.

6.2.1 Twist

A second dependent variable can be added to the analysis to account for wire twist with respect to the supporting surfaces. If the extra angle of twist is f, then the wire twist is augmented by df/ds and the additional changes in curvature and twist can be written

$$\begin{aligned} \Delta\kappa &= f\kappa' = f\frac{\cos^2\alpha_0}{R} \\ \Delta\kappa' &\approx 0 \\ \Delta\tau &= \frac{df}{ds} \end{aligned} \tag{6.2}$$

At the end fitting f is zero. The variables α and γ still describe the wire orientation and position on the supporting surfaces, these not being directly affected by f. In addition, work is done by the wire as its extra twist angle requires the supporting surfaces to be moved. Assuming that the radius remains constant and that lateral movement is not suppressed by the surface deformation, the only further addition to the functional terms is work done, which can be treated as work done against an externally applied force. This could be assumed to be linearly dependent on displacement giving work done W as

$$W = \tfrac{1}{2}K_1 f^2 \tag{6.3}$$

assuming that f remains fairly small. Constant K_1 is dependent on the surface materials.

For example in the axial model case, proceeding with these additional terms, the original Euler equation terms affected are

$$EI_1 \frac{d^2\alpha}{ds^2} \rightarrow EI_1\left(\frac{d^2\alpha}{ds^2} - \frac{df}{ds}\frac{\cos^2\alpha_0}{R}\right)$$

$$\frac{G_1k_1I_2}{R^2}\left(1-2\sin^2\alpha_0\right)^2\alpha \rightarrow \frac{G_1k_1I_2}{R}\left(1-2\sin^2\alpha_0\right)\left(\left(1-2\sin^2\alpha_0\right)\frac{\alpha}{R}+\frac{df}{ds}\right) \tag{6.4}$$

A second Euler equation results for f, which is

$$G_1k_1I_2\left(\frac{1}{R}\left(1-2\sin^2\alpha_0\right)\frac{d\alpha}{ds}+\frac{d^2f}{ds^2}\right) = EI_1\frac{\cos^2\alpha_0}{R}\left(\frac{\cos^2\alpha_0}{R}f-\frac{d\alpha}{ds}\right)+Kf \tag{6.5}$$

From (6.5) $d\alpha/ds$ can be written in terms of f and d^2f/ds^2, which can then be substituted into the first Euler equation to get a fourth order O.D.E. in f.

6.2.2 Friction

The inclusion of friction alters the problem by introducing energy dissipation. However, the frictionless results indicate that wire displacements grow with growing tension and curvature. If the work done against friction is treated as work done against applied conservative forces, the resulting conservative system will not be any different provided that the loading increases steadily from the initial state to the final state, therefore allowing the continued application of the Euler-Lagrange equation.

For a typical 6mm x 3mm tensile armour wire axially stressed at 125 MPa, the tension is 2.25 kN. If it is helically wound on a cylinder at a helical angle of 45° and radius 0.1m then

$$T\kappa' = 11.25 \times 10^3 \text{ N/m}$$

which is the major contributor to the normal force per unit length X. For this to be sufficient to hold the wire from slipping if the supporting cylinder is bent then

$$\frac{dT}{ds} \leq \mu X \tag{6.6}$$

everywhere. The maximum value of the tension gradient is

$$\left(\frac{dT}{ds}\right)_{\max} = EA\left(\frac{\cos\alpha_0}{R}\right)\frac{R}{\rho}\sin^2\alpha_0 \tag{6.7}$$

and putting this equal to μX with $\mu = 0.2$ gives a radius of curvature for the pipe of roughly 600m. This suggests that even when friction is present slip will very quickly be fully developed in the region of the end fitting.

Equilibrium

Love's thin rod equilibrium equations are quoted in full in Chapter 2 (2.30). They contain three applied forces per unit length and three applied moments per unit length. Normal force X and twisting moment θ are already present in the absence of friction owing to the support from the neighbouring surfaces. Forces per unit length Y and Z will both now be present also. Applied moments per unit length K and K' may also be present, but owing to the small dimensions of the wire cross-section and to the likely behaviour of the neighbouring surfaces they are neglected in the following.

The dynamic friction is lower than the static friction, but at what point does the wire-surface interface become dynamic? For a helical line on a cylinder, the line will shear when an axial force is applied to the cylinder, but a wire on the helix will turn to follow the new line rather than shear with it. This suggests that everywhere the dynamic level of friction should be chosen. This also suggests that K will exist although friction would have to be very high to make it significant, and the shear strength too of the supporting surfaces.

Axial Model

With friction, the model length will be shorter than without, as the straight helical region away from the end restraint is incompatible with any lateral slip, which would require some lateral curvature. The location of the boundary varies as strain increases, leading to a transitional region of slip, and would need to be checked for equilibrium afterwards.

As there is no appreciable axial slip in these cases work done is dependent only on $(Y-\gamma)$, the contact forces and the coefficient of friction. Total work is

$$W = \mu\int_0^{L(T)}\int_0^{(Y-\gamma)}\left(T\kappa_0' + 2pw\right)\left|d(Y-\gamma)_1\right|ds \tag{6.8}$$

where p is the contact pressure at the armour wire surfaces. It is reasonable to asssume that p remains constant as T increases but that $(Y-\gamma)$ is linearly dependent on T. T can also be considered to be independent of s. Hence

$$W = \mu\int_0^{L(T)}\left(\tfrac{1}{2}T_{\max}\kappa_0'(Y-\gamma)^2 + \left|2pw(Y-\gamma)\right|\right)ds \tag{6.9}$$

A problem remains with the modulus in (6.9) although this can be approximated by $(Y-\gamma)^2/(Y-\gamma)_{\max}$ with $(Y-\gamma)_{\max}$ to be checked and updated if necessary. Finally the moving boundary can be examined as tension increases, with a transitional region over which the work done depends also on the value of T at the beginning of slip.

The new terms resulting from the minimisation are

$$\mu(\gamma - Y)\left(T_{\max}\kappa_0' + \frac{4pw}{(Y-\gamma)_{\max}}\right) \tag{6.10}$$

Flexural Model

In flexural cases the direction of the friction force is less easy to say as there will also be axial slip. Hence the expression (6.8) becomes

$$W = \mu \int_0^{L(T)} \int_0^{l} \left(T\kappa_0' + 2pw\right) \left| dl_1 \right| ds \tag{6.11}$$

where

$$(dl_1)^2 = (d(Y-\gamma))^2 + (df_1(s))^2$$

in which $f_1(s)$ represents the axial slip which can be taken directly from the surface strain due to applied curvature. If the tension T is assumed not to vary significantly during flexure it can be taken as a constant. In this case

$$W = \mu \int_0^{L(T)} \left(T\kappa_0' + 2pw\right) \left((Y-\gamma)^2 + f_1(s)^2\right)^{\frac{1}{2}} ds \tag{6.12}$$

and the new term resulting from the minimisation is

$$\mu\left(T\kappa_0' + 2pw\right)(\gamma - Y)\left((Y-\gamma)^2 + f_1(s)^2\right)^{-\frac{1}{2}} \tag{6.13}$$

The problem with this result is that the differential equation for γ is now non-linear. This might be overcome, especially for low levels of friction, by using the frictionless result for γ in the square root in (6.13).

6.2.3 Change in Radius

The effects of varying radius along the pipe length, a possibility if the pipe is restricted at the end fitting but otherwise more free to expand, could also be assessed using a further Euler equation in the small variable ΔR.

7 REFERENCES

Boas M L, 1983, Mathematical Methods in the Physical Sciences, 2nd Ed., Wiley.

Cook R D, 1995, Finite Element Modelling for Stress Analysis, Wiley.

Costello G A, 1990, Theory of Wire Rope, Springer-Verlag, New York.

D'Oliveira J G, Goto Y, Okamoto T, 1985, Theoretical and Methodological Approaches to Flexible Pipe Design and Application. Offshore Technology Conference, OTC5021.

Ericksen, J and Truesdell, C, 1957-58, Exact Theory of Stress and Strain in Rods and Shells, Archives of Rational Mechanics and Analysis, Vol. 1, pp 295-323.

Fee D A, O'Dea J, 1986, Technology for Developing Marginal Offshore Oilfields. Elsevier Science.

Feret J J, Bournazel C L, 1987, Calculation of Stresses and Slip in Structural Layers of Unbonded Flexible Pipes, Journal of Offshore Mechanics and Arctic Engineering, Vol. 109, pp 263-269.

Fuku T, Ishii K, 1992, Fatigue Properties and Analysis of Flexible Riser, OTC6876.

Hay G E, 1942, The Finite Displacement of Thin Rods, Transactions of the American Mathematical Society, Vol. 51, pp 65-102.

Hruska F H, 1951, Calculation of Stresses in Wire Ropes, Wire, pp 766-801.

Hruska F H, May 1952, Radial Forces in Wire Ropes, Wire and Wire Products, Vol. 27, No. 5, pp 459-463.

Hruska F H, May 1953, Tangential Forces in Wire Ropes, Wire and Wire Products, Vol. 28, No. 5, pp 455-459.

Jolicoeur C, Cardou A, December 1991, A Numerical Comparison of Current Mathematical Models of Twisted Wire Cables Under Axisymmetric Loads, ASME Journal of Energy Resources Technology, Vol. 113, pp 241-249.

Knapp R H, 1979, Derivation of a New Stiffness Matrix for Helically Armoured Cables Considering Tension and Torsion, International Journal for Numerical Methods in Engineering, Vol. 14, pp 515-529.

Kreyszig, Advanced Engineering Mathematics, 7th Ed., Wiley, Chapter 8.

Lanteigne J, June 1985, Theoretical Estimation of the Response of Helically Armoured Cables to Tension, Torsion and Bending, Journal of Applied Mechanics, Vol. 52, pp423-432.

Lipschutz M, 1969, Theory and Problems of Differential Geometry, McGraw-Hill.

Love A E H, 1944, A Treatise on the Mathematical Theory of Elasticity, 4th Ed., Dover, New York.

Lutchansky M, 1969, Axial Stresses in Armour Wires of Bent Submarine Cables, ASME Journal of Engineering for Industry, Vol. 91, pp 687-693.

Marinflex, 1995, Proceedings of the Second European Conference on Flexible Pipes, Umbilicals and Marine Cables – Structural Mechanics and Testing, edited by MH Patel and JA Witz, Ch 4, p22.

Mathpages, Constant Headings and Rhumb Lines, [online]. Available from : http://www.mathpages.com/home/kmath502/kmath502.htm [cited 28/3/06]

McIver D B, 1995, A Method of Modelling the Detailed Component and Overall Structural Behaviour of Flexible Pipe Sections, Elsevier Science, Engineering Structures, Vol. 17, No. 4, pp 254-266.

McIver D B, 1998, Behaviour of Helically Wound Wires Sliding Under Friction on a Bent Cylinder, MAI Consultants Ltd, Epsom, Surrey, UK.

Moaveni S, 1999, Finite Element Analysis – Theory and Application with ANSYS, Prentice-Hall.

Oden J T, Ripperger E A, 1981, Mechanics of Elastic Structures, 2nd Ed., McGraw-Hill.

Out J M M, von Morgen B J, 1997, Slippage of Helical Reinforcing on a Bent Cylinder, Elsevier Science, Engineering Structures, Vol. 19, No. 6, pp 507-515.

Patel M H, Seyed F B, 1992, Mathematics of Flexible Risers Including Pressure and Internal Flow Effects, Elsevier Science, Marine Structures 5, pp 121-150.

Patel M H, Tan Z, Witz J A, 1993, Damage Assessment of Subsea Umbilicals During Installation, Department of Mechanical Engineering, UCL.

Patel M H, Witz J A, Tan Z, 1993, A Flexible Riser Design Manual, Bentham Press, London.

Prager W, 1961, Introduction to Mechanics of Continua, Ginn and Company.

Principal Metals Online, [online]. Available from : http://www.principalmetals.com [cited 24/3/06]

Ramsey H, 1988, A Theory of Thin Rods with Application to Helical Constituent Wires in Cables, International Journal of Mechanical Sciences, Vol. 30, No. 8, pp 559-570.

Ramsey H, 1990, Analysis of Interwire Friction in Multilayered Cables under Uniform Extension and Twisting, International Journal of Mechanical Sciences, Vol. 32, No. 18, pp 709-716.

Ramsey H, 1991, Localized Effect of Clamped or Socket End Connections on Helical Wires in Multilayered Cables, International Journal of Solids and Structures, Vol. 28, No. 6, pp 779-790.

Raoof M, Hobbs R E, 1984, The Bending of Spiral Strand and Armoured Cables Close to Terminations, ASME Journal of Energy Resources Technology, Vol. 106, pp 349-355.

Rees D W A, 1990, The Mechanics of Solids and Structures, McGraw-Hill, London.

Roark R J, Young W C, 1975, Formulas for Stress and Strain, 5th Ed., McGraw-Hill, New York.

Routh E J, 1905, Elementary Part of a Treatise on the Dynamics of a System of Rigid Bodies, 7th Ed., Macmillan, London.

Routh E J, 1905, Advanced Part of a Treatise on the Dynamics of a System of Rigid Bodies, 6th Ed., Dover, New York.

Sævik S, 1993, A Finite Element Model for Predicting Stresses and Slip in Flexible Pipe Armouring Tendons, Computers and Structures, Vol. 46, No.2, pp 219-230.

Saevik S, Giertsen E, Olsen G P, 1998, A New Method for Calculating Stresses in Flexible Pipe Tensile Armours, SINTEF Civil and Environmental Engineering, Norway, / Norsk Hydro Research Centre, Norway.

Seyed F B, Sept. 1989, Ph.D. Thesis, Department of Mechanical Engineering, University College London.

Society for Underwater Technology (SUT), 2005, The Life-Cycle of Flexible Risers and Flowlines, Course Notes, Aberdeen.

Sødahl N R, 1991, Methods for Design and Analysis of Flexible Risers, Dr Ing Thesis, Division of Marine Structures, Norwegian Institute of Technology, Trondheim.

Sokolnikov, 1956, Mathematical Theory of Elasticity, 2nd Ed., McGraw-Hill.

Stevenson A, Materials Engineering Research Laboratory Ltd, Polymers as Structural Engineering Materials, Lecture Notes.

Thompson J F, Warsi Z U A, Wayne Mastin C, 1985, Numerical Grid Generation: Foundations and Applications.

Timoshenko S P, 1941, Strength of Materials, 2nd Ed., Macmillan, London.

Timoshenko S P, Woinowsky-Krieger S, 1959, Theory of Plates and Shells, 2nd Ed., McGraw-Hill.

Timoshenko S P, Goodier J N, 1970, Theory of Elasticity, 3rd Ed., McGraw-Hill.

Vasselin, T P, 2000, Use of Polyamide 11 in Corrosive Applications, Elf Atochem North America, Technical Paper.

Washizu K, 1974, Variational Methods in Elasticity and Plasticity, 2nd Ed., Pergamon Press.

Waters E O et al, 1937, Formulas for Stresses in Bolted Flanged Connections, Transactions of the ASME, Fuels and Steam Power, FSP-59-4, pp 161-169.

Williams J G, 1973, Stress Analysis of Polymers, Longman, London.

Witz J A, Tan Z, 1992 (i), On the Flexural Structural Behaviour of Flexible Pipes, Umbilicals and Marine Cables, Elsevier Science, Marine Structures 5, pp 229-249.

Witz J A, Tan Z, 1992 (ii), On the Axial-Torsional Behaviour of Flexible Pipes, Umbilicals and Marine Cables, Elsevier Science, Marine Structures 5, pp205-227.